UNIVERSIDAD DE CHILE
FACULTAD DE CIENCIAS FíSICAS Y MATEMÁTICAS
DEPARTAMENTO DE INGENIERÍA ELÉCTRICA

HIERARCHICAL ENERGY MANAGEMENT SYSTEM BASED ON FUZZY PREDICTION INTERVALS FOR OPERATION AND COORDINATION OF MICROGRIDS

TESIS PARA OPTAR AL GRADO DE
DOCTOR EN INGENIERÍA ELÉCTRICA

LUIS GABRIEL MARÍN COLLAZOS

PROFESOR GUÍA:
DRA. DORIS SÁEZ HUEICHAPAN

PROFESOR CO-GUÍA:
DR. MARK SUMNER
PROFESOR CO-GUÍA 2:
DR. ALFREDO NUÑEZ VICENCIO

MIEMBROS DE LA COMISIÓN:
DR. RODRIGO MORENO VIEYRA
DR. DANIEL SBÁRBARO HOFER
DR. MATÍAS NEGRETE PINCETIC

SANTIAGO DE CHILE
2018

RESUMEN DE LA TESIS PARA OPTAR
AL TÍTULO DE DOCTOR EN INGENIERÍA ELÉCTRICA
POR: LUIS GABRIEL MARÍN COLLAZOS
FECHA: 2018
PROFESOR GUÍA: DRA. DORIS SÁEZ HUEICHAPAN

HIERARCHICAL ENERGY MANAGEMENT SYSTEM BASED ON FUZZY PREDICTION INTERVALS FOR OPERATION AND COORDINATION OF MICROGRIDS

La integración de un gran número de Recursos Energéticos Distribuidos (DERS, por sus siglas en inglés) en el sistema de distribución puede ocurrir mediante el refuerzo de los activos existentes de la red, o con el manejo activo de los recursos flexibles en las distintas secciones de la red de distribución. El diseño de estrategias de control es necesario para la administración activa de la red de distribución y lograr una integración eficiente y confiable a gran escala de los DERs. Además del beneficio de soportar el uso de fuentes de energía renovable, los DERs juegan un papel importante en la mejora de la resiliencia y sostenibilidad del sistema de distribución de energía, además en la generación de nuevas oportunidades de mercado.

En esta tesis, la administración activa de los DERs se propone utilizando un sistema de administración energético (EMS, por sus siglas en inglés) jerárquico, y aplicado a Comunidades Energéticas. Las comunidades energéticas corresponden a un concepto que permite a diferentes usuarios finales cooperar en sus interacciones energéticas con el propósito de maximizar su auto-consumo, minimizar los costos energéticos, reducir los niveles de picos de potencia, o una combinación de estos y cumplir con otras metas beneficiosas. El EMS jerárquico propuesto permite la incorporación de mecanismos que aseguran la realización del balance de potencia en el corto tiempo, y el manejo a largo plazo de la energía, beneficiando al propietario de la micro-red así como al operador de la red de distribución.

El EMS jerárquico se diseña en dos niveles: a nivel de red principal, y a nivel de micro-red. A nivel de micro-red, se propone el uso de un controlador en tiempo real basado en reglas, y en el alto nivel, un modelo de control predictivo robusto (MPC) basado en modelos de intervalos de predicción difusos con el fin de ayudar al sistema a estar preparado para errores en las predicciones que pueden ocasionar decisiones subóptimas.

Diferentes casos de estudio se utilizaron para evaluar el desempeño del EMS jerárquico para la operación y coordinación de micro-redes. El EMS robusto basado en modelos de intervalos de predicción difusos es comparado con un EMS determinístico y con un EMS básico sin un sistema de almacenamiento de energía (ESS). Estos resultados muestran que el EMS determinístico y el EMS robusto proveen mejoras con respecto al caso sin ESS, puesto que ofrecen mecanismos para una administración eficiente de la energía. La incorporación de un ESS en la comunidad energética beneficia tanto al usuario final al reducir los costos de la energía, así como al operador de la red de distribución al limitar los niveles de picos de potencia y permitiendo una mayor penetración de generación distribuida (DG). Adicionalmente, el EMS jerárquico es capaz de mantener el flujo de potencia de la comunidad cerca de la potencia de referencia definida por el controlador de alto nivel con el menor costo de energía, dentro de otros beneficios. Finalmente, los usuarios finales que operan como comunidades de energía pueden optimizar el uso de la DG y el tamaño del ESS requerido.

Abstract

The integration of large numbers of Distributed Energy Resources (DERs) into the distribution system could take place either by reinforcement of the existing network assets, or the incorporation of active management of flexible resources into different sections of the distribution network. For active management of a distribution network, the design of control strategies is necessary for an efficient and reliable large-scale integration of DERs. Besides the benefit of supporting the use of renewable energy sources, DERs play an important role in improving the resilience and sustainability of the electricity distribution system and also in the generation of new market opportunities.

In this thesis, the active management of DERs is proposed using a hierarchical energy management system (EMS) applied to "Energy Communities". Energy communities are a concept which allows different end users to cooperate in their energy interactions with the aim of maximising their self-consumption, minimising energy costs, reducing peak power levels or a combination of these and other beneficial goals as well. The hierarchical EMS proposed allows incorporating mechanisms to ensure both the realisation of short-term power balancing objectives and long-term energy management, benefiting the microgrid owner and the distribution network operator.

The hierarchical EMS is designed in two levels: main grid level and microgrid level. At the microgrid level, a real-time local rule-based controller is proposed and at the higher level, a Robust model predictive control (MPC) is used to manage the uncertainty associated with renewable distributed generation and electricity demand. The uncertainty is incorporated into the Robust MPC controller based on fuzzy prediction interval models in order to help the system to be prepared for errors in the predictions that might yield sub-optimal decisions.

Several case studies are used to test the performance of the hierarchical EMS for the operation and coordination of microgrids. Robust EMS based on fuzzy prediction interval models is compared to the deterministic EMS and with a basic EMS without energy storage system (ESS). The results show that the deterministic and Robust EMSs provide improvements over the case without ESS, as they offer mechanisms for efficient energy management. The incorporation of an ESS into the energy community benefits both the end user, by reducing energy cost, and the distribution network operator, by limiting the peak power levels and enabling increased penetration of distributed generation (DG). Additionally, the hierarchical EMS is able to keep the community power flow close to the reference power defined by the higher level controller with minimum energy cost, among other benefits. Finally, end users operating as Energy Communities can optimise the use of DG and the size of the ESS required.

To my aunt Hilda Collazos (RIP), you will always be in my heart. To my parents, Luis Antonio and Carlina, for all the love and support they have given me throughout my life. To my son Manuel Andrés, who I love with all my heart and is my main motivation to keep on going. To my sister Eliana for her unconditional support. Finally, to my nieces Anama and Isa who will always be my beautiful "Abichuchas".

Luis Gabriel Marín Collazos

Acknowledgements

I would like to express my sincere gratitude to my supervisors Prof. Doris Sáez Hueichapan, Prof. Mark Sumner and Prof. Alfredo Núñez for their commitment, guidance, support and patience during the course of my studies. Also, to the rest of the commission members for their valuable comments and recommendations: Prof. Rodrigo Moreno, Prof. Daniel Sbárbaro and Prof. Matías Negrete.

I am also grateful for the productive advice and support offered by Dr. Felipe Valencia, Dr. Diego Muñoz-Carpintero and Dr. Seksak Pholboon.

To all friends that I have met during these years in the University of Chile: Tomislav, Raúl, Nicolás (Creator), Alex, Claudio, Daniel, Oscar, Enrique, Erwin, Felipe, Matías D., Manuel, Leonel L., Matías U., Cristian, Carolina, Victor, Antonio, Leonel G., and Patricio. Thanks for the friendship and help.

Thanks to Jacqueline, Elizabeth, Vanessa, Rosana, Francisco (Panchito), Diego (el de Jacque), Aramis (Chiquillo), Juan (Juanito), Carlos (Rulitos) and Leonardo (la amiga) for being such great friends and for making these years in Chile a wonderful experience. Thanks for sharing so many important moments, conversations and advice in the appropriate times.

This study was partially supported by the Complex Engineering Systems Institute, CONICYT–PIA–FB0816, the Solar Energy Research Centre SERC-Chile, CONICYT/FONDAP Project under Grant No. 15110019, FONDECYT Grant No. 1170683 "Robust Distributed Predictive Control Strategies for the Coordination of Hybrid AC and DC Microgrids", FONDECYT Grant No. 1140775 "Design of Robust Predictive Control Strategies for the Operation of Microgrids with High Penetration of Renewable Energy", and FONDEF ID14I10063 "Design and Implementation of an Experimental Prototype of Microgrid for Mapuche Communities".

Finally, I would like to thank COLCIENCIAS and CONICYT-PCHA/Doctorado Nacional para Extranjeros/2014-63140093 for providing the financial support that made this research possible, also to the Vice-Presidency of Academic Affairs of the University of Chile for the short-term research scholarship.

Contents

List of Figures

List of Tables

Chapter 1

Introduction

1.1 Research Motivation

The distributed energy resources (DERs) are comprised of various forms of dispatchable or nondispatchable resources, including distributed generation (DG) units and controllable loads [3, 7, 8]. DGs span from typical fossil-fuelled engines to renewable energy (RE) sources such as wind turbines (WT) and photovoltaic power (PV). RE sources are cleaner and more sustainable than the traditional forms of energy and, therefore, their penetration has increased into the electric power transmission and distribution systems to reduce gas emissions, and enhance sustainable development. In addition, governments and societies are convinced that the use of the RE can help to decrease global warming and climate change, and the introduction of a tariff policy has, in particular, encouraged the adoption of RE systems at domestic level [7].

The integration of large numbers of DERs into the distribution system may play an important role in improving the resilience and sustainability of the electricity distribution system and in generating new market opportunities. However, when high penetrations of DG occur, the management of local and national power flow may be compromised and power quality may move outside allowed national standards [9, 10]. Therefore, the massive adoption of DERs presents new technological challenges that must yet be overcome to ensure that the present levels of grid performance as reliability, resilience and power quality are not significantly affected, and the potential benefits of DG units are fully taken advantage [3].

At a microgrid workshop in 2012 sponsored by the U.S. Department of Energy, the concept of microgrid was defined as: "a group of interconnected loads and distributed energy resources within clearly defined electrical boundaries that acts as a single controllable entity with respect to the grid. A microgrid can connect and disconnect from the grid to enable it to operate in both grid-connected or island-mode" [11]. Based on this definition, microgrids appear as an alternative for overcoming the challenges of integrating clusters of DERs and load into power system, reducing the control burden on the main grid [12, 13, 14].

The concept of multiple microgrids is developed when the penetration level of microgrids into the distribution network is increased. As explained in [15], this corresponds to a situa-

tion in which most of the low voltage networks turn into active microgrids. Fig. 1.1 shows an example of a smart distribution system and its division into multiple microgrids. In this scheme, the coordination among different microgrids and the distributed network operator (DNO) brings new challenges because the coordinated operation of multiple microgrids increases the complexity and dimension of the system to be controlled. Currently, effort is being put into the design of control strategies for overcoming these challenges. Therefore, energy management systems (EMSs) are proposed in order to guarantee a reliable, secure and economical operation of the whole electrical system composed of multiple microgrids. Additionally, when the uncertainties introduced by the variability in end-user profiles and the intermittency of renewable energy sources are included, the design of suitable EMS is necessary.

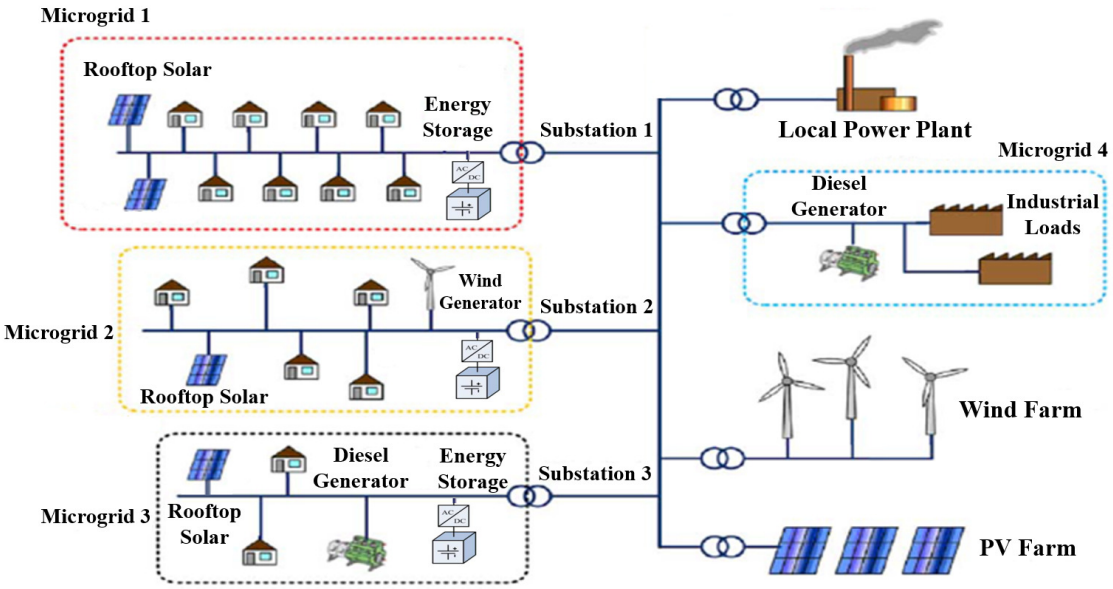

Figure 1.1: Distribution System divided into Several Microgrids. Adapted from [1]

1.2 Problem Statement

This thesis presents a new strategy for employing active management of DERs within a distribution network using an energy management system (EMS) applied to "Energy Communities". The concept of "Energy Communities" enables energy exchange between the DERs of community members to maximise their self-consumption, minimise their energy costs, reduce peak power levels or a combination of these and other beneficial goals. An energy community could be considered to be a microgrid if it is seen from the main distribution grid as a single element responding to appropriate control signals within defined electrical boundaries [7, 16], and this could be applicable to a community that is geographically co-located or to a community that exists as a virtual entity distributed around a much larger system, with their capabilities "aggregated" by inter-communications via web-type services. For the latter case, the option of "island" operation is not possible, but in most other aspects it can be considered to be a microgrid capable of providing energy and fast power response.

The distribution system to be considered is illustrated in Fig. 1.2. It can be considered as an "Energy Community" comprising separate microgrids, but it also could have other loads (the "local loads" in the diagram, which may be factories, commercial parks or other community loads) and larger generation (labelled "bulk generation" in the diagram and this may be fossil fuel based, or PV/Wind "farms").

The proposed EMS has been created as a hierarchical control approach for the microgrids, which is designed specifically to address the stochastic nature of renewable energy generation and load consumption. The EMS is split into two levels: main grid level and microgrid level, as shown in Fig. 1.2. The Robust Model Predictive Control (Energy Profiler) at the higher level allows the operation and coordination of multiple microgrids and must have the ability to communicate with individual local controllers at the microgrid level.

At the microgrid level, a real-time control strategy is adopted to ensure the short-term objectives of the end-user and this controller operates based on the instantaneous and dynamic variation of the power flow of DERs, and load consumption of each of the microgrids. Additionally, this real-time local controller follows a power reference (P^{i}_{mgref}) set by the Robust MPC (Energy Profiler). The power reference should be calculated with an understanding of what can be met by the microgrid energy resources (PV, storage system, load) so that there will always be a high likelihood that the power target (P^{i}_{mgref}) can be followed reasonably well.

The Robust MPC implements an optimization of the predicted performance of the energy community dynamics and the electricity market prices over a prediction horizon while considering the uncertainty associated with predictions of the renewable generation and electrical

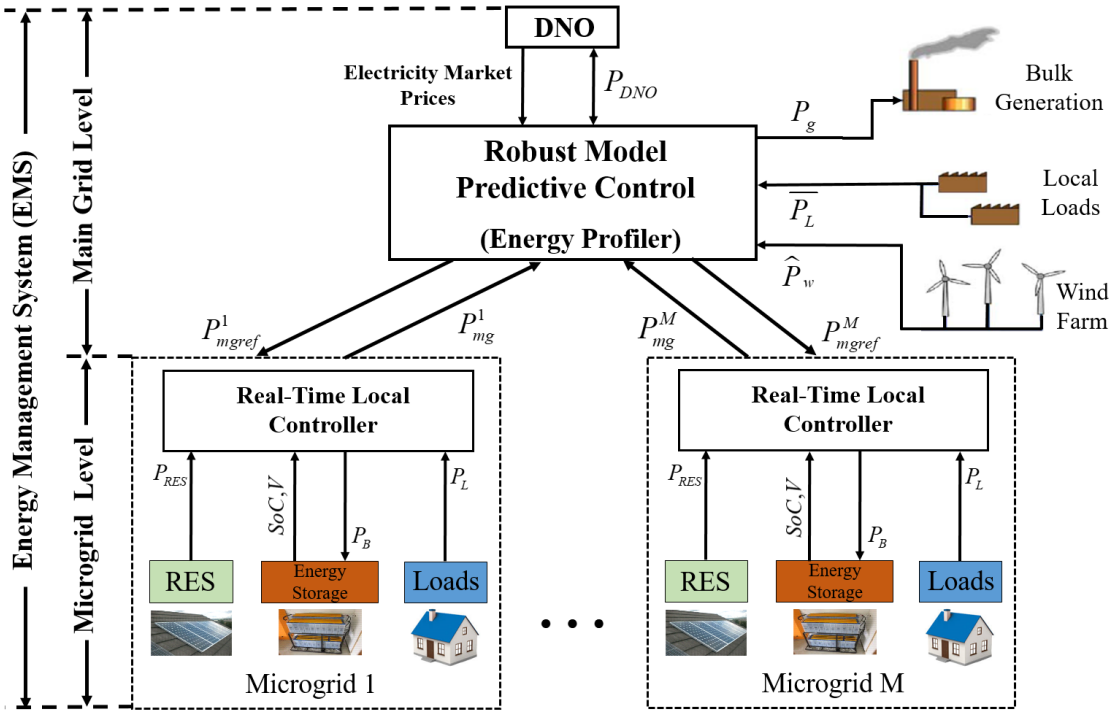

Figure 1.2: Hierarchical Control Structure Proposed

demand. In this thesis, the uncertainty is handled using fuzzy prediction interval models tuned to a desired coverage probability. Finally, the outputs at this level are the power references (P^{i}_{mgref}) to all the microgrids associated with the Robust MPC and are updated each 30 min. This sample time is selected because energy markets tend to operate with a half-hourly update rates.

1.3 Hypotheses

The hypotheses associated with this work are:

1. Energy management system based on a robust control strategy for the coordinated operation of multiple microgrids and distribution network system demands an accurate representation of uncertainty of loading profiles and renewable generation profiles.

2. Energy storage used at distribution level can be of benefit to both the end user (reducing energy costs) and the network operator (limiting peak power levels, enabling increased penetration of DG) for electricity distribution systems.

3. End users trading as energy communities can reduce peak power flows and aid with asset utilization at distribution system level – for example by exploiting complementary power profiles such as schools with daytime consumption, households with peak morning and evening consumption.

4. End users trading as energy communities can optimise the use of DG and the size of energy storage required - by increasing the number of end users within a community, the load profile reduces in variability and becomes much more predictable and this can then enable the development of effective energy storage systems, which can be used at distribution system level.

1.4 Objectives

1.4.1 General Objective

To design novel hierarchical energy management system for the operation and coordination of microgrids, including the uncertainty associated with both renewable distributed generation and load.

1.4.2 Specific Objectives

1. To propose a real-time control strategy that allows integration of the distributed energy resources, ensuring the short-term power balancing objectives of each microgrid.

2. To design new prediction interval models for characterising the uncertainties associated with distributed energy resources and load included in the proposed framework.

3. To design novel robust predictive control strategy based on prediction interval models to ensure the long-term energy management objectives, including constraints imposed by the distribution network system.

4. To validate the proposed framework with the hierarchical control strategy developed by simulation, taking into account various conditions and scenarios to determine the reliable and efficient operation of the clusters of microgrids.

5. To demonstrate that the concept of Energy Communities can be beneficial to both end users and network operators.

1.5 Contributions

This project considers the development of a suitable hierarchical energy management system (EMS) for energy communities, which can work effectively in the presence of the variability in end user profiles and the intermittency of renewable energy sources. Within each microgrid a low level control is executed to control the net power flowing from the main grid to each microgrid according to a reference sent from a central "Energy Profiler" which calculates these microgrid power references. The research and development of this hierarchical EMS forms the main objective of this project, thus, the main contributions of this work are:

- Development of a new modelling methodology for constructing prediction intervals based on fuzzy numbers and its extension to fuzzy and neural network prediction interval models, and the appropriate method for identifying the parameters of these prediction interval models.

- Development of a novel two-stage Energy Management System (EMS) for the operation and coordination of multiple microgrids. The EMS includes a real-time controller at the microgrid level and a Robust Model Predictive Control at the main grid level.

- Formulation of Robust Model Predictive Control (MPC) using prediction interval models to characterise the uncertainty of renewable resources and the load. Robust MPC can be designed using uncertainty sets, such as the prediction interval models, combining the worst-case analysis with a min–max formulation to obtain optimal solutions that are robust against variations in the system parameters with respect to a nominal value (optimal worst-case scenario).

- Incorporation at the real-time controller (lower level of the hierarchical EMS) of stochastic filtering techniques to estimate the state of the charge (SoC) of the energy storage system (ESS) and an estimator of the maximum available power from the ESS. The objective to include these estimators is for guaranteeing safe operation of the ESS without violating the operating limits for the current, voltage, and SoC.

1.6 Publications

1.6.1 Journal Publications

L. G. Marín, N. Cruz, D. Sáez, M. Sumner, and A. Núñez. Prediction interval methodology based on fuzzy numbers and its extension to fuzzy systems and neural networks. *Expert Systems with Applications*, 119:128–141. https://doi.org/10.1016/j.eswa.2018.10.043, Oct. 2018.

L. G. Marín, M. Sumner, D. Muñoz-Carpintero, D. Köbrich, S. Pholboon, and D. Sáez. Hierarchical energy management system for microgrid operation under uncertainty. *Submitted.*

L. G. Marín, M. Sumner, D. Muñoz-Carpintero, D. Köbrich and D. Sáez. Hierarchical energy management system for microgrid coordination. *Preparing for submission.*

J. Llanos, R. Morales, A. Núñez, D. Sáez, M. Lacalle, **L. G. Marín**, R. Hernández, and F. Lanas. Load estimation for microgrid planning based on a self-organizing map methodology. *Applied Soft Computing*, 53:323–335. https://doi.org/10.1016/j.asoc.2016.12.054, Jan. 2017.

T. Roje, **L. G. Marín**, D. Sáez, M. Orchard, and G. Jiménez-Estévez. Consumption modeling based on markov chains and bayesian networks for a demand side management design of isolated microgrids. *International Journal of Energy Research*, 41(3):365–376. https://doi.org/10.1002/er.3607, Aug. 2016.

F. Valencia, J. Collado, D. Sáez, and **L. G. Marín**. Robust energy management system for a microgrid based on a fuzzy prediction interval model. *IEEE Transactions on Smart Grid*, 7(3):1486–1494. https://doi.org/10.1109/TSG.2015.2463079, May 2016.

D. Sáez, F. Ávila, D. Olivares, C. Cañizares and **L. G. Marín**. Fuzzy prediction interval models for forecasting renewable resources and loads in microgrids. *IEEE Transactions on Smart Grid*, 6(2):548–556. https://doi.org/10.1109/TSG.2014.2377178, March 2015.

1.6.2 Conference Publications

N. Cruz, **L. G. Marín**, and D. Sáez. Neural network prediction interval based on joint supervision. *In 2018 International Joint Conference on Neural Networks (IJCNN)*, pages 1–8. https://doi.org/10.1109/IJCNN.2018.8489264, July 2018.

L. G. Marín, F. Valencia, and D. Sáez. Prediction interval based on type-2 fuzzy systems for wind power generation and loads in microgrid control design. *In 2016 IEEE International Conference on Fuzzy Systems (FUZZ-IEEE)*, pages 328–335. https://doi.org/10.1109/FUZZ-IEEE.2016.7737705, July 2016.

R. Morales, D. Sáez, **L. G. Marín**, and A. Nuñez. Microgrid planning based on fuzzy

interval models of renewable resources. *In 2016 IEEE International Conference on Fuzzy Systems (FUZZ-IEEE)*, pages 336–343. https://doi.org/10.1109/FUZZ-IEEE.2016.7737706, July 2016.

F. Veltman, **L. G. Marín**, D. Sáez, L. Guitierrez, and A. Núñez. Prediction interval modeling tuned by an improved teaching learning algorithm applied to load forecasting in microgrids. *In 2015 IEEE Symposium Series on Computational Intelligence*, pages 651–658. https://doi.org/10.1109/SSCI.2015.100, Dec. 2015.

1.7 Thesis Outline

The rest of this thesis is structured as follows:

- **Chapter 2** presents the state-of-the-art of the main topics related to this thesis: hierarchical control of microgrids, architectures and methodologies for EMS scheduling. Additionally, prediction interval models are presented as an alternative to including the uncertainty into the Robust EMS formulation. Finally, studies related to the coordination of microgrids are discussed.

- **Chapter 3** develops a new prediction interval modelling methodology based on fuzzy numbers. Fuzzy and neural network prediction interval models are developed based on this proposed methodology. The developed models are compared with a covariance-based prediction interval method and these models are tested by forecasting up to two days ahead of the load of the residential dwellings in the town of Loughborough, UK.

- **Chapter 4** proposes a two-level hierarchical EMS which realises both short-term power balancing and long-term energy management, benefiting both the energy community members and the distribution network operator. The proposed EMS addresses both the uncertainty of the renewable energy resources and the variability in end-user consumption profiles by means of prediction intervals and has been evaluated using data from a typical urban community made up 30 dwellings with a photovoltaic (PV) power level of up to 50% penetration, and an energy storage system of up to 135kWh.

- **Chapter 5** presents the design of an EMS for microgrid coordination, including the uncertainty associated with renewable DG and load. The performance of the proposed hierarchical EMS is tested with two case studies. The first case study corresponds to an energy community made up of two microgrids with different numbers of dwellings, renewable energy (Photovoltaic and Wind Energy) and ESS based on lead-acid batteries. The second case study corresponds to an energy community made up of three microgrids. For this case, a microgrid with a school demand profile is included with the aim to exploiting complementary power profiles.

- **Chapter 6** gathers the main conclusions made from different stages of this thesis. Additionally, the recommended future work is presented.

Chapter 2

Literature Review

This chapter presents the state-of-the-art of the main topics related to this thesis. First, the effects that the integration of distributed generation (DG) could have on the distribution network, regarding operational issues over the existing network are described. Next, different hierarchical control approaches adopted to successfully integrate DERs into the distribution system are detailed. These architectures of control can improve the power quality and reliability of the electrical network and ensure that the potential benefits of DG are fully harnessed. Then, the most reported architectures and methodologies for energy management system (EMS) scheduling are discussed. Additionally, the common techniques for the formulation of the EMS with the management of uncertainty are described. Later, prediction interval models are presented as an alternative to including the uncertainty of nonconventional energy sources and electrical demand into the Robust EMS formulation. Finally, studies related to the coordination of microgrids are discussed.

2.1 Introduction

Integration of renewable generation (RG) at the transmission level and the high penetration of DERs in the distribution system have to be economically efficient and reliable [17]. To achieve this, a level of intelligence should be incorporated into the electric system through active management technologies and communication systems. These intelligent electric power systems are referred to as smart grids [18, 19, 20]. The concept of the smart grid includes the technological developments on the current electrical grid that make it more flexible. The information technologies are the key to the smart grid due to their allowing the monitoring and control of the reliable operation of the power system in a economical manner [21].

One way to manage the smart grid is to split the distribution system into small clusters or microgrids, considering control strategies for coordinating these multiple microgrids [19, 20]. Some objectives of the microgrids could be maintaining power balance, maximising self-consumption from renewable energy (RE), guaranteeing power quality, minimising grid energy during peak periods, minimising system losses, maximising the lifetime of energy storage, minimising customer cost, and minimising CO_2 emissions.

The microgrids can operate either in grid-connected or islanded modes. In the grid-connected mode, the microgrid is connected to the host power system on the distribution level at a single point of connection, or point of common coupling (PCC). In this scenario, the main grid can supply the power deficit of the microgrid, and the surplus power generated in the microgrid can be traded with the distribution network operator (DNO) and can provide ancillary services. The islanded mode of microgrid operation represents a more critical case, in which the active and reactive power generated within the microgrid must be in balance with the demand of local loads [22, 23].

Therefore, the microgrid concept is an alternative for overcoming the challenges of integrating DER units, including RE sources, into power systems [3, 16]. The main issues to be overcome in order to allow seamless deployment of microgrids, include [3]:

- Scheduling and dispatching of units with a high penetration level of DERs, and considering the variability in the renewable generation and load.
- Designing appropriate Demand Side Management (DSM) schemes.
- Developing new voltage, frequency, and power control techniques to take the increase in power-electronics-interfaced distributed generation into account.
- Designing new electrical market models that allow promoting green-energy technologies.
- Implementing new protection schemes and control system that ensure reliable, secure and economical operation of microgrids in either grid-connected or stand-alone mode.

In the next section, the impact of the integration of distributed generation units (DG) on a distribution system network will be presented.

2.2 Impact of the Integration of Distributed Generation on a Distribution Network

DG is an electric power source connected directly to the distribution network, or to the customer side of the meter [24]. DG is characterised by relatively small generated power, and the possibility of choosing the location in the network area freely. The renewable energy (RE) and energy storage system (ESS) are particular DG units [9, 25]. In [9], the authors report that the main advantage of DG is that it is close to the consumer loads. The disadvantage is that the distribution systems are designed such that the power flows in one direction, and when the DG power is greater than the downstream load, it sends power upstream, reversing the direction of the power flow. Because the interconnection of the DG to the distribution system may have significant effects on the system, some of these effects are analysed below.

In [25] some benefits and issues of DG were explained based on a simulation for the IEEE 14 test system with a 3MW wind turbine. The authors explain that the greater benefit of DG is that the electricity is generated near the place of consumption. The increase in the power supply security related to the use of different energy sources, reduction of power losses in

the network, competitive energy markets, reduced environmental impacts where RE sources are used, and deferred investments for upgrading existing systems are the other benefits of including DG. On the other hand, increases in short circuit level, voltage profile changes along the network, and congestions in system branches could be some of the problems of including DG. In general, the power quality and reliability may be affected, and the network protections may not function properly.

In [26], the author says that the inclusion of DG in the distribution network can result in several benefits for both the utility and the customers. The benefits for a simple case of a radial distribution feeder with concentrated load and distributed generator were quantified. The result shows that DG can reduce the electrical line losses, but this depends on the dimension of DG with respect to the load, location, and operating power factor. In [45], the results showed that with the inclusion of DG in the distribution network, the fault current levels could increase, and the protection system schemes might need to be changed.

Summarizing, DG may play a significant role in improving the reliability of the grid, improving the power quality, and providing voltage and frequency support in order to provide in an efficient and stable operation of the whole electric system. Additionally, the DG can reduce greenhouse gas emission by providing clean and efficient energy (see Fig. 2.1) [9, 10, 27]. However, when DG penetration occurs, the topics mentioned above can sometimes become issues for the distribution system.

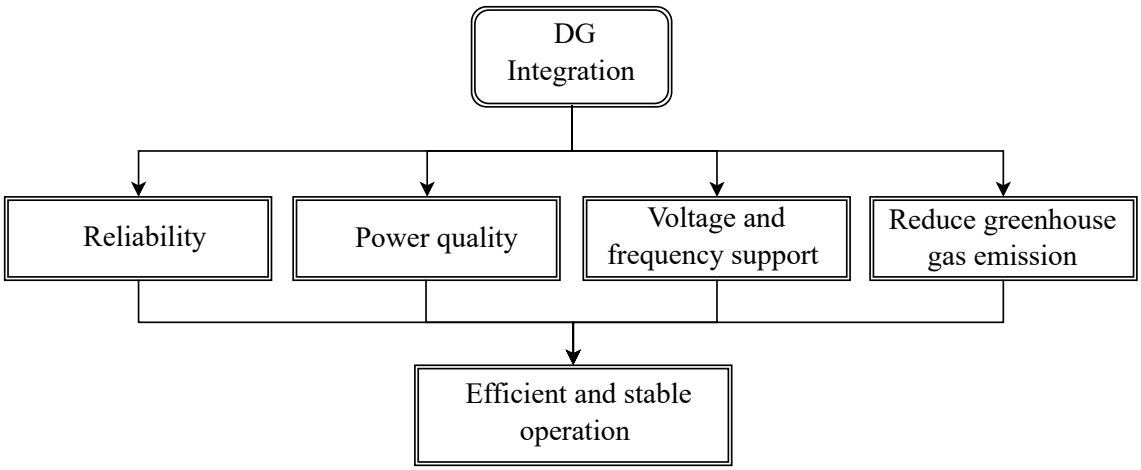

Figure 2.1: Benefits DG Integration into the Distribution System

The authors in [28, 29, 30, 31, 32] reported that active management of DG units and controllable loads into different sections of the distribution network provides an acceptable approach to increasing of the penetration of DG into a passive distribution network, in order to avoid the costs of network reinforcement. Active management of a distribution network requires the integration of control strategies at different levels in a smart grid framework and communication technologies that allow the connection of DG units to the network. Next section presents the approaches to control of microgrid reported in the literature in order to successfully integrate DERs into the distribution system and that their potential benefits are fully harnessed.

2.3 Control of Microgrids

The design of control and protection systems are needed in order to successfully integrate DERs into the distribution system, ensuring that the reliability of the system is not significantly affected and that the potential benefits of integrating DG are entirely exploited [3]. Hierarchical control structure is the most common architecture used in the power system's control because this approach achieves a compromise between the centralized and decentralized control schemes [3, 7]. In the hierarchical architecture, the defined control levels differ in their speed of response, in the time frame in which they operate, and in the infrastructure requirements, for instance, the communication requirements. Next, an overview of different hierarchical control structures is presented from the perspective of microgrids.

Three control levels are typically used in the hierarchical architecture for microgrids operation [14, 33, 34, 35, 36, 37, 38]. The first level is named primary control, and its function is load sharing between converters, based on decentralized control. The performance and stability of the system can be improved, adjusting both the frequency and output voltage, because the active and reactive power are shared among DG units at this control level. The second level (secondary control), is responsible for removing any steady-state error introduced by the primary control level. When a load change is realized, the frequency and voltage values must be restored to their nominal values by this control level. Finally, the decision of importing or exporting energy for the microgrid is the responsibility of the third level (tertiary control), named energy management system (EMS). The energy flows are optimised by adjusting the set points of the microgrid inverters. This level is responsible for the economical and optimal operation of the microgrid. In different studies, several control strategies (belonging to the different control levels) have been designed for the operation of only one single microgrid, adopting this hierarchical control structure (three layers).

In [2] a hierarchical control architecture is proposed for a smart grid that is comprised of multiple microgrids. Three control levels are considered: a distribution network operator (DNO) and market operator (MO), a microgrid central controller (MCC), and local controllers (LCs) associated with each DER unit and load, as is shown in Fig. 2.2.

In this approach, the DNO and MO operate in an area in which more than one microgrid exists. These two entities can be considered as part of the main grid, but not the microgrid itself. The MCC functionalities include maximising the use of locally generated power, and coordinating the LCs. The MCC is the main interface between the DNO/MO and the microgrid. At the MCC level, the microgrid operation is optimised according to the open market prices, the bids received by the DG units, and the forecasted loads. In general, the MCC level is responsible for the reliable, secure, and economical operation of microgrids in either grid-connected or stand alone mode. The LC is placed at the lowest level of the proposed hierarchical structure, and controls the DGs and controllable loads. In a centralised aprroach, each LC receives set points from a corresponding MCC, and in a decentralised approach, each LC can communicate with the MCC and other LCs in order to share knowledge, request/offer a service, and/or exchange any other information relevant to the operation of the microgrid, but the decisions of each LC are made locally.

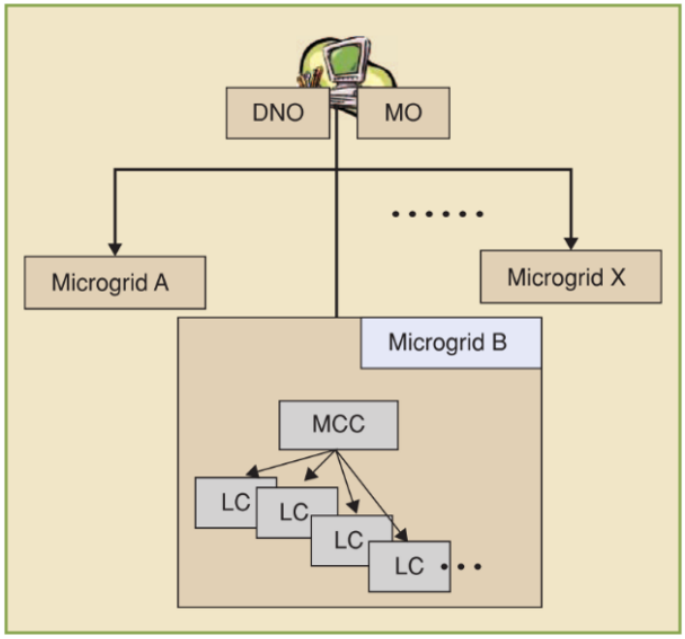

Figure 2.2: A Microgrid Supervisory Control Architecture. Figure taken from [2]

A similar approach to the previous one is presented in [3] and [23] for microgrid operation. The hierarchical control structure adopted is presented in Fig. 2.3. The primary and secondary control levels are associated with the operation of the microgrid itself, and the tertiary level refers to the coordinated operation of the microgrids and the operator network. In [2], short-term power balancing and long-term energy management objectives of the microgrid operation are distinguished, but the optimisation or control algorithms that could provide power balancing and energy management are not mentioned. In [3] the state-of-the-art of primary control and EMS levels is presented. Nevertheless, the control level related to microgrid coordination is not discussed in detail. The authors explain that this level could provide the set points to the EMS of each microgrid, based on the requirements of the main grid, and that it operates in the order of several minutes.

In [4], another hierarchical control structure with three levels is proposed. In this case, the hierarchical optimisation method optimises the operation of the system by scheduling the operation of several resources with sufficient storage capability for maximising the benefit to the utility and its customers. Fig. 2.4 shows the proposed approach, and the multiple objectives at each level: distribution feeder optimisation, substation optimisation, and system optimisation. At the feeder optimisation, the problem is formulated as a quadratic optimisation problem. At the substation and the system optimisation levels, a stochastic dynamic programming problem is formulated for capturing the uncertainty associated with the integration of renewable energy.

The substation optimisation generates the target value that each feeder should achieve to ensure optimal operating of the substation over the planning period (24 hours) and every 15 minutes the targets are updated. The feeder optimisation schedules the controllable resources in order to attain these imposed targets. In that study, each feeder can be seen as a microgrid.

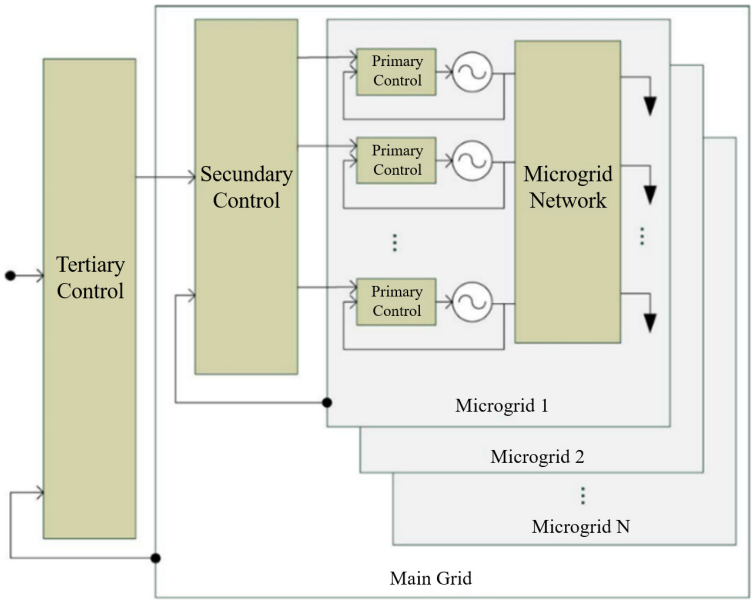

Figure 2.3: Hierarchical Control Levels for Microgrids Operation. Figure taken from [3]

The aggregated model of all feeders fed from the same substation, and the targets received from the system optimisation level are used at the substation optimisation to generate the individual targets for every feeder (microgrid) at the lower level. The system optimisation level generates the targets that each substation should achieve to guarantee optimal operation. At this level, the aggregate substation models and short-term forecasted data are used as input to the optimisation process. The approach proposed in that study can be applied to a distribution system independently of the size of the system because of the flexibility for the scalability at each level. The interconnected operation of the different levels is driven through the generated targets as reference for feeder and substation optimisation levels. In that study is not clear how the uncertainty of renewable energy and load are characterised. Additionally, at each level, only optimisation methods are proposed to solve the different problems.

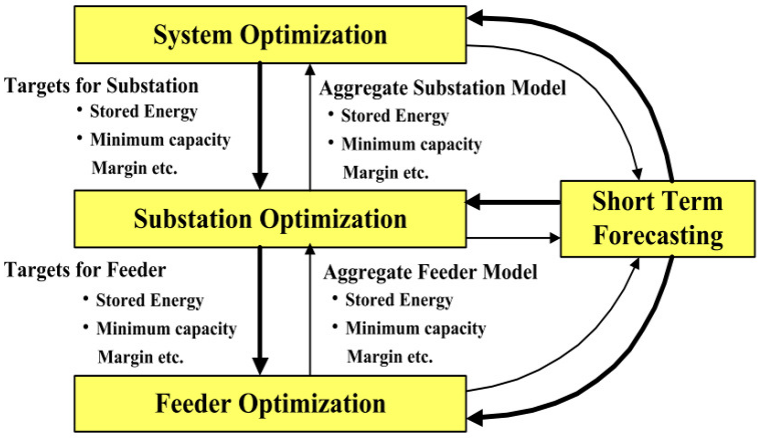

Figure 2.4: Hierarchical Optimisation Approach Proposed in [4]

The authors in [39, 40] and [5] have adopted a hierarchical control framework for a smart grid, similar to the approach explained previously (see Fig. 2.5). The lowest level corresponds to the microgrids and is named community's central control platform. The control aim at this level is to ensure the realization of short-term power balancing through real time power control, following targets set (PF_T) by the cluster's central control platform, which is the next level in this approach. The optimisation objective at the cluster's central control platform is to minimise distribution losses and avoid overloading the local network assets, considering the constraints imposed by the distribution network operator. The optimisation objective at the highest level is to maximise the use of renewable energy, and maintain stability of the distribution network. The output at the distribution network level is the power flow set point (PF_{TC}) for each microgrid cluster associated with this distribution network operator (see Fig. 2.5).

In these studies, the authors have suggested heuristic optimisation techniques at the distribution network operator and the cluster central control platform levels at different rates of execution, since the accuracy of the load forecast could be different at each level. Unlike [4] in which a quadratic optimisation problem at the lower level is suggested, in [39] and [41] the authors proposed an algorithm with fast decision-making capabilities based on the instantaneous and dynamic values of power. This algorithm is implemented because the demand prediction at the lower level could be unreliable due to low aggregation, and because the power flow is highly stochastic and variable.

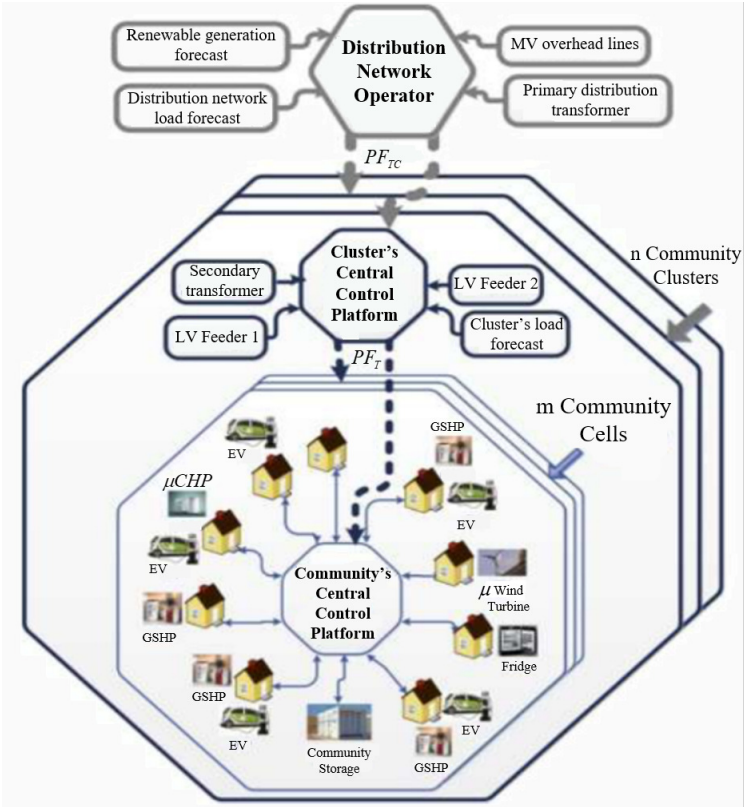

Figure 2.5: A Hierarchical Multilevel Control Framework for a Smart Grid. Figure taken from [5]

The Community Power Flow Control (CPFC) deterministic algorithm proposed in [39] and [41] runs in real time and manages the resources in the microgrid, determining the correct number of microgrid devices to dispatch in a coordinated manner. The active power flow has been chosen as the primary control parameter, and the voltage and current measurement at the point of common coupling are used to calculate the microgrid power flow. The algorithm is developed at the lower level, and the following targets are set by the cluster's central control platform.

Derived from the literature review of hierarchical control approaches to the operation of smart grids, and in particular, for microgrids, the following observations can be highlighted:

The control at the lowest level in the hierarchical structure corresponds to the control of the power electronic converter of the DG units that make up a microgrid. These control strategies should ensure that voltage and frequency values are within the allowable limits, and follow the reference values sent by adjacent levels, to guarantee the power quality and stability of the microgrid. The control at the lowest level must be operated at the fastest response. The models of the DG units that are adopted in this thesis assume that the control strategies of the power electronic converter are working appropriately.

The next level in hierarchical structure is often called the Energy Management System (EMS). The aims of the EMS consist of finding the optimal operation of the microgrid, according to both short-term power and long-term energy objectives. The EMS tasks may be constructed on one or more levels, as evidenced in the literature review concerning hierarchical control structures. Finally, the highest level in all the approaches presented corresponds to market and business models that can be made by the distribution network operator and market operator. The objectives at this level could be to maximise the use of renewable generation, and maintain stability of the distribution network.

In this thesis, a two level EMS (main grid and microgrid level) is developed to achieve the objectives of operation and coordination of microgrids, which considers the uncertainty of the renewable energy resources and the variability in end-user load profiles. The design of the first level (microgrid level) is in accordance with short-term power balancing objectives. The second level (main grid level) ensure the long-term energy management objectives. In the next section, a review of the literature on the different approaches for the EMS scheduling is presented.

2.4 Energy Management System

The microgrid scheduling problem can be reviewed from the point of view of the architecture and scheduling methodology of the EMS [7]. The selection of architecture and scheduling methodology of the EMS depend on technical, economical, and environmental aims to be achieved in the microgrid operation. Fig. 2.6 shows the most frequently reported approaches to microgrid scheduling, which are described below.

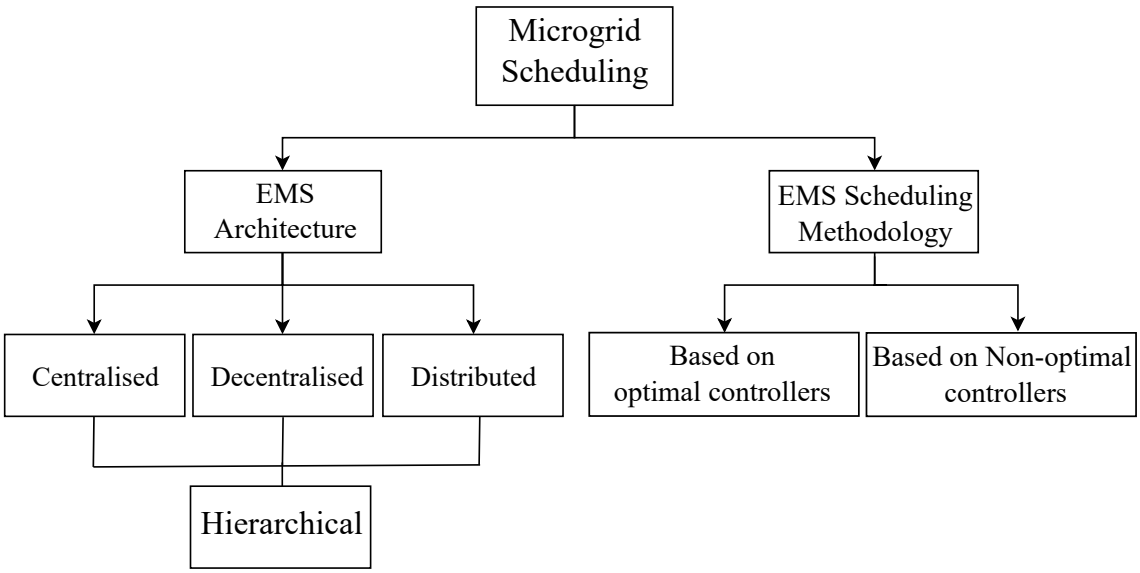

Figure 2.6: Architecture and Methodology for EMS Scheduling

With respect to the architecture of the EMS: centralised, decentralised, and distributed are the main approaches reported in the literature [3, 7, 42, 43]. The centralised architecture is based on a central controller that determines the dispatch of the resources according to established objectives, considering relevant information about the microgrid, as well as information from forecasting systems. The fully centralised approach is difficult to implement when a large number of DER units are included in the microgrid, because increase the complexity of the problem and require a higher capacity of the communication network.

The decentralised architecture aims to achieve economical operation of a microgrid while providing the highest possible autonomy to the different DERs by local controllers. This approach can simplify the complexity of the problem by reducing it into subproblems and solving them locally. Nevertheless, the fully decentralised approach is not always possible due to the strong couplings among the operation of several units of the system, requiring a minimum level of coordination that cannot be achieved by using only local controllers.

In the distributed architecture, each component of the microgrid is considered as an agent with the ability of making decisions, and the optimal schedule is obtained using iterative data transfer among the agents. The multi-agent systems are the approaches used most, to implement distributed control. For more details about these architectures proposed for EMSs, see [3, 7] and [42], which several works that use these approaches are reported.

Each architecture proposed offers its own benefits and drawbacks and therefore hierarchical schemes have been proposed to exploit the benefits of different approaches [2, 34, 44]. In a hierarchical structure, different levels can be defined to incorporate control strategies that ensure the realisation of short-term power balancing objectives and long-term energy management, benefiting the microgrid owner/members and the distribution network operator [40].

The scheduling methodology of the EMS tends to be divided into two groups: one based on non-optimal controllers and the other based on optimal controllers [45]. Most approaches reported in the specialized literature with regard to the scheduling methodology of EMSs

are based on optimal controllers, in which the behaviour of the load and energy resources available must be predicted.

Optimal EMS based on a receding horizon control (RHC) strategy (also known as model predictive control (MPC)) has been proposed. The principle behind of this approach is to anticipate the expected behaviour of both the renewable resources and the load demand over a prediction horizon, and, when this predicted behaviour is available, the commitment and dispatch of the DER units is performed in accordance with the selected performance criteria [46, 47]. For instance, an EMS based on a rolling horizon strategy for an isolated microgrid composed of photovoltaic panels, two wind turbines, a diesel generator, and an energy storage system is proposed in [48]. The EMS considers a two-day-ahead forecast of renewable sources and demand. Finally, the optimisation problem is solved using mixed integer linear programming, ensuring near-optimality. In [49] a novel double-layer coordinated control approach for a microgrid EMS is proposed for both the grid-connected and stand-alone modes. Two layers are proposed: the scheduling layer, and the dispatch layer. The scheduling layer has an economical operation scheme based on forecasting data, while the dispatch layer provides the power of controllable units based on real-time data. The results show that the revenues are maximised according to DG bids and market price in the grid-connected mode, with total load supplied, and total renewable sources used.

Other examples of EMSs based on MPC approaches are reported in [23, 50, 51, 52, 53]. In general, the goal of the EMS is to manage the DERs economically to meet certain power quality standards. With the MPC approach, an optimisation problem is solved at each time step to determine a plan of action over a future time horizon. However, only the command for the next time-step is implemented.

The effectiveness of these control approaches depends mainly on the accuracy of the prediction models, which in turn depends on the sampling time and aggregation level, as is reported in [54]. Additionally, longer calculation times compared with non-optimal controls are required, particularly when using nonlinear predictors. Therefore, when prediction models are not suitable for capturing the behaviour of the system or cannot be implemented in real-time, an alternative approach is to use a control with real-time decision-making capabilities based on the instantaneous power flow and the availability of the DERs and loads, rather than prediction profiles. This "Community Power Flow" approach has been shown to effectively schedule DERs in [41].

Additionally, mixed integer linear programming (MILP), continuous relaxation (CR), and the fuzzy logic controller (FLC) were the control strategies used for optimal energy flow with a home energy management system (HEMS) in [55]. The results showed that the three approaches can optimise the energy consumption. The MILP gave the lowest optimisation cost but required the highest computational time. The CR reduced the computational complexity but increased the cost compared with the MILP. The authors suggest that FLC is the best approach for a real-life application, since it reduces the computational time, has good performance in cost optimisation, and needs no forecast data.

The authors in [40, 41, 56, 57] and [58] presented several "rule-based" control approaches for microgrid management, with [59, 60, 61] and [62] describing fuzzy rule approaches. In [60], the electricity price is considered as an input parameter of the fuzzy controller. The

authors in [59] suggests including the uncertainties of renewable energy in the design of the fuzzy controller, by using, for instance, a type-2 fuzzy systems. In general, the proposed objectives were to maximize the use of renewable energy in satisfying the local demand, and optimising the use of the battery to benefit the consumer by reducing the energy cost, while the maintaining the reliability of the whole electrical system.

The approaches discussed above are some examples of EMSs based on non-optimal controllers with real-time decision-making, and the studies reported demonstrate their effectiveness for microgrid management. These methods do not require a detailed model of the system, and can have a fast response to changes in the system. However, they require design and commissioning, and the creation of generalised procedures to support the application of these types of EMS are not yet in place. For example, parameters such as the minimum required RES penetration level and the correct sizing of energy storage elements are necessary so that the rule based algorithm can meet the demand in an optimal way.

In this thesis, a two level EMS is developed for microgrid management, which considers the uncertainty of the renewable energy resources and the variability in end-user load profiles. The aim is to incorporate the benefits of schemes based on both receding horizon control and real-time decision-making. Therefore, the proposed EMS comprises a real-time control strategy which uses a rule-based approach at the lower level, and a Robust MPC at the higher level for operation and coordination of microgrids. In the next section, common techniques for the formulation of the EMS with the management of uncertainty, particularly those based on MPC are presented.

2.4.1 EMS with management of uncertainty

Common techniques for the formulation of the EMS with the management of uncertainty, particularly those based on MPC, are Stochastic Optimisation (SO) and Robust Optimisation (RO).

In the SO approach, an appropriate number of scenarios with their probabilities is required to achieve a good representation of the uncertainty [63]. In [64, 65, 66, 67, 68] several studies on stochastic-based management of microgrids with high penetration of renewable resources were presented. The results of these approaches showed superior performance in terms of energy cost compared to that of a deterministic EMS. Although SO EMS formulations appear to be feasible solutions for addressing the uncertainty, the selection of the probability density functions (PDFs) for modelling the uncertainty is difficult, and the computational burden might increase.

RO has become popular since it can be applied using uncertainty sets rather than probabilistic models, reducing the difficulties related to the identification of PDFs for renewable resources and loads. The RO approach combines the worst-case analysis with a min–max formulation to obtain optimal solutions that are robust against variations in the parameter with respect to a nominal value (optimal worst-case scenario) [63]. The RO methods were proposed in [63, 69, 70, 71, 72] for optimal scheduling of microgrids. Aspects associated with economic and environmental performance, together with reliability were considered in the

presence of high penetration levels of RES resources and distributed storage systems.

In this thesis, the proposed Robust EMS is based on MPC, thus it requires models to predict the expected value and the variability of the demand and the energy available from the renewable resources, over a prediction horizon. Clearly, the performance of the Robust MPC depends on the quality of these models. Therefore, prediction intervals appear as an alternative solution for providing not only the expected future resources, but also a measure of their variability, and could be used as a solution for generating scenarios for Robust EMS formulation. The Prediction interval quantifies the uncertainty associated with the difference between the measured data and the predicted value, and it takes both the uncertainty in model structure, and the noise in data into account. The region defined by the upper and lower bounds of the prediction intervals is interpreted as the region to which the modelled phenomenon belongs with certain coverage probability, and therefore, a reduced number of scenarios can be obtained. In this work, the Robust MPC formulation uses prediction interval models to characterise the uncertainty of renewable resources and the load. Next, prediction interval modelling is presented and its use in Robust MPC formulation.

2.5 Prediction Interval Modelling

In recent decades, several methodologies have been proposed to solve nonlinear model identification problems that use a finite number of measured data and consider an optimality criterion [73]. Many studies have examined methods for improving the accuracy of these approaches to obtain higher precision in expected value prediction [74, 75]. Although these methodologies exhibit adequate performance in estimation and prediction, uncertainty is not typically quantified by these modelling approaches, and only expected value is obtained. However, information on the dispersion of the output of the model provides more information about the phenomena modelled with uncertainty and more useful information from a decision-making point of view than the models with only expected value [76, 77].

Confidence intervals and prediction intervals have been proposed to model the uncertainties of a system. Confidence intervals are used to capture uncertainties in the unknown parameters of a model. Confidence intervals are usually associated with parameters rather than with observations. Prediction intervals are used to capture uncertainties in random variables yet to be observed and provide a probability that the random variable will be within a given interval [78, 79, 80, 81]. Prediction intervals consider more sources of uncertainty than do confidence intervals; these additional sources of uncertainty include model error and noise variance. The predicted outputs (black lines in Fig. 2.7) are intervals that represent (with a given coverage probability) the most likely region defined by the upper and lower bounds of the interval to which the output (targets) of the uncertain phenomena will belong, as shown in Fig. 2.7. Point prediction (Fig. 2.7) gives a value close to mean or median and is unable to predict that level of randomness or uncertainty [76]. In [82] and [76] a literature review on methods for construction of prediction intervals is explored and summarised.

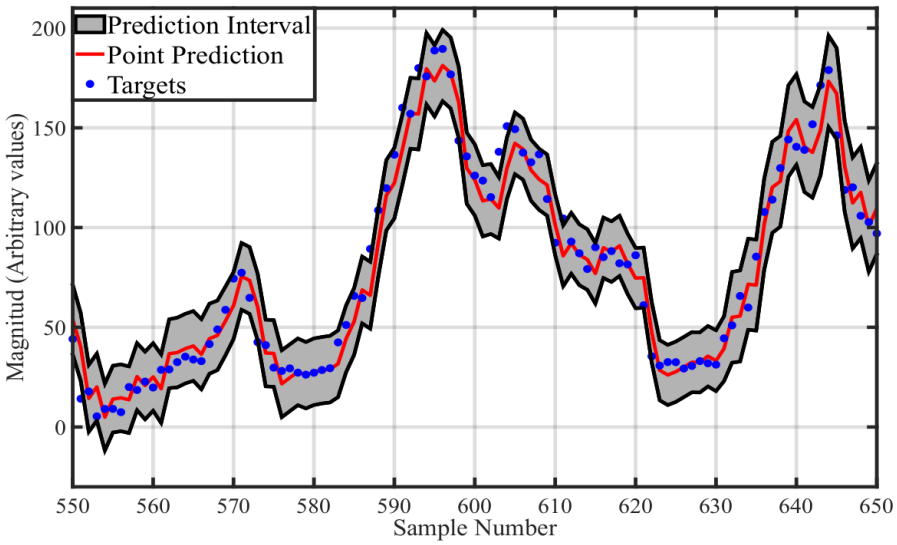

Figure 2.7: Rough sketch for representing a Prediction Interval

In this thesis, prediction interval models are used to represent both nonlinear behaviour and uncertainty derived from nonconventional energy sources and electrical demand. The uncertainties associated with wind and photovoltaic power are due to the stochastic intermittency of the primary input (wind speed and solar radiation), and the uncertainty of the demand profiles in energy communities (microgrids) is due to minor load variations, which can generate large changes in the total profile [7]. Moreover, for control of microgrids, the uncertainty associated with intermittent power sources and load is typically handled using a Robust MPC in the formulation of the EMS [83].

For instance, in the work of [84], a wind-based energy source was modelled by a fuzzy prediction interval based on the method reported in the work of [85], and a Robust EMS was achieved using the convex sum of the lower (worst case) and upper (best case) bounds of the available wind energy. In a similar way, in the works of [86] and [87], prediction interval models of the solar power, wind power, and electrical demand of a microgrid were generated to formulate a scenario-based Robust EMS. In [86], the combination of all the lower and upper bounds of the prediction intervals allowed the various scenarios for Robust EMS to be defined, and the solution was obtained using a second-order cone optimization problem. In [87], scenarios were generated via Taguchi's orthogonal array testing method using the prediction intervals of the uncertain variables modelled, and the optimization problem was solved using a search strategy based on an orthogonal array. The results of the previous studies showed that a more secure and reliable operation is achieved with Robust EMS than with EMS without uncertainty. However, the performance of a Robust EMS depends on the quality of the prediction interval models over the future time horizon; therefore, improved prediction interval model designs are required [7, 83, 88].

In this thesis, a two level EMS is developed for microgrids management and the uncertainty is explicitly incorporated in the formulation of the Robust MPC controller by means of prediction intervals. Finally, an important topic in this thesis is the coordination of multiple microgrids since the majority of the studies reported consider only a single microgrid. A review of the importance and benefits of coordinated control in microgrids will be presented in the next section.

2.6 Coordination of Microgrids

Most studies related to microgrid scheduling have considered a single microgrid. When the distribution system is composed of multiple microgrids, the coordination between microgrids and distribution network operators can improve the operation and reliability of the whole system. As explained in [15]: "The concept of multiple microgrids is related to a structure formed at the medium voltage (MV) level, consisting of low voltage (LV) microgrids and DER units connected on adjacent MV feeders. The main issue when dealing with control strategies for multiple microgrid systems is the use of individual controllers, which should have a certain degree of autonomy, and be able to communicate with each other in order to implement specific control actions".

A hierarchical control approach is justified by the increase in both the dimension and the complexity of the system so that the management of a multiple microgrid system requires the use of a more flexible control and management architecture. Recent studies show that connecting multiple microgrids in a coordinated manner to a smart distribution system can improve the operation and reliability of the electric system, particularly at the medium voltage level [89].

For instance, in [6] a typical urban network with several microgrids and a total installed capacity limited to 20% of the microgrid peak load was considered. Each microgrid had 25% renewable energy, mainly PV, and 75% controllable units, such as micro-turbine. In Fig. 2.8 the area below the curve indicates the amount of energy needed to be bought from the utility. The results show higher energy production by microgrids, and therefore, lower amounts of energy that need to be bought. As can be seen in Fig. 2.9, a congestion level reduction at the peak hour in the ten most congested lines, especially for periods of high electricity prices, is achieved. The results show a 7.9% congestion level reduction in the most congested line compared to a case without microgrids installed, with typical electricity prices, and a reduction of 15.7% in the most congested line during a period of high electricity market prices. Fig. 2.10 shows an active loss reduction, reaching a value of 23.7% at the peak hour, for a period of high electricity prices compared to the case without microgrids.

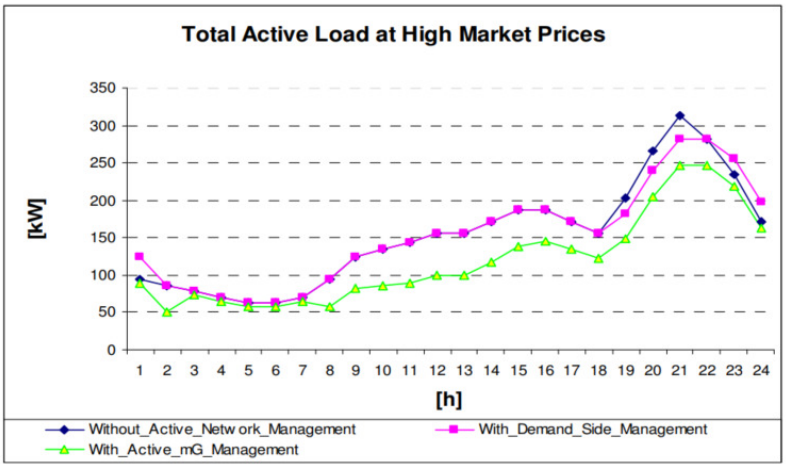

Figure 2.8: Total Active Load in a Period of High Electricity Market Price. Figure taken from [6]

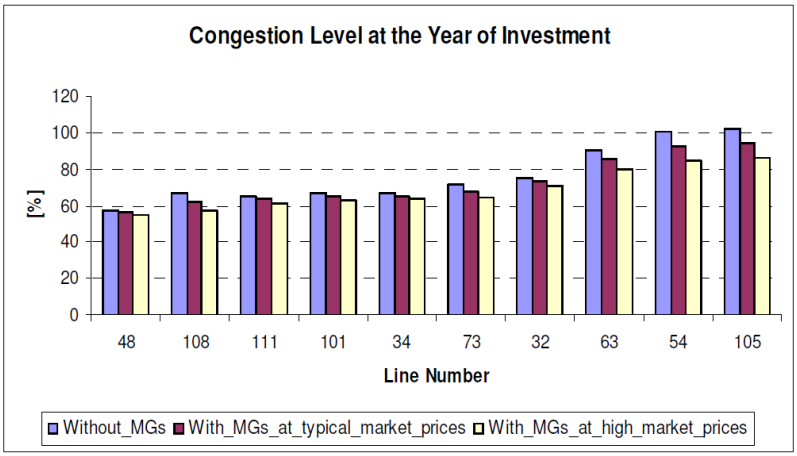

Figure 2.9: Congestion Level at the Ten most Congested Lines at the Year of Investment. Figure taken from [6]

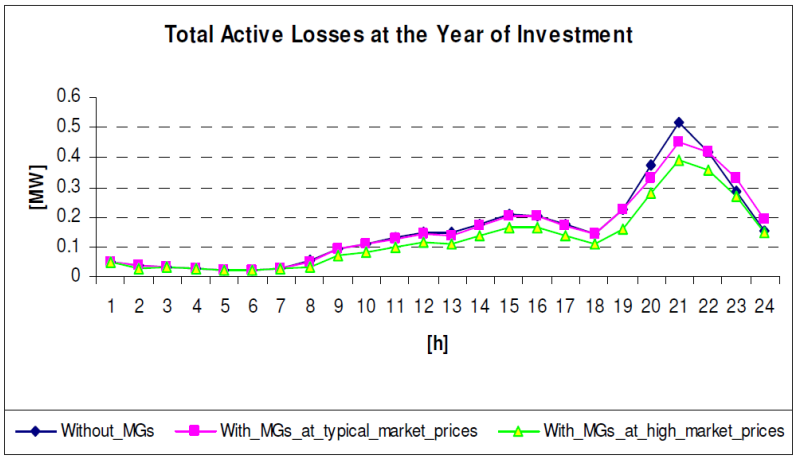

Figure 2.10: Total Active Losses in an MV Urban Network for a day of Typical and High Electricity Market Prices. Figure taken from [6]

There are several studies related to the coordination of different microgrids, and between a distribution network operator and microgrids, in which the benefits of dividing the smart grid into multiple microgrids are demonstrated. For instance, the authors in [90], present a MPC for optimal power exchanges in a smart network of microgrids. The global benefits are maximised with an innovative control strategy for a cluster of interconnected microgrids. A MPC-based algorithm is used to determine the future scheduling of power exchanges among microgrids, as well as the charging/discharging in each local energy storage system for the future time horizon, based on information on power prices, power generation, and load forecasts. The results demonstrated that the cooperation among microgrids has advantages and benefits for each microgrid operation in terms of facing the deficiency or excess of power production caused by uncontrollable renewable energy behaviour. Another conclusion is that the uncertainties in predictions may have effects on the optimal control scheduling.

Other works related to coordination of multiple microgrids are presented in [1, 91, 92, 93, 94, 95]. In general, the results show that the coordination among different microgrids decreases the distribution system total operating cost while maintaining the rated frequency and voltage for each participating microgrid, the power quality and the reliability of the electrical network and economically optimising the exchanged power.

In the studies presented above, the coordination between multiple microgrids, as well as the stochastic nature of renewable energy and load, have not been considered simultaneously. Few studies have included uncertainty in the control strategies for multiple microgrids operation. For instance, in [96] an optimisation problem for economical operation of multiple microgrids based on the power transaction between the microgrids and the main grid is presented. The optimal power dispatch problem considers the uncertainties in load and probabilistic modelling of generated power by renewable energy resources. In order to deal with these uncertainties, the PDF associated with power generation and load is considered as input to a probabilistic load flow problem. The problem is solved with a particle swarm optimisation (PSO) algorithm. Results show that it is possible to regulate the power demand and transaction between each microgrid and its neighbours, and between each microgrid and the main grid. Additionally, it is indicated that the power sharing between microgrids with main grid can reduce the total operation cost of the distribution network. The difficulties in this study are related to the identification of PDFs of renewable units and load; and to the lack of a guarantee that the optimal solution is achievable by the heuristic method used to solve the problem.

In [97] a control strategy for the coordinated operation of networked microgrids in a distribution system is proposed. The distribution network operator and each microgrid are considered as different entities with individual objectives to minimise the operation cost. The cost of a microgrid includes the operation costs of DGs, and the cost of buying electricity from a utility. The incomes of a microgrid result from selling electricity to a utility. The costs of the distribution network operator correspond to operation costs of DGs connected to the medium voltage (MV) network, and the cost of buying electricity from microgrids and the connected high voltage (HV) system. The revenues include selling electricity to the HV system, and to consumers connected to the MV system and microgrids. A stochastic bi-level problem was formulated for taking the uncertainties of DG into account, with the distribution network operator at the upper level and microgrids at the lower level. The scenarios for characterising

the uncertainties of renewable resources are generated from a Monte Carlo Simulation, and the reduction scenario method is applied for increasing the calculation speed in the solution. In this work, the uncertainty associated with the load is not considered, and the uncertainty of renewable units is modelled by the beta function for representing the prediction error, where the parameters for characterising this beta function are not easily obtained. Finally, in the approaches already reported, only optimisation methods for EMS scheduling are used.

2.7 Discussion

A group of interconnected loads and distributed energy resources (DERs) that acts as a single controllable entity with respect to the main grid is called a microgrid. The energy management system (EMS) is responsible for reliable and economical microgrid operation, managing the power and the energy between sources and loads.

When the distribution system is made up of several microgrids, and distributed generation units and load are connected to adjacent medium voltage feeders, the design of new control strategies and protection schemes is necessary for optimal operation. In this scenario, the EMS is responsible for coordinating the operation between the distribution network operator and the microgrids, or among different microgrids. The proposed objectives in the operation system must comply with technical, economical, and environmental requirements to guarantee the power quality and the reliability of the electrical network. Moreover, the operational constraints, such as energy balance, load management, and DER limitations, should be considered in multiple microgrids scheduling.

In this thesis, a hierarchical EMS is adopted, since allows incorporating a mechanism to ensure both the realisation of short-term power balancing objectives, and long-term energy management, benefiting both the microgrid owner and the distribution network operator.

Regarding the scheduling methodology of the EMS, two approaches are included: non-optimal controllers and optimal controllers. Adopting an approach depends on the level at which it is used in the hierarchical architecture, and the characteristics of the system to be considered. Therefore, in this thesis, a two levels EMS is considered: the microgrid (energy community) level and the main grid level. At the microgrid level, a real-time local controller is proposed and at the higher level, Robust MPC controller is proposed to manage the uncertainty by means of prediction interval models.

Chapter 3

Prediction Interval Methodology Based on Fuzzy Numbers

Prediction interval modelling has been proposed in the literature to characterize uncertain phenomena and provide useful information from a decision-making point of view. In most of the reported studies, assumptions about the data distribution are made and/or the models are trained at one step ahead, which can decrease the quality of the interval in terms of the information about the uncertainty modelled for a higher prediction horizon. In this chapter, a new prediction interval modelling methodology based on fuzzy numbers is proposed to solve the abovementioned drawbacks. Novel fuzzy and neural network prediction interval models are developed based on this proposed methodology by minimizing a criterion that includes the coverage probability and normalized average width. The fuzzy number concept is considered because the affine combination of fuzzy numbers generates, by definition, prediction intervals that can handle uncertainty without requiring assumptions about the data distribution. The developed models are compared with a covariance-based prediction interval method, and high-quality intervals are obtained, as determined by the narrower interval width of the proposed method. Additionally, the proposed prediction intervals are tested by forecasting up to two days ahead of the load of the residential dwellings in the town of Loughborough, UK. The results show that the proposed models are suitable alternatives to electrical consumption forecasting because they obtain the minimum interval widths that characterize the uncertainty of this type of stochastic process. Furthermore, the information provided by the obtained prediction interval could be used to develop robust energy management systems that, for example, consider the worst-case scenario.

3.1 Introduction

In this chapter, prediction interval modelling based on fuzzy numbers provides a systematic framework for representing uncertainty and nonlinear dynamics, which makes it useful for forecasting the uncertainty associated with stochastic variables, such as renewable energy-based generation variables. Next, the general interval modelling problem is detailed.

The result of mapping an input vector $Z(k)$ onto a nonlinear real continuous g function can be written as follows:

$$y(k) = g(Z(k), w) + \varepsilon(k) \qquad k = 1, \ldots, N \tag{3.1}$$

where $Z(k) = \{z_1(k), z_2(k), \ldots, z_p(k)\}$ represents the input vector of all measurements at time k, $y(k)$ is the output obtained from the set of measured data at time k, w is the true parameter set, and random variable $\varepsilon(k)$ is noise. The aim of the model is to find a real function $g \in \mathcal{G}$ that belongs to the model class $\mathcal{G}$, such that g is the best representation of the system [77]. The condition for selecting the model is $\|y(k) - \hat{y}(k)\| \leq \varepsilon_0 \; k = 1, \ldots, N$, where $\hat{y}(k) = g(Z(k), \hat{w})$ is the model output at time k, $\hat{w}$ are the estimated parameters and ε_0 is the desired error model. The error may be due to unknown or unobserved variables that affect the model output $\hat{y}(k)$ [81, 79]. When the nonlinear real function g is an uncertain function, it can be assumed that it is a member of the following family of functions [73, 85]:

$$\mathcal{G} = \{g : S \to \mathbb{R}^1 \,|g\,(Z(k)) = g_{nom}\,(Z(k)) + \Delta_g\,(Z(k))\} \tag{3.2}$$

where g_{nom} represents the nominal function and Δ_g models the uncertainty and satisfies $\sup_{Z \in S} |\Delta_g(Z)| \leq c, c \in \mathbb{R}$. According to (3.2), the function $g \in \mathcal{G}$ can be used to predict a new observation, and its uncertainty based on observed data. This type of function ($g \in \mathcal{G}$) is called a prediction interval model. The goal of prediction interval modelling is to find the lower function $\hat{y}_L$ and the upper function $\hat{y}_U$ that satisfy:

$$\hat{y}_L(k) \leq g(Z(k), w) \leq \hat{y}_U(k) \qquad \forall Z(k) \in S \tag{3.3}$$

In this respect, a function g from the class $\mathcal{G}$ can be found in the band defined by the upper and lower functions. The prediction intervals are developed with a certain coverage probability $(1 - \alpha)\%$ that future observations of the uncertain phenomena belong to the interval defined by the lower $\hat{y}_L$ and upper $\hat{y}_U$ [98]:

$$P\left\{\hat{y}_L(k) \leq y(k) \leq \hat{y}_U(k)\right\} \geq (1 - \alpha) \tag{3.4}$$

As in the works of Veltman et al. [99], Marín et al. [88], Shrivastava et al. [77], and Khosravi et al. [100, 101, 102], in this work, the prediction interval coverage probability *(PICP)* and the prediction interval normalized average width *(PINAW)* are the metrics to be incorporated in the identification process of prediction intervals. *PICP* is used to quantify the number of measured values that fall within the interval defined by the model, and *PINAW* is used to measure the width of the interval.

In this chapter, new prediction interval models based on the concept of fuzzy numbers are derived such that the width defined by the upper $\hat{y}_U(k)$ and lower $\hat{y}_L(k)$ values of the interval is as narrow as possible while the interval contains a certain percentage of measured data $y(k)$.

This condition implies that, to generate prediction intervals, the average width measured by *PINAW* must be minimized while considering a certain desired coverage probability measured by *PICP*. In the next section, the proposed prediction interval models based on fuzzy and neural network modelling are presented.

3.2 Prediction Interval Models Based on Fuzzy Numbers

In this section, a new approach to developing prediction intervals based on fuzzy and neural network models is derived. In general, the models consider a set of p inputs ($z_1(k) \in Z_1, \ldots, z_p(k) \in Z_p$) that represent the input measurement data at time step k.

When an affine linear model is used, the model output $\hat{y}(k)$ at time k is defined as follows:

$$\hat{y}(k) = \theta_o + \theta_1 z_1(k) + \cdots + \theta_p z_p(k), \tag{3.5}$$

where θ_{i} ($\mathrm{i} = 0, 1, \ldots, p$) are the regression coefficients. In this approach, to include uncertainty, the coefficients θ_{i} are defined as interval fuzzy numbers [103, 104]. Therefore, the parameters are expressed as a fuzzy set that defines a fuzzy interval for representing the value of θ_{i}.

Thus, the parameters θ_{i} (interval fuzzy numbers) are characterized by a mean (m) and spread (s). The uncertainty distribution regarding the expected value is characterized using various spread values, i.e., $\theta_{\mathrm{i}} = [m_{\mathrm{i}} - \underline{s}_{\mathrm{i}}, m_{\mathrm{i}} + \overline{s}_{\mathrm{i}}]$. The lower bound ($\hat{y}_L$) and upper bound ($\hat{y}_U$) that define the prediction interval are defined based on the theorem of the affine combination of type-1 interval fuzzy numbers (see Karnik and Mendel in [105] and Mendel in [103] for details on this theorem):

$$\hat{y}_L(k) = \sum_{\mathrm{i}=1}^{p} m_{\mathrm{i}} z_{\mathrm{i}}(k) + m_0 - \sum_{\mathrm{i}=1}^{p} |z_{\mathrm{i}}(k)|\, \underline{s}_{\mathrm{i}} \tag{3.6}$$

$$\hat{y}_U(k) = \sum_{\mathrm{i}=1}^{p} m_{\mathrm{i}} z_{\mathrm{i}}(k) + m_0 + \sum_{\mathrm{i}=1}^{p} |z_{\mathrm{i}}(k)|\, \overline{s}_{\mathrm{i}} \tag{3.7}$$

Based on (3.6) and (3.7), the expected value is characterized by the mean (m_{i}). The last term in both equations is associated with the prediction interval, and it is characterized by the parameters ($\overline{s}_{\mathrm{i}}, \underline{s}_{\mathrm{i}}$).

In this interval modelling approach, the parameters associated with spread ($\overline{s}_{\mathrm{i}}, \underline{s}_{\mathrm{i}}$) are obtained to assure the desired coverage probability $(1-\alpha)\%$ with the smallest interval width at the defined future prediction horizons. The proposed method for identifying these parameters (spreads) is described in Section 3.3. The models thus provide the values of the upper ($\hat{y}_U$) and lower ($\hat{y}_L$) bounds given a coverage probability and the expected value $\hat{y}(k)$.

The proposed method is used to characterize uncertainty. Uncertainty corresponds to the fitting error between the prediction $\hat{y}(k)$ and the actual output $y(k)$; thus, uncertainty is defined by the interval $[\hat{y}_L, \hat{y}_U]$ to which the predicted value could belong. In the next section, both fuzzy and neural network prediction interval models based on fuzzy numbers are presented.

3.2.1 Fuzzy Prediction Interval Modelling

Mathematically, a fuzzy system is defined by a set of p inputs ($z_1(k) \in Z_1, \ldots, z_p(k) \in Z_p$), a set of rules, and an output $\hat{y}^j(k)$ related to each rule at time k. The rules of the Takagi-Sugeno models are expressed as follows:

$$\begin{aligned} R^j : \mathrm{if}\ z_1(k)\ \mathrm{is}\ F_1^j\ and \cdots and\ z_p(k)\ \mathrm{is}\ F_p^j\ then \\ \hat{y}^j(k) = \theta_o^j + \theta_1^j z_1(k) + \cdots + \theta_p^j z_p(k) \end{aligned} \tag{3.8}$$

$j = 1, \ldots, M$, where M is the number of rules. Let $F^j\left(Z(k)\right) = \prod_{\mathrm{i}=1}^{p} \mu_{F_\mathrm{i}^j}\left(z_\mathrm{i}(k)\right)$ be the activation degree of each rule. Then, the normalized activation degree $\beta^j(Z(k))$ is defined as follows:

$$\beta^j(Z(k)) = \frac{F^j(Z(k))}{\sum_{j=1}^{M} F^j(Z(k))} \tag{3.9}$$

In this work, singleton fuzzification, Gaussian membership functions (F_i^j), and the t-norm product are used to provide the output of the fuzzy system:

$$\hat{y}(k) = \sum_{j=1}^{M} \beta^j(Z(k))\hat{y}^j(k) \tag{3.10}$$

Considering the proposed interval modelling framework, in the fuzzy prediction interval models, the consequence parameters (θ_i^j) of each rule (see (3.8)) can be considered as interval fuzzy numbers with their corresponding means (m_i^j) and spreads ($\overline{s}_\mathrm{i}^j, \underline{s}_\mathrm{i}^j$). Thus, the local interval output for each rule (j) is calculated as follows:

$$\hat{y}_L^j(k) = \sum_{\mathrm{i}=1}^{p} m_\mathrm{i}^j z_\mathrm{i}(k) + m_0^j - \sum_{\mathrm{i}=1}^{p} |z_\mathrm{i}(k)|\, \underline{s}_\mathrm{i}^j \tag{3.11}$$

$$\hat{y}_U^j(k) = \sum_{\mathrm{i}=1}^{p} m_\mathrm{i}^j z_\mathrm{i}(k) + m_0^j + \sum_{\mathrm{i}=1}^{p} |z_\mathrm{i}(k)|\, \overline{s}_\mathrm{i}^j \tag{3.12}$$

Finally, the lower $\hat{y}_L(k)$ and upper $\hat{y}_U(k)$ bounds are calculated considering the activation degrees (see (3.9)) and the local outputs of each rule (see (3.11)) and (3.12)) as follows:

$$\hat{y}_L(k) = \sum_{j=1}^{M} \beta^j(Z(k))\hat{y}_L^j(k) \tag{3.13}$$

$$\hat{y}_U(k) = \sum_{j=1}^{M} \beta^j(Z(k))\hat{y}_U^j(k) \tag{3.14}$$

In this study, a fuzzy clustering method is considered for defining the rule numbers and the parameters (centre and standard deviation) of the Gaussian membership functions (F_{i}^j). The means (m_{i}^j) of the consequences are estimated by the minimum least-squares optimization method [106]. The method for tuning the spreads ($\overline{s}_{\mathrm{i}}^j, \underline{s}_{\mathrm{i}}^j$) is explained in Section 3.3.

The lower and upper bounds of the fuzzy prediction model for forecasting the output of future steps are defined as follows:

$$\hat{y}_L(k+h) = f^{fuzzy}(Z(k+h), \beta^j(Z(k+h)), m_{\mathrm{i}}^j, \underline{s}_{\mathrm{i}}^j(k+h)) \qquad \forall h = 1, \ldots, N_p \tag{3.15}$$

$$\hat{y}_U(k+h) = f^{fuzzy}(Z(k+h), \beta^j(Z(k+h)), m_{\mathrm{i}}^j, \overline{s}_{\mathrm{i}}^j(k+h)) \qquad \forall h = 1, \ldots, N_p \tag{3.16}$$

where $j = 1, \ldots, M$ is the rule number, $\mathrm{i} = 1, \ldots, p$ is the input number, and N_p is the prediction horizon. Note that the parameters $\underline{s}_{\mathrm{i}}^j(k+h)$ and $\overline{s}_{\mathrm{i}}^j(k+h)$ are the spreads tuned $\tilde{h}$ steps ahead, where $\tilde{h} \in \{1, \ldots, N_p\}$, using experimental data with certain coverage probability at the future steps. After the tuning process is completed and the prediction interval is obtained, these parameters are held constant through horizon prediction, i.e., $\underline{s}_{\mathrm{i}}^j(k+h) = \underline{s}_{\mathrm{i}}^j(k+\tilde{h})$ and $\overline{s}_{\mathrm{i}}^j(k+h) = \overline{s}_{\mathrm{i}}^j(k+\tilde{h})$ for $h = 1, \ldots, N_p$. More details about the tuning method are provided in Section 3.3.

3.2.2 Neural Network Prediction Interval Modelling

Mathematically, a neural network system is defined by a set of p inputs ($z_1(k) \in Z_1, \ldots, z_p(k) \in Z_p$), a set of of weights ($w$) and biases ($b$) per layer, and an activation function per layer. If the neural network uses a hyperbolic tangent activation function for the hidden layer and a linear activation function for the output layer, the output of the neural network at time k is defined as follows:

$$\hat{y}_l(k) = \sum_{j=1}^{L} w_{j,l}^0 \left(\tanh \left(\sum_{\mathrm{i}=1}^{p} w_{j,\mathrm{i}}^h z_{\mathrm{i}}(k) + b_j^h \right) \right) + b_l^0 \tag{3.17}$$

$j = 1, \ldots, L$, where L is the number of hidden layer units and l is the number of output units; in this study, $l = 1$. The hidden weights, hidden bias, output weights and output bias are $w_{j,\mathrm{i}}^h$, b_j^h, $w_{j,l}^0$ and b_l^0 respectively. The neural network in (3.17) can be written as follows:

$$\hat{y}(k) = \sum_{j=1}^{L} w_j^0 \tilde{Z}_j(k) + b^0 \tag{3.18}$$

where:

$$\tilde{Z}_j(k) = \tanh\left(\sum_{\mathrm{i}=1}^{p} w_{j,\mathrm{i}}^h z_{\mathrm{i}}(k) + b_j^h\right) \tag{3.19}$$

In this work, Bayesian regularization is used to train the neural network. Bayesian regularization consists of a paradigm designed to minimize overfitting of neural networks. The method provides a Bayesian criterion for terminating training, thus generating better results for the test dataset [107].

In this approach, the neural network prediction interval is developed such that the output weights (w_j^0) are considered interval fuzzy numbers with their means (m_j) and spreads ($\underline{s}_j, \overline{s}_j$). The lower and upper bounds of the prediction interval can be calculated as follows:

$$\hat{y}_L(k) = \sum_{j=1}^{L} m_j \tilde{Z}_j(k) + b^0 - \sum_{j=1}^{L} \left|\tilde{Z}_j(k)\right| \underline{s}_j \tag{3.20}$$

$$\hat{y}_U(k) = \sum_{j=1}^{L} m_j \tilde{Z}_j(k) + b^0 + \sum_{j=1}^{L} \left|\tilde{Z}_j(k)\right| \overline{s}_j \tag{3.21}$$

The neural network can be defined as a neural network whose outputs are the upper and lower bounds and the target prediction. As fuzzy prediction interval models, neural network prediction interval models are used to forecast the output of future steps as follows:

$$\hat{y}_L(k+h) = f^{NN}(\tilde{Z}_j(k+h), m_j, \underline{s}_j(k+h)) \qquad \forall h = 1, \ldots, N_p \tag{3.22}$$

$$\hat{y}_U(k+h) = f^{NN}(\tilde{Z}_j(k+h), m_j, \overline{s}_j(k+h)) \qquad \forall h = 1, \ldots, N_p \tag{3.23}$$

where $j = 1, \ldots, L$ is the number of hidden layer units and N_p is the prediction horizon. Note that the parameters $\underline{s}_{\mathrm{i}}^j(k+h)$ and $\overline{s}_{\mathrm{i}}^j(k+h)$ are the spreads tuned $\tilde{h}$ steps ahead, where $\tilde{h} \in \{1, \ldots, N_p\}$, using experimental data with certain coverage probability at the future steps. After the tuning process is completed and the prediction interval is obtained, these parameters are held constant through horizon prediction.

Next, the method for identifying the parameters of the prediction interval based on fuzzy systems and neural networks is explained.

3.3 Method for Developing Prediction Interval based on Fuzzy Numbers

The identification procedure for deriving the prediction interval models is shown in Fig. 3.1. The first part of this procedure corresponds to the identification method of the fuzzy and neural network models for obtaining the expected value, and the second part is the method for prediction interval parameter (spreads) identification.

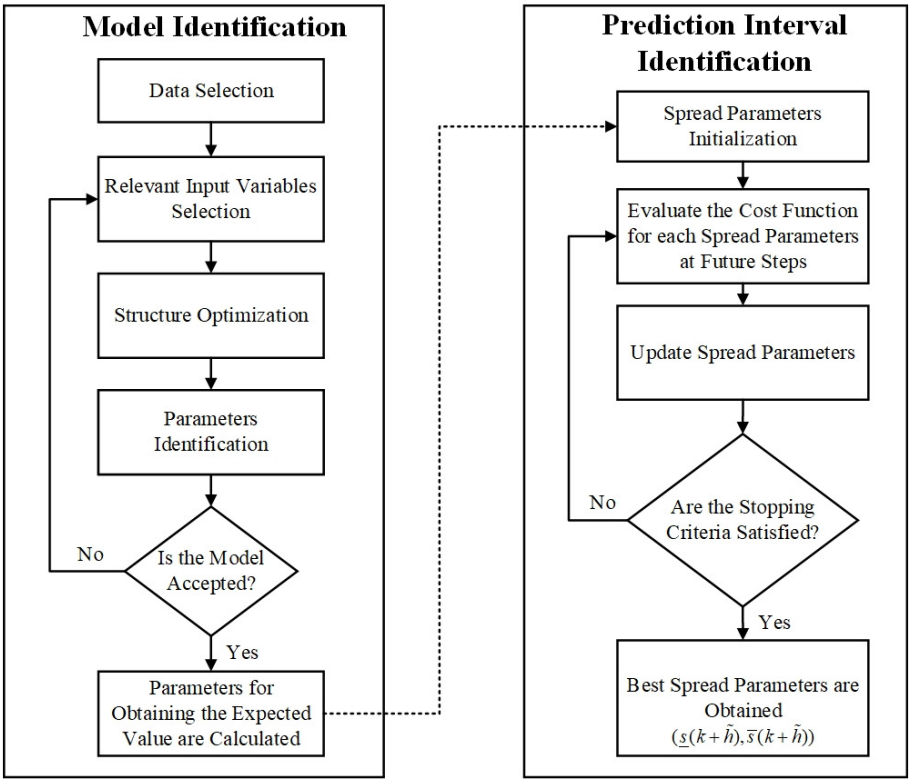

Figure 3.1: Methodology for Developing Prediction Intervals

Regarding model identification (Fig. 3.1), the first step involves data collection for training, validation and testing; sufficient information is collected to represent the various operational points of the process to be modelled. The training dataset is used to obtain the model parameters. The validation dataset is not directly used in the training process; however, it allows the model generalization capacity given by the model behaviour to be evaluated under a new dataset. Finally, the test dataset is used to evaluate the performance of the obtained model.

In this procedure, a structural optimization is made. The structural optimization of fuzzy and neural network models consists of proposing several structures. Specifically, several fuzzy models are obtained when the number of clusters (rules) is modified, and several neural network models are obtained by modifying the hidden neuron number. Then, relevant input variables are selected via sensitivity analysis, and a structural optimization is made. Finally, the parameters necessary for obtaining the expected value are calculated using the relevant input variables, the optimal structure and the training dataset. As proposed in [108], the best

structure is defined when the validation error is either increased or stabilized in comparison with the training error when the structure of the model increases in complexity.

For the fuzzy models, the Gustafson-Kessel clustering algorithm is used to obtain the premise parameters, and the consequence parameters are estimated by the minimum least-squares optimization method. Bayesian regularization is used to obtain the parameters of the neural network models. Finally, the model is evaluated using a test dataset to verify model performance. Then, if the performance of the model is not suitable, the model identification procedure in previous steps must be reviewed; otherwise, this procedure is completed [108].

After the model identification procedure, the parameters associated with providing the expected value are obtained. In fuzzy models, the standard deviation and centre of the Gaussian functions (F_{i}^{j}) of the fuzzy model are found, where p ($\mathrm{i} = 0, 1, \ldots, p$) are the relevant inputs identified and M ($j = 1, \ldots, M$) is the rules number. These parameters are necessary for obtaining the normalized activation degree ($\beta^{j}(Z(k))$) of the premises. The identified consequence parameters (θ_{i}^{j}) (see (3.8)) are assigned to the mean values ($m_{\mathrm{i}}^{j} = \theta_{\mathrm{i}}^{j}$) required in (3.11) and (3.12), and the expected value (see (3.10)) can be obtained.

Regarding neural network models, hidden weights ($w_{j,\mathrm{i}}^{h}$) and hidden biases (b_{j}^{h}) are found. With these parameters, the term $\tilde{Z}_{j}(k)$ in (3.19) is calculated, where p ($\mathrm{i} = 1, \ldots, p$) are the relevant inputs identified and L ($j = 1, \ldots, L$) is the number of hidden layer units. Additionally, the output weights (w_{j}^{0}) and output bias (b^{0}) are identified. Finally, the output weights are used to obtain the expected value, where $m_{j} = w_{j}^{0}$ (used in (3.20) and (3.21)). After the model identification stage, the spreads of the parameters for developing the prediction interval at future steps must be identified (see Fig. 3.1). This method is described in the following section.

3.3.1 Parameters Identification for Prediction Intervals

This identification method stage obtains the parameters (spreads) of the prediction interval models such that the upper and lower values of the interval are as narrow as possible and the interval contains a certain percentage of measured data. The prediction interval models derived in this work can include endogenous $y(k)$ and exogenous variables $u(k)$, where $Z(k) = [y(k-1), \ldots, y(k-q_1), u(k-1), u(k-2), \ldots, u(k-q_2)]^{T}$ is the vector of regressors associated with the output and input variables. Then, the prediction interval is a function of the real and/or prediction data, depending on the number of future steps [83]. In this study, the spreads for developing the prediction interval are tuned according to the required steps ahead. Then, based on the formulation described in the previous sections for developing the prediction interval models and the metrics for evaluating the performance of the prediction interval, the spread identification procedure consists of the solution to the following optimization problem (3.24):

$$\begin{aligned} &\min_{\underline{s}(k+\tilde{h}),\overline{s}(k+\tilde{h})} \quad PINAW \\ &st.\ PICP = 1 - \alpha \end{aligned} \tag{3.24}$$

where $\tilde{h} \in \{1, \ldots, N_p\}$ is the number of steps ahead and $(1-\alpha)\%$ is the desired coverage probability. The prediction interval normalized average width *(PINAW)* and the prediction interval coverage probability *(PICP)* for N_p steps ahead are defined as follows:

$$PICP = \frac{1}{N} \sum_{k=1}^{N} \delta_{k+h} \times 100\% \tag{3.25}$$

$$PINAW = \frac{1}{N \cdot R} \sum_{k=1}^{N} (\hat{y}_U(k+h) - \hat{y}_L(k+h)) \times 100\% \qquad \forall h = 1, \ldots, N_p \tag{3.26}$$

where $\delta_{k+h} = 1$ if $y(k+h) \in [\hat{y}_L(k+h), \hat{y}_U(k+h)]$; otherwise, $\delta_{k+h} = 0$. The parameters $(\underline{s}(k+\tilde{h}), \overline{s}(k+\tilde{h}))$ are the decision variables in the optimization problem, and the dimensionalities of these parameters depend on the model selected. For fuzzy models, $2pM$ parameters that correspond to the spreads $(\underline{s}_{\mathrm{i}}^{j}(k+\tilde{h}), \overline{s}_{\mathrm{i}}^{j}(k+\tilde{h}))$ and $2L$ parameters for the neural network model that corresponds to the spreads $(\underline{s}_j(k+\tilde{h}), \overline{s}_j(k+\tilde{h}))$ should be identified. Then, the parameters $(\underline{s}(k+\tilde{h}), \overline{s}(k+\tilde{h}))$ (see (3.24)) must be computed such that i) *PICP* is greater than or equal to the desired coverage probability $(1-\alpha)\%$ and ii) *PINAW* is as small as possible at future steps. The equality constraint $PICP = (1-\alpha)\%)$ in (3.24) is a hard constraint and is therefore included in the optimization problem as a barrier function to relax this constraint. Therefore, the solution of the minimization problem (3.24) is computed following the procedure for the unconstrained minimization problem:

$$\min_{\underline{s}(k+\tilde{h}), \overline{s}(k+\tilde{h})} \quad J = \eta_1 PINAW + \exp^{-\eta_2(PICP-(1-\alpha))} \tag{3.27}$$

In (3.27), η_1 is a weighting factor and η_2 is a penalty factor. These parameters are chosen such that, if *PICP* is less than $(1-\alpha)\%$, the term $\exp^{-\eta_2(PICP-(1-\alpha))}$ is the dominant term in the cost function; otherwise, *PINAW* is dominant. Finally, the solution to the nonlinear optimization problem (3.27) is computed using particle swarm optimization (PSO), as outlined in the next section.

3.3.2 Solution Method

To solve the nonlinear optimization problem in (3.27), traditional algorithms, such as gradient descent methods, are not adequate. These methods entail a risk of falling into a local optimum when solving non-convex optimization problems. Therefore, other optimization methods are needed [109]. In this work, PSO is used to solve the problem because it generally outperforms other algorithms in terms of success rate and solution quality, as reported in [110]. In PSO, the generated solutions are called particles, and each particle has a position vector with an associated velocity vector [111]. The first step in the algorithm consists of the initialization of particle positions $x_{\mathrm{i},j}$ and velocities $v_{\mathrm{i},j}$ for the $j-th$ dimension of the $\mathrm{i}-th$ particle. In this study, the particle positions are all the spread parameters $(\underline{s}(k+\tilde{h}), \overline{s}(k+\tilde{h}))$ required to develop the prediction interval model, as explained in Section 3.2.

The velocity $v_{\mathrm{i},j}$ and position $x_{\mathrm{i},j}$ in the $j-th$ dimension of every $\mathrm{i}-th$ particle are updated according to the following relations:

$$\begin{aligned} v_{\mathrm{i},j}(t+1) &= Wv_{\mathrm{i},j}(t) + c_1 rand()(Pbest_{\mathrm{i},j}(t) - x_{\mathrm{i},j}(t)) + c_2 rand()(gbest_j(t) - x_{\mathrm{i},j}(t)) \\ x_{\mathrm{i},j}(t+1) &= x_{\mathrm{i},j}(t) + v_{\mathrm{i},j}(t+1) \end{aligned} \tag{3.28}$$

$\mathrm{i} = 1, 2, \ldots, NP$, where NP is the number of particles, and $j = 1, 2, \ldots, N_0$ is the total number of parameters to be identified, which depends on the type of model used (fuzzy or neural). W is an inertia factor, $Pbest$ is the best previous solution of the particle, and $gbest$ is the best solution of the swarm up to the current step. The terms c_1 and c_2 are called the cognitive and social acceleration constants, and $rand()$ is a random number between 0 and 1. The training termination criterion is set when a minimum error or a defined maximum number of iterations is achieved. Once the training process terminates, the $gbest$ value is chosen as the spread parameter to generate the prediction interval model.

PINAW and *PICP* are used as metrics for the evaluation of the quality of the interval. Additionally, the root mean square error *(RMSE)* and the mean absolute error *(MAE)* are included as performance indices to evaluate the accuracy of the prediction model associated with the expected value. All indices are evaluated for several prediction horizons with the test dataset. In this study, the prediction interval models based on fuzzy systems and neural networks are used to represent the nonlinear behaviour and uncertainty derived from electricity demand and renewable resources; however, the proposed methodology can be used to describe a large family of uncertainty nonlinear functions.

3.4 Experiment and Results

A comparative analysis between the proposed prediction interval models based on interval fuzzy numbers (PI-IFN) and covariance prediction interval models is presented following the definition presented in [81, 73] and [83]. The prediction interval based on the covariance establishes the interval based on the error between the observed data $y(k)$ and the model output $\hat{y}(k)$. This method is based on the assumption that the noise is normally distributed with a zero mean value and variance σ^2 that is expressed as $\mathrm{e} = N(0, \sigma^2)$ [73].

As indicated in (3.18), the neural network model is a linear model of the parameters. Therefore, the lower and upper bounds of the neural network prediction interval based on the covariance method can be developed using (3.29) and (3.30), following the definition presented in [81]:

$$\hat{y}_L(k+h) = \tilde{Z}^*(k+h)^T W^0 + b^0 - \alpha_{k+h} I^{NN} \tag{3.29}$$

$$\hat{y}_U(k+h) = \tilde{Z}^*(k+h)^T W^0 + b^0 + \alpha_{k+h} I^{NN} \tag{3.30}$$

where:

$$I^{NN} = \sigma_{\mathrm{e}}\left(1 + \tilde{Z}^{*T}\left(\tilde{Z}^T\tilde{Z}\right)^{-1}\tilde{Z}^*\right)^{1/2} \tag{3.31}$$

where σ_{e} is the variance of the error, α_{k+h} is the parameter related to the interval width tuned h steps ahead, where $h \in \{1, \ldots, N_p\}$, $\tilde{Z}^*$ is the new datum used to predict the future observation and $\tilde{Z}$ is the matrix that considers all data used in the training process in which the output weights and output bias were determined.

On the other hand, the local fuzzy output for rule j at time k can written as [73]:

$$\hat{y}^j(k) = [1\ Z(k)]\theta_j, \tag{3.32}$$

where θ_j is the coefficients vector of the consequence associated with each rule. Therefore, the total output of the fuzzy model is defined by:

$$\hat{y}(k) = \sum_{j=1}^{M} \beta^j(Z(k))[1\ Z(k)]\theta_j = \sum_{j=1}^{M} \psi_j^T\theta_j \tag{3.33}$$

where $\psi_j^T = \beta^j(Z(k))[1\ Z^T(k)]$, $j = 1, \ldots, M$. The expression (3.33) can also be written in matrix form: $\hat{y}(k) = \Psi^T\Theta$, where $\Psi^T = [\psi_1^T, \ldots, \psi_M^T]$ is the fuzzy regression matrix and $\Theta^T = [\theta_1, \ldots, \theta_M]$ is the matrix of the coefficients for all the rules. The lower and upper bounds of the fuzzy prediction interval based on the covariance method [73] can be defined by:

$$\hat{y}_L(k) = \hat{y}(k) - \alpha I^{TS}(k) \tag{3.34}$$

$$\hat{y}_U(k) = \hat{y}(k) + \alpha I^{TS}(k) \tag{3.35}$$

with the fuzzy interval given by:

$$I^{TS}(k) = \sum_{j=1}^{M} \beta^j(Z^*(k))I_j^{TS}(k), \tag{3.36}$$

where $I_j^{TS}(k) = \hat{\sigma}_j(1 + \psi_j^{*T}(\psi_j\psi_j^T)^{-1}\psi_j^*)^{1/2}$ is a component associated with the covariance matrix and the current input ψ_j^{*T} associated to a new datum $Z^*(k)$. The fuzzy prediction at future steps ahead can be obtained as follows:

$$\hat{y}(k+h) = \sum_{j=1}^{M} \beta^j(Z(k+h))\hat{y}^j(k+h) \tag{3.37}$$

It has been proposed in [83] that the expected covariance of the error between the observed data and the local model output along with some tuning parameters α_{k+h} can be used to find the fuzzy prediction interval for a desired coverage probability at future steps ahead. Therefore, the lower ($\hat{y}_L$) and upper ($\hat{y}_U$) bounds are given by:

$$\hat{y}_L(k+h) = \hat{y}(k+h) - \alpha_{k+h} I^{TS}(k+h) \tag{3.38}$$
$$\hat{y}_U(k+h) = \hat{y}(k+h) + \alpha_{k+h} I^{TS}(k+h) \tag{3.39}$$

Finally, the parameter α_{k+h} defines the interval width and it is tuned using experimental data to achieve the desired coverage probability at future steps ahead. In the next section, the results of a benchmark and the load forecast with the proposed prediction interval models are presented.

3.4.1 Benchmark

In this work, the original Chen series in [112] is modified and used to evaluate the prediction interval models:

$$\begin{aligned} y(k) = {} & (0.8 - 0.5\exp(-y^2(k-1)))y(k-1) - (0.3 + 0.9\exp(-y^2(k-1)))y(k-2) + \\ & u(k-1) + 0.2u(k-2) + 0.1u(k-1)u(k-2) + \mathrm{e}(k) \end{aligned} \tag{3.40}$$

where the system noise $\mathrm{e}(k) = 0.5\exp(-y^2(k-1))\gamma(k)$ depends on the previous state of the output model and $\gamma(k)$ is white noise. The system input $u(k)$ is band-limited Gaussian white noise. The system is simulated, and 10,000 data points are generated. The data are divided into training, validation and testing sets accounting for 55%, 25% and 20% of the total dataset, respectively. Fig. 3.2 shows the input, output and noise of the modified Chen series simulation for 400 training data. As shown in Fig. 3.2, the noise level is high when the output $y(k)$ is close to zero.

The regressors $u(k-1)$, $u(k-2)$, $y(k-1)$ and $y(k-2)$ are defined as the inputs for deriving the prediction interval models. Regarding the structure of the fuzzy model, five rules are defined, whereas eight hidden layer units are defined for the neural network model. With these structures defined, the parameters associated with providing the expected value are obtained as explained in Section 3.3. The PSO algorithm is used to identify the spread parameters for generating the prediction interval at future steps. The desired coverage probability $(1-\alpha) = 90\%$, the weighting factor $\eta_1 = 250$ and the penalty factor $\eta_2 = 150$ in (3.27) are defined. A particle size of 50 and the parameters $c_1 = 2.5$ and $c_2 = 1.5$ are used. Finally, W runs from 0.9 to 0.3 during offline optimization. The number of iterations for PSO is set to 5,000, the optimizations are executed several times, and the best solution is selected. The cost function value (J) in (3.27) and the developed metrics are reported in Table 3.1 for the test dataset using various numbers of steps ahead.

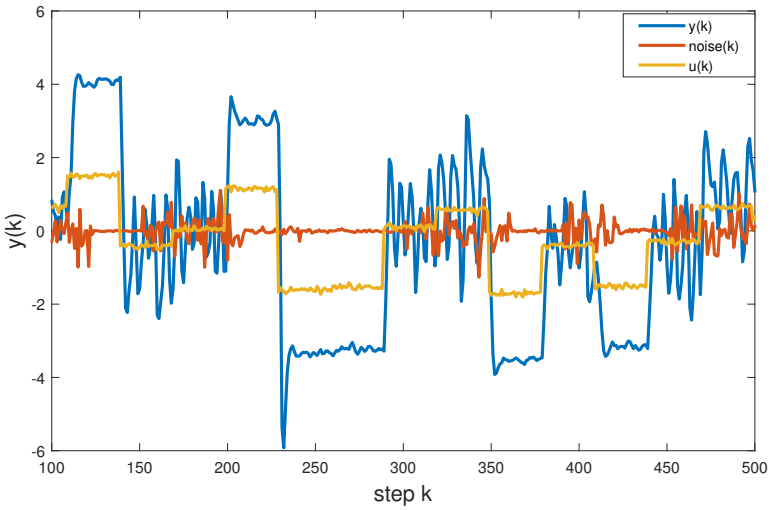

Figure 3.2: Modified Chen Series for 400 Training Data

As shown in Table 3.1, the fuzzy and neural network models provide cost function values (J) lower than those of the linear model, which is consistent with the nonlinear benchmark structure. These results are expected because of the ability of the fuzzy and neural network models to better fit the dynamics and nonlinearities of the systems, which are more notable for longer future-step predictions. Additionally, it can be observed that the cost function of the proposed method (see (3.27)) is lower than that of the covariance method for all models (i.e., linear, fuzzy and neural network). The *RMSE* and *MAE* values are equal in the proposed and covariance methods because the identification method is the same. However, the prediction error increases for a larger horizon prediction because the accumulative error of the model is larger when the steps of the horizon increase, as shown in Table 3.1.

Furthermore, it can be observed that the *PICP* term is close to 90% because the interval models are trained to maintain *PICP* near the desired value for various steps ahead. In terms of prediction intervals, the proposed method (PI-IFN) provides narrower intervals for all step-ahead forecasts. While the covariance method maintains a constant width for the interval (see Fig. 3.3(a), Fig. 3.4(a) and Fig. 3.5(a)), the proposed method achieves a narrower interval in states with little noise and an interval with a width similar to that of the covariance method in states with high noise.

Importantly, the information level delivered by a prediction interval is directly related to its width [113, 88]; thus, the proposed method yields a better information level regarding the covariance method (smaller widths). Wider intervals could produce a higher *PICP*, but these intervals provide less useful information about the uncertainty of the modelled phenomena. In this respect, the neural network models exhibit sharper prediction intervals than the linear and fuzzy models.

Fig. 3.3, Fig. 3.5 and Fig. 3.4 show sixteen-step-ahead forecasts of the linear, fuzzy and neural network prediction interval models. The figures show that nearly all the data are included in the interval; only the outliers of the time series are left outside the region constructed by the prediction interval. Additionally, the intervals produced by the proposed

Table 3.1: Performance Indices for the Benchmark

Prediction Horizon	Performance Indices	Linear Models		Fuzzy Models		Neural Models	
		Covariance	PI-IFN	Covariance	PI-IFN	Covariance	PI-IFN
One	J	52.23	32.62	26.26	23.60	20.93	18.20
step	RMSE	0.4312	0.4312	0.3517	0.3517	0.2372	0.2372
ahead	MAE	0.2883	0.2883	0.2253	0.2253	0.1241	0.1241
	PINAW (%)	20.89	12.40	10.09	9.37	7.90	6.85
	PICP (%)	98.15	89.68	89.98	91.18	89.89	89.95
Four	J	57.71	47.47	40.27	35.56	36.58	24.36
steps	RMSE	0.6124	0.6124	0.5266	0.5266	0.4076	0.4076
ahead	MAE	0.5010	0.5010	0.3765	0.3765	0.2446	0.2446
	PINAW (%)	23.05	17.35	15.14	13.73	14.18	9.18
	PICP (%)	91.62	89.06	89.41	89.86	89.92	89.77
Eight	J	57.98	49.32	43.39	39.48	39.94	32.62
steps	RMSE	0.6761	0.6761	0.5621	0.5621	0.5105	0.5105
ahead	MAE	0.4647	0.4647	0.4015	0.4015	0.3127	0.3127
	PINAW (%)	23.19	18.16	17.08	15.29	15.13	11.72
	PICP (%)	93.26	89.09	90.25	89.85	89.50	89.20
Sixteen	J	58.16	50.75	45.21	41.40	45.93	36.15
steps	RMSE	0.6814	0.6814	0.5839	0.5839	0.5937	0.5937
ahead	MAE	0.4717	0.4717	0.4167	0.4167	0.3685	0.3685
	PINAW (%)	23.26	18.97	17.85	15.98	18.20	14.10
	PICP (%)	93.19	89.20	90.36	89.75	90.57	90.07

method (PI-IFN) are narrower than those obtained by the method used for comparison, as shown in the figures.

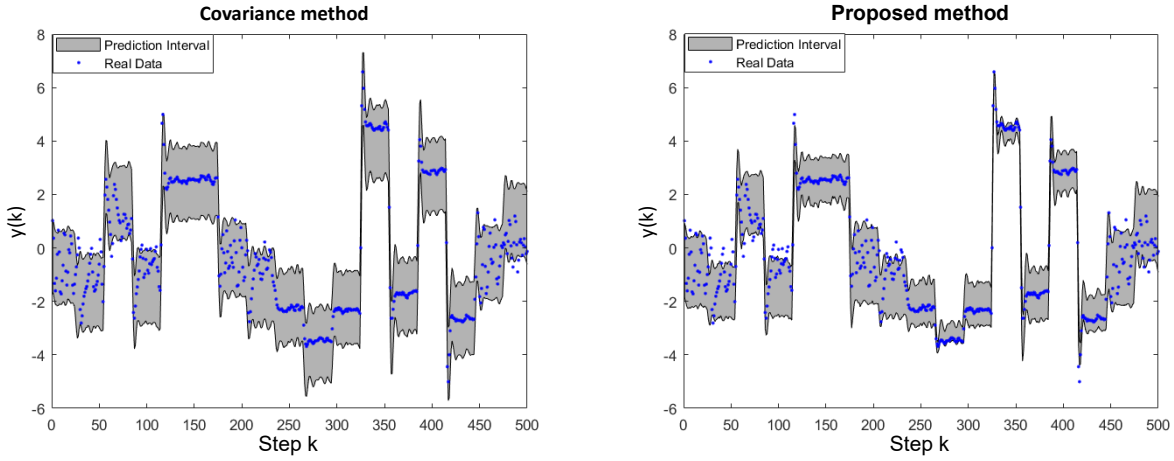

(a) (b)

Figure 3.3: Sixteen-step-ahead Linear Prediction Interval Model: (a) Covariance and (b) Proposed Methods

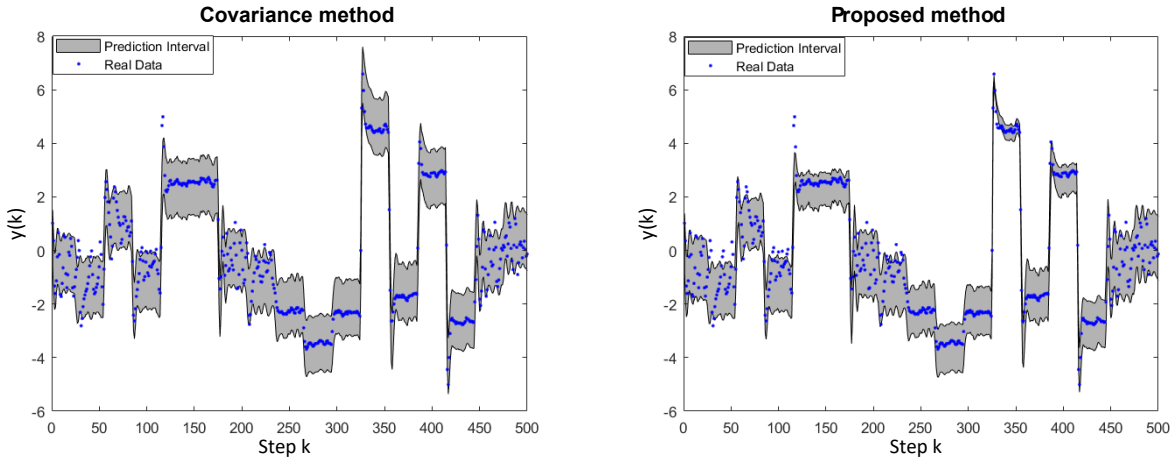

(a) (b)

Figure 3.4: Sixteen-step-ahead Fuzzy Prediction Interval Model: (a) Covariance and (b) Proposed Methods

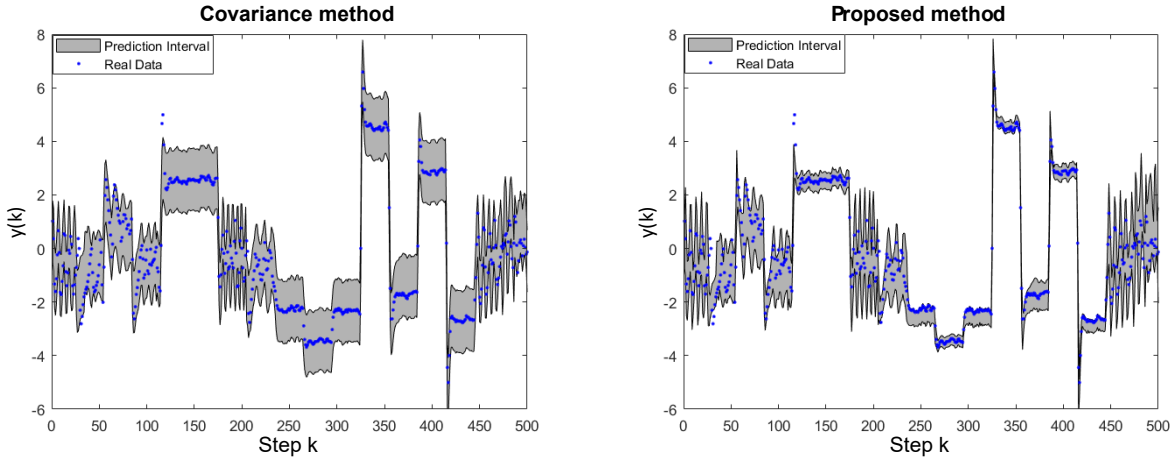

(a) (b)

Figure 3.5: Sixteen-step-ahead Neural Network Prediction Interval Model: (a) Covariance and (b) Proposed Methods

3.4.2 Application for Load Forecasting

In this section, both fuzzy and neural network prediction interval models based on the concept of interval fuzzy numbers (PI-IFN) are used to develop the domestic load consumption prediction interval models supported by the results obtained with the benchmark.

The load data from 20 dwellings in the town of Loughborough, UK [114], are used to develop fuzzy and neural network prediction interval models using the proposed method (PI-IFN). The available load data correspond to the year 2008; however, only summer data are

used to develop the prediction interval. Therefore, a period of 94 days is used, which is divided into 52 days for training, 23 days for validation and 19 days for test data, corresponding to 55%, 25% and 20% of the total dataset, respectively. The maximum electric load is 29.54 kW with a sample time of 15 minutes.

Equations (3.41) and (3.42) show the relevant regressors obtained during the model identification process for the fuzzy and neural network models, respectively:

$$\begin{aligned}\hat{p}_L(k) = f^{fuzzy}(&p_L(k-1), p_L(k-2), p_L(k-3), p_L(k-5), p_L(k-6), p_L(k-8), ... \\ &p_L(k-90), p_L(k-91), p_L(k-92), p_L(k-93), p_L(k-94), ... \\ &p_L(k-95), p_L(k-96), p_L(k-97), p_L(k-98))\end{aligned} \tag{3.41}$$

$$\begin{aligned}\hat{p}_L(k) = f^{NN}(&p_L(k-1), p_L(k-2), p_L(k-3), p_L(k-4), p_L(k-5), p_L(k-91), ... \\ &p_L(k-92), p_L(k-95), p_L(k-96), p_L(k-97), p_L(k-100))\end{aligned} \tag{3.42}$$

Three rules and nine neurons in the hidden layer correspond to the optimal structure for the fuzzy and neural network models, respectively. Note that exogenous variables are not included in the models. Specifically, in this study, one-step-ahead (15 minutes), one-hour-ahead, one-day-ahead, and two-day-ahead prediction horizons are considered. For both models (fuzzy and neural network), the performance indices are computed based on the method described in Section 3.3 for the prediction horizons considered.

As shown in Table 3.2, the fuzzy and neural models provide similar performances in terms of *RMSE* and *MAE* for the test dataset. The maximum *RMSE* is 2.6054 kW for a peak load of 29.54 kW, corresponding to the fuzzy model at two days ahead. The coverage probability *(PICP)* for all prediction horizons with respect to the training data is in accordance with the desired coverage probability.

These results suggest that the prediction interval is tuned appropriately to 90% of the desired *PICP*. However, Table 3.2 shows that the *PICP* values for the test data are higher than the desired coverage probability as the prediction horizon increases. For instance, the *PICP* values are 93.86% and 94.06% at one-day-ahead for the fuzzy and neural network models, respectively. These results are obtained because of the high variability of the data used in this study case, as shown in Fig. 3.6.

As explained in Section 3.3, to calculate the spread parameters of all prediction interval models, the coverage probability is fixed in the optimization problem (see (3.24)). The interval width finding therefore corresponds to the minimum width at the step ahead defined for characterizing the uncertainty of the modelled demand, given the desired *PICP*. The interval width *(PINAW)* increases with the prediction horizon.

Fig. 3.6 shows the one-day-ahead prediction intervals of the fuzzy and neural network models, with interval widths of 47.54% and 47.93%. Despite the widths of these intervals, the relationship between the coverage probability and the interval width for this study case provides sufficient information about the uncertainty modelled, and this information could be useful, for instance, for the design of a robust energy management system.

Table 3.2: Performance Indices for the Load Prediction Models

Prediction Horizon	Performance Indices	Fuzzy Model	Neural Network Model
One step ahead	J	93.07	92.33
	RMSE (kW)	20.678	20.613
	MAE (kW)	15.225	15.147
	PINAW (%)	36.68	36.44
	PICP (%)	89.79	89.86
One hour ahead	J	110.64	110.17
	RMSE (kW)	22.942	22.910
	MAE (kW)	17.269	17.139
	PINAW (%)	44.25	44.05
	PICP (%)	92.73	92.12
One day ahead	J	118.85	119.83
	RMSE (kW)	23.429	22.984
	MAE (kW)	18.076	17.403
	PINAW (%)	47.54	47.93
	PICP (%)	93.86	94.06
Two days ahead	J	128.23	128.05
	RMSE (kW)	26.054	25.532
	MAE (kW)	20.665	19.422
	PINAW (%)	51.29	51.22
	PICP (%)	94.63	94.22

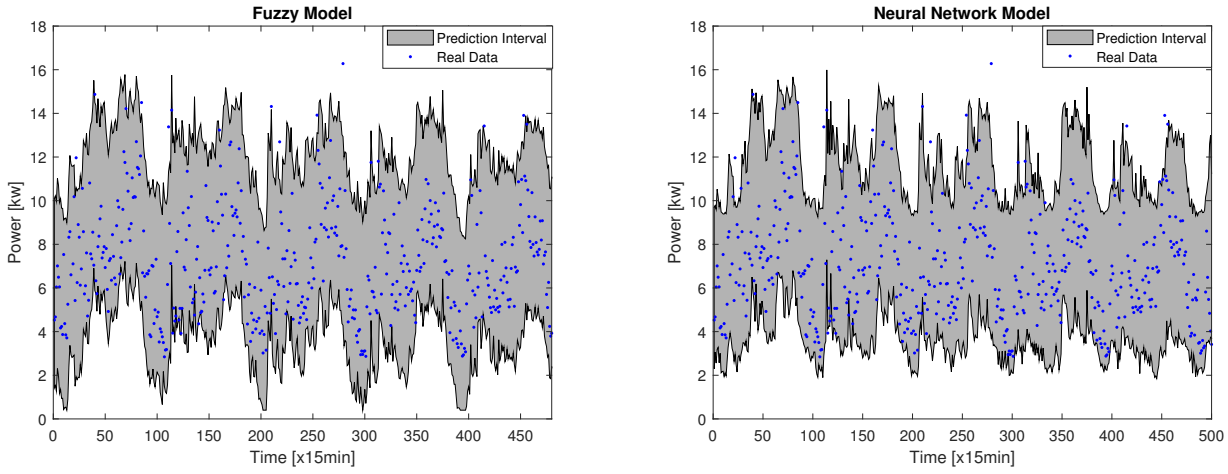

(a) (b)

Figure 3.6: One-day-ahead Prediction Interval: (a) Fuzzy Model and (b) Neural Network Model

3.5 Discussion

In this chapter, a new prediction interval modelling framework based on the concept of interval fuzzy numbers was proposed to represent nonlinear dynamics and uncertainties. These models provide the upper and lower bounds of the predicted values given a coverage probability with the minimum interval width at future prediction horizons. This prediction interval modelling was extended to fuzzy systems and neural networks to describe a large family of uncertain nonlinear functions. In this approach, the fuzzy number concept was used because the affine combination of interval fuzzy numbers generates, by definition, interval models that can address the uncertainty of the modelled phenomena without requiring assumptions to be made about the data or the noise distribution. In this methodology, the spreads of the prediction interval models were tuned at future steps based on a novel criterion that minimizes the width of the interval given a desired coverage probability.

Prediction intervals models are capable of quantifying the uncertainty using just three information points: expected value, lower and upper bounds, thus making them the most understandable uncertainty quantification mechanism, when compared to other methods such as: probability density function (PDF), cumulative probability density function (CDF) and probabilistic forecast [76]. In the prediction interval model, the expected value provides a solution where the statistical error is the lowest possible defined by error metrics, such as the root mean square error (RMSE) and the mean absolute percentage error (MAPE). Additionally, the lower and upper bounds of the interval can be derived probabilistically and provide information on the dispersion of the output of the model. Furthermore, it delivers more useful information from a decision-making point of view than the models where only the expected value is considered. The prediction interval models can capture the nonlinearity, the temporal dynamics and the uncertainty of the modelled phenomena derived from nonconventional energy sources and electrical demand.

Based on a benchmark problem, the proposed method was compared with a covariance prediction interval method. The results show that the proposed prediction interval models generated a narrow interval width and retained the desired coverage probability. In this sense, narrow width prediction intervals provide more information about the uncertainty phenomena modelled. Furthermore, the proposed method was used to represent the future load uncertainty of residential dwellings in the town of Loughborough, UK for several prediction horizons. The results indicated that the proposed method for developing prediction intervals is suitable for load forecasting in applications of energy communities. In this thesis, the proposed Robust EMS is based on MPC, thus it requires models to predict the expected value and the variability of the demand and the energy available from the renewable resources, over a prediction horizon. Therefore, fuzzy prediction interval models are used in the formulation of the optimization problem.

Chapter 4

Hierarchical Energy Management System for Microgrid Operation

The concept of "Energy Communities" enables energy exchange between community members to maximise their self-consumption, minimise their energy costs, reduce peak power levels or a combination of these and other beneficial goals. To achieve a stable, robust and cost effective energy community, the system must use a suitable energy management system (EMS). This chapter proposes a two level hierarchical EMS which realises both short-term power balancing and long-term energy management, benefiting both the energy community members and the distribution network operator (DNO). The two level structure addresses both the uncertainty of the renewable energy resources and the variability in end-user consumption profiles. At the lowest level, a real-time control strategy comprising a rule-based decision system, is employed to control power with a sample rate of one-minute. For the higher level, a Robust Model Predictive Control (MPC) is used with a sample period of 30 min to optimise energy usage. The hierarchical EMS proposed has been evaluated using data from a typical urban community made up 30 dwellings with a photovoltaic (PV) power level of up to 50% penetration, and an energy storage system of up to 135kWh. Simulation results show that the proposed hierarchical EMS can accurately control power levels draw by the community to follow references set by the Robust MPC and can also operate at minimum energy cost. Additionally, the structure maintains safe operation of the battery bank as well as reducing peak load levels drawn by the community. It is shown that the Robust EMS with explicit uncertainty compensation creates a more uniform grid power draw (flatter) compared to a deterministic EMS, which can provide benefit for the distribution network operator.

4.1 Introduction

This work considers a hierarchical energy management system (EMS) as proposed in [39]. This EMS comprises two levels: the microgrid (energy community) level and the main grid level as is shown in Fig. 4.1. Within this framework, the proposed microgrid is composed of domestic demand (non-controllable loads), photovoltaic arrays (PV), and an energy storage

system (ESS) based on lead-acid batteries. The ESS is included as part of this approach since it can benefit both the end user (reducing energy costs) and the distribution network operator (DNO) (limiting peak power levels and enabling increased penetration of DG). Additionally, the ESS is required to increase robustness to uncertainty.

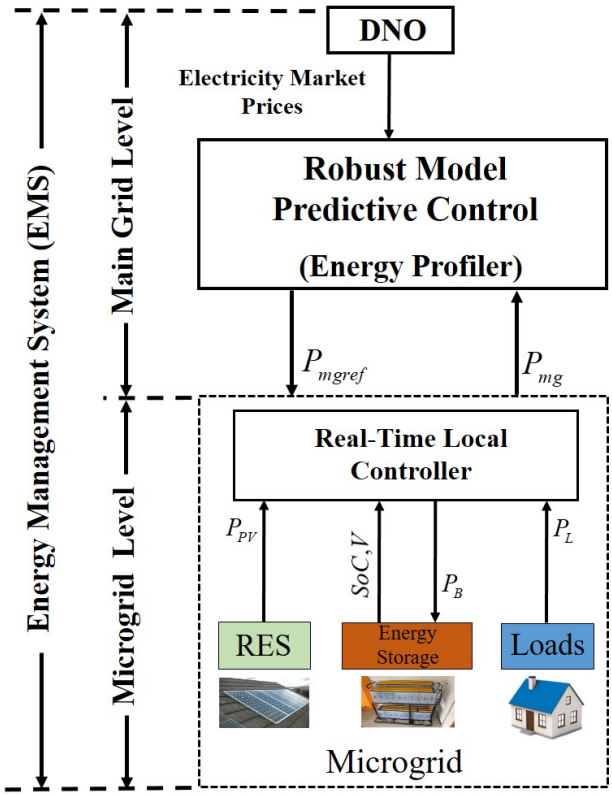

Figure 4.1: Hierarchical EMS Structure

At the main grid level, a Robust MPC controller operates to provide realistic power references (P_{mgref}) for the microgrid: this is the "Energy Profiler". The microgrid level controller aims to track these references and so that the system works for example with minimum energy costs. To achieve this goal, the Robust MPC implements an optimization of the predicted performance cost of the microgrid over a prediction horizon, while considering the uncertainty associated with predictions of the renewable generation and consumer load, safe limit constraints for the ESS and power transfer to and from the main grid. In this study, the uncertainty is handled using fuzzy prediction interval models tuned to a desired coverage probability. A sample time of 30 min is considered, which defines the update frequency of P_{mgref}. This sample time is selected because energy markets tend to operate with a half-hourly update rates.

At the microgrid level, a real-time local controller is proposed with the objective of satisfying the demand whilst guaranteeing safe operation of the ESS. This controller is executed with a sample time of one-minute to control the net power flowing from the main grid to the microgrid (P_{mg}) or vice versa so that it tracks the power reference (P_{mgref}) sent from the central Energy Profiler at the main grid level. Therefore, P_{mg} corresponds to import/ export power from the main grid. The following sections present the details of the real-time controller at microgrid level and the Robust MPC for the main grid level.

4.2 Real-time Controller at Microgrid Level

The ESS is the only dispatchable DER in the proposed microgrid, and therefore the real-time controller can only set the charging/discharging power profile (P_B) of the ESS (as shown in Fig. 4.2) in order to track the target (P_{mgref}) provided by the Energy Profiler. Note that the ESS consists of a power converter and battery packs, however in this framework, converter losses are not considered.

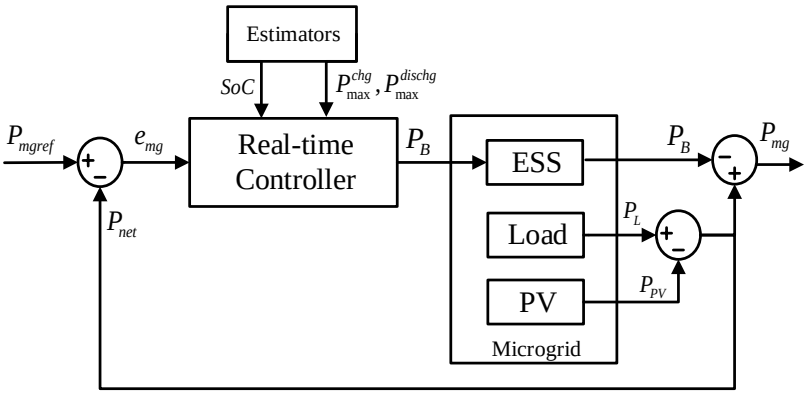

Figure 4.2: Block Diagram at the Microgrid Level

The active power of both the microgrid consumption (P_L) and photovoltaic array (P_{PV}) are measured at the point of common coupling (PCC) with a sample rate of one minute to calculate the net power (P_{net}) of the microgrid (give by $P_{net}(k) = P_L(k) - P_{PV}(k)$). The error between the microgrid power target and the net power is given by:

$$\mathrm{e}_{mg}(k) = P_{mgref}(k) - P_{net}(k), \tag{4.1}$$

which corresponds to a power surplus (positive error) or deficit (negative error) with respect to P_{mgref}. Therefore, e_{mg} is the required power from the ESS so that the instantaneous microgrid power P_{mg} tracks the target P_{mgref} provided by the Robust MPC in the Energy Profiler.

For safe operation of the ESS, the maximum available power for charging (P_{max}^{chg}) and discharging ($P_{max}^{\mathrm{dischg}}$) is calculated based on methods proposed in [115] and [116]. These power values are obtained to prevent battery damage by over/under charge (SoC) or voltage, or by exceeding the rated current or power limit (for details of this estimator see appendix A3). The ESS power P_B cannot exceed these values. Additionally, the SoC value is estimated based on an Unscented Kalman Filter (UKF) [117], with outer feedback correction loops as presented in [118] (for details of this estimator see appendix A2). This is because Bayesian estimation algorithms have been demonstrated be a well-suited tool estimation for nonlinear problems, such as SoC estimation, and they present several advantages such as real-time implementation and use of empirical models that deal better with limited and noisy data compared to methods such as ampere-hour counting, internal impedance measurement and the open circuit voltage measurement (OCV), among others [119, 120].

In this work, positive power from the ESS indicates the ESSs is discharging (generation) and negative power indicates the ESS is charging (load). Finally, the controller output (ESS power reference) P_B is determined according to the following rules:

$$\begin{aligned}
&R1: \text{if } \mathrm{e}_{mg}(k) \geq 0 \text{ and } SoC(k) \geq SoC_{max} \text{ then } P_B(k) = 0 \\
&R2: \text{if } \mathrm{e}_{mg}(k) \geq 0 \text{ and } SoC(k) < SoC_{max} \text{ then } P_B(k) = -\min(\mathrm{e}_{mg}(k), P_{max}^{chg}(k)) \\
&R3: \text{if } \mathrm{e}_{mg}(k) < 0 \text{ and } SoC(k) \geq SoC_{min} \text{ then } P_B(k) = \min(-\mathrm{e}_{mg}(k), P_{max}^{\mathrm{dischg}}(k)) \\
&R4: \text{if } \mathrm{e}_{mg}(k) < 0 \text{ and } SoC(k) < SoC_{min} \text{ then } P_B(k) = -\min(P_{PV}(k), P_{max}^{chg}(k))
\end{aligned} \tag{4.2}$$

where $SoC_{min} = 0.2$ and $SoC_{max} = 0.8$ are the minimum and maximum defined values range for the SoC with the aim to increase the lifespan, because capacity fade is typically accelerated by operating profiles with high average SOC levels and deep discharges [121]. As is shown in Fig. 4.2, the instantaneous microgrid power (P_{mg}) is calculated as:

$$P_{mg}(k) = P_{net}(k) - P_B(k) \tag{4.3}$$

Thus, according to rules in (4.2), P_{mg} tracks P_{mgref} as long as the resulting values of P_B and SoC do not violate safety constraints.

4.3 Model Predictive Control for Microgrid Operation

The higher level controller aims to calculate the reference power (P_{mgref}) which will minimize the energy cost for the community, such that the low level real-time controller can follow this power target reasonably well based on the available resources (P_B and P_{PV}) and the load (P_L). In this way, the controller at the higher level is seen as a supervisory controller, as shown in Fig 4.3.

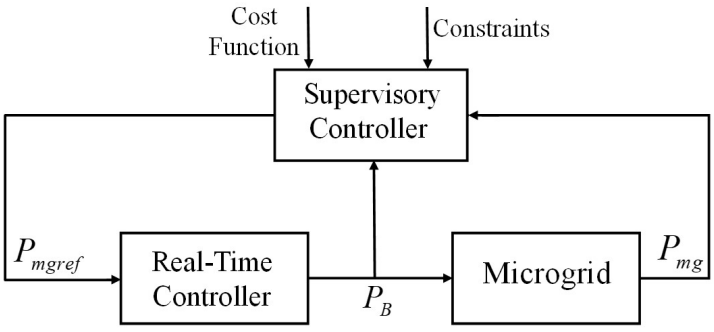

Figure 4.3: Block Diagram at Main Grid Level

The Robust EMS chosen operates with receding horizon control, and it is necessary to generate models that anticipate the behavior of the expected value over a prediction horizon,

and the variability of both the demand and the energy available from the renewable resources. Therefore, the performance of the Robust EMS depends on the accuracy of the prediction system employed, and the method used for characterising the uncertainty.

4.3.1 Deterministic EMS

The role of the supervisory controller at the main grid level is to minimize the power delivered to the microgrid (energy community) from the main grid. This is achieved by means of an MPC controller, which uses a model of the energy community dynamics to predict its behaviour one day ahead, with a sample time (T_s) of 30 min (thus using a prediction horizon of $N = 48$ samples). At each discrete time instant k, an optimization problem uses this model to find the optimal sequence of $P_{mgref}(k+j), j = 0, \ldots, N-1$ that minimizes the energy consumption during the prediction horizon N. For this work, three energy price levels $C(k+j)$ have been used based on a time of use (ToU) tariff scheme.

The dynamical component of the system is given by a simplified linear model of the energy evolution of the ESS (E_B). These dynamics must be included in the MPC optimization, and are described by:

$$E_B(k+j+1) = E_B(k+j) - TsP_B(k+j), \tag{4.4}$$

where $j = 0, \ldots, N-1$ and $P_B(k+j)$ is positive if it injects power (discharging) into the microgrid and negative for the charging process. The prediction of the future states requires an estimation of the current state, particularly the SoC. Here, it is estimated by UKF (see appendix A2) at the microgrid level which sends this information to the upper layer.

The power balance at microgrid level must also be imposed in the MPC optimization. This constraint is invoked as:

$$P_{mgref}(k+j) = P_{net}(k+j) - P_B(k+j). \tag{4.5}$$

where $P_{net}(k+j) = P_L(k+j) - P_{PV}(k+j)$. In the deterministic approach, the net power P_{net} of the microgrid is characterised by its expected value $\hat{P}_{net}$. Note that predictions of $\hat{P}_{net}(k+j)$ are required to solve the optimization problem, and therefore the fuzzy model is used to obtained these values. Other constraints that must be considered in the optimization include the minimum and maximum limits of battery capacity:

$$E_{min} \leq E_B(k+j) \leq E_{max} \tag{4.6}$$

where minimum and maximum limits of use of the battery capacity are defined: $E_{min} = 0.2C_n$ and $E_{max} = 0.8C_n$, and C_n is the nominal capacity.

The limits for the maximum power for charging and discharging of the ESS are calculated using the following linear equations:

$$P_{max}^{\mathrm{dischg}}(k+j) = \alpha_{\mathrm{d}} P_B^{max} SoC(k+j) \tag{4.7}$$

$$P_{max}^{chg}(k+j) = \alpha_c P_B^{max}(1 - SoC(k+j)) \tag{4.8}$$

where P_B^{max} is the maximum instantaneous power given by the manufacturer, α_{d} and α_c are tuned parameters which avoid under/over SoC limits, respectively.

The overarching aims of the EMS are to maximise self-consumption (i.e. minimise energy exported to the main grid) and to minimise the power drawn from the main grid during peak periods. Therefore the minimum grid power is $P_{grid}^{min} = 0$, and the maximum grid power (P_{grid}^{max}) can be defined. With these considerations, the optimal control problem to be solved at time k is given by:

$$J = \min_{P_{mgref}(k+j)} \sum_{j=0}^{N-1} C(k+j) P_{mgref}(k+j) T_s \tag{4.9}$$

Subject to:

$$P_{mgref}(k+j) = \hat{P}_{net}(k+j) - P_B(k+j) \tag{4.9a}$$
$$-P_{grid}^{min} \leq P_{mgref}(k+j) \leq P_{grid}^{max} \tag{4.9b}$$
$$-P_{max}^{chg}(k+j) \leq P_B(k+j) \leq P_{max}^{\mathrm{dischg}}(k+j) \tag{4.9c}$$
$$E_B(k+j+1) = E_B(k+j) - TsP_B(k+j) \tag{4.9d}$$
$$E_{min} \leq E_B(k+j) \leq E_{max} \tag{4.9e}$$

Problem (4.9) is a linear program, whose solution can be found with any suitable solver. Matlab is used to code the optimization problem and it is solved by an interior-point algorithm. Finally, only the first element of the sequence, $P_{mgref}(k+j)$, is actually sent as a reference to the microgrid according to the RHC strategy, and the procedure is repeated at the discrete time instant $k+1$ (i.e. 30 min ahead).

4.3.2 Robust EMS with Explicit Uncertainty Compensation

The formulation of section 4.3.1 ignores the uncertainty of the predictions of the net power (P_{net}) drawn by the microgrid. While the closed-loop nature of the MPC controller provides some robustness to uncertainty, this is not explicitly incorporated in the controller. Including the uncertainty in the formulation may bring benefits in performance. This section deals with the uncertainty handling in the controller formulation.

Fuzzy prediction interval models are used to define the uncertainty of P_{net} predictions: ($\Delta\hat{P}_{net}(k+j)$). Therefore, net power P_{net} is characterised by the expected value $\hat{P}_{net}$ with

its variability: $P_{net}(k+j) = \hat{P}_{net}(k+j) + \Delta\hat{P}_{net}(k+j)$. This variability ($\Delta\hat{P}_{net}(k+j)$) is the deviation of the actual value from the prediction, therefore, is the uncertain component, but satisfies:

$$\Delta\hat{P}_{net}(k+j) \in [\Delta\hat{P}^{min}_{net}(k+j), \Delta\hat{P}^{max}_{net}(k+j)],$$

where

$$\Delta\hat{P}^{max}_{net}(k+j) = \overline{\hat{P}}_{net}(k+j) - \hat{P}_{net}(k+j) \tag{4.10}$$

$$\Delta\hat{P}^{min}_{net}(k+j) = \underline{\hat{P}}_{net}(k+j) - \hat{P}_{net}(k+j), \tag{4.11}$$

for $j = 1, \ldots, N-1$. $\overline{\hat{P}}_{net}$ and $\underline{\hat{P}}_{net}$ are the upper and lower bounds of the fuzzy prediction interval model. In this work, the prediction interval is designed to have a minimum interval width and to guarantee that the future real values are within the interval with a certain coverage probability level.

The solution for deterministic optimal control problems, as the one in deterministic MPC, is a sequence of control actions. This is not enough when there are uncertain components, as this ignores that there will be a correction of the disturbances by the closed-loop operation. It is shown in [122] that a computationally efficient alternative to acknowledge these corrections in the optimization is to explicitly compensate the uncertain terms with linear gains $L(k+j)$. In this study, the Robust MPC formulation proposed follows this idea. The following control laws for the predicted inputs of the optimization at time k, P_B and P_{mgref} are proposed:

$$P_B(k+j) = \hat{P}_B(k+j) + L(k+j)\Delta\hat{P}_{net}(k+j) \tag{4.12}$$

$$P_{mgref}(k+j) = \hat{P}_{mgref}(k+j) + (1 - L(k+j))\Delta\hat{P}_{net}(k+j), \tag{4.13}$$

where $\hat{P}_{mgref}(k+j)$, $\hat{P}_B(k+j)$ and $L(k+j)$ are the optimization variables, for $j = 0, \ldots, N-1$. This can be interpreted as follows: if $P_{net}(k+j) = \hat{P}_{net}(k+j)$ (thus $\Delta\hat{P}_{net}(k+j) = 0$), then $P_B(k+j) = \hat{P}_B(k+j)$. Otherwise, the predicted input to be applied to the system is compensated by $L(k+j)\Delta\hat{P}_{net}(k+j)$. Likewise, the compensation $(1-L(k+j))\Delta\hat{P}_{net}(k+j)$ is different for $P_{mgref}(k+j)$ in order to satisfy the balance equation (see 4.5) with the expected values of P_{mgref}, P_{net} and P_B:

$$\hat{P}_{mgref}(k+j) = \hat{P}_{net}(k+j) - \hat{P}_B(k+j) \tag{4.14}$$

Note that the predicted control laws of (4.12) and (4.13) depend on the uncertain values $\Delta\hat{P}_{net}(k+j)$, and this dependence is reflected in the use of the ESS (only dispatchable DER). However, the optimization problem as proposed in (4.9), cannot be solved with uncertain values. A worst case approach is taken then, where $\Delta\hat{P}_{net}(k+j)$ are assigned to take the worst possible values according to some criterion. In the Robust approach proposed, the constraints associated with the limits for the power reference (P_{mgref}) are equivalent to:

$$\hat{P}_{mgref}(k+j) + (1 - L(k+j))\Delta\hat{P}_{net}(k+j) \leq P_{grd}^{max}, \tag{4.15}$$

$$-\hat{P}_{mgref}(k+j) - (1 - L(k+j))\Delta\hat{P}_{net}(k+j) \leq P_{grd}^{min}. \tag{4.16}$$

These inequalities depend on $\Delta\hat{P}_{net}(k+j)$, which is uncertain. Therefore they are implemented by setting $\Delta\hat{P}_{net}(k+j)$ to take the values that are more constraining for $\hat{P}_{mgref}(k+j)$ in each of them: $\Delta\hat{P}_{net}^{\max}(k+j)$ and $\hat{P}_{net}^{\min}(k+j)$, respectively. Thus, they are invoked in the optimization as:

$$\hat{P}_{mgref}(k+j) + (1 - L(k+j))\Delta\hat{P}_{net}^{max}(k+j) \leq P_{grid}^{max} \tag{4.17}$$

$$-\hat{P}_{mgref}(k+j) - (1 - L(k+j))\Delta\hat{P}_{net}^{min}(k+j) \leq P_{grid}^{min} \tag{4.18}$$

Indeed, satisfying these constraints for the worst cases, as defined, will ensure that the power reference sent does not instruct the lower level to sell energy to the grid and that the power bought is greater than the upper limit.

Additionally, the proposed prediction interval provides several operating conditions of the microgrid from the perspective of the net power. The uncertainty limits $\Delta\hat{P}_{net}^{\min}$ and $\Delta\hat{P}_{net}^{\max}$ are interpreted as best and worst-case operating conditions, respectively, from the perspective of the demand (P_L) and available photovoltaic power (P_{PV}). Then, for all constraints associated to the ESS, the worst case is considered to be that where P_{net} is the largest; i.e. $\Delta P_{net}(k+j) := \Delta\hat{P}_{net}^{max}(k+j)$. This is the case with the most deficit of renewables with respect to demand, which is the instant where the ESS is the most needed to provide flexibility and reduce the energy bought from the grid. Therefore, the constraints associated with the minimum and maximum limits of use of the ESS and the limits of maximum power for charging and discharging of the ESS are defined as:

$$-Ts\sum_{\mathrm{i}=0}^{j}\hat{P}_B(k+\mathrm{i}) - Ts\sum_{\mathrm{i}=0}^{j}L(k+\mathrm{i})\Delta\hat{P}_{net}^{max}(k+\mathrm{i}) \leq E_{\max} - E_B(k) \tag{4.19}$$

$$Ts\sum_{\mathrm{i}=0}^{j}\hat{P}_B(k+\mathrm{i}) + Ts\sum_{\mathrm{i}=0}^{j}L(k+\mathrm{i})\Delta\hat{P}_{net}^{max}(k+\mathrm{i}) \leq -E_{\min} + E_B(k) \tag{4.20}$$

$$\hat{P}_B(k+j) + L(k+j)\Delta\hat{P}_{net}^{max}(k+j) \leq P_{max}^{\mathrm{dischg}}(k+j) \tag{4.21}$$

$$-\hat{P}_B(k+j) - L(k+j)\Delta\hat{P}_{net}^{max}(k+j) \leq P_{max}^{chg}(k+j) \tag{4.22}$$

where $j = 0, \ldots, N-1$. Note that because the microgrid is generally not operating all the time under the worst operating condition, a robust solution for the operation of the microgrid

is achieved. Therefore, with these considerations, the optimization problem to be solved at each time k is:

$$J = \min_{\substack{\widehat{P}_{mgref}(k+j) \\ \widehat{P}_B(k+j) \\ L(k+j)}} \sum_{j=0}^{N-1} C(k+j)\hat{P}_{mgref}(k+j)\ T_s \tag{4.23}$$

Subject to:

$$Eqs.\ (4.14), (4.17), (4.18), (4.19), (4.20), (4.21), (4.22) \tag{4.23a}$$
$$0 \leq L(k+j) \leq 1 \tag{4.23b}$$

The Robust MPC formulation is linear and can be tackled with suitable solvers. In this case, by an interior-point algorithm.

4.4 Case Study

In order to test the performance of the hierarchical EMS, a community connected to the main grid made up of 30 dwellings with a 50% level of photovoltaic power penetration has been considered (i.e. 15 dwellings have a photovoltaic array). The winter season data from a town in the UK is used. Fig. 4.4 shows a typical day's load profile (P_{Load}), photovoltaic power (P_{PV}) and the energy tariff used with a sample time of one minute.

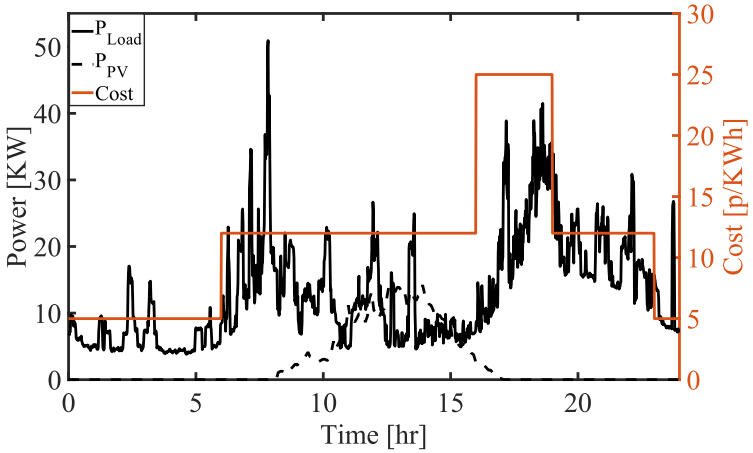

Figure 4.4: Profiles of Load, PV and Cost of a typical day

For this scenario, a three level ToU tariff (similar to [123]) has been considered for buying energy from the grid (in pence of pound sterling per kWh) - see Table 4.1. The same profile is used for each day of the simulation. For the scenario without an ESS, the surplus energy is exported to the main grid, therefore, 5p/kWh (pence per KWh) is used to quantify the financial benefit of this trade.

Table 4.1: Energy price during the day

Hours	Energy Cost
00:00 - 06:00	5 p/KWh
06:00 - 16:00	12 p/KWh
16:00 - 19:00	25 p/KWh
19:00 - 23:00	12 p/KWh
23:00 - 24:00	5 p/KWh

As was explained in Section 4.2, the ESS is the only dispatchable DER in the proposed microgrid, therefore, the storage capacity provides operational flexibility of the microgrid in order to achieve an optimal operation. Thereby, the ESS size is an important factor that could determine the effectiveness of the proposed EMS. In this study, an appropriate battery bank size is defined according to the community size and penetration level of renewable energy. Next, the proposed method to define the battery size is presented.

4.4.1 Sizing of Energy Storage System

From the simulation analysis, it was found that there exists a trade-off between the battery size and some performance indices that benefit the operation of the microgrid and the main grid. Therefore, the ESS size is selected based on the battery technology used, the controller proposed (which was explained in Section 4.2 and 4.3) and the specific operating conditions that will be explained below. In this approach, investment and replace metrics of the ESS are not included.

In this study, Trojan T-105 lead-acid batteries are considered, and the different sizes of the ESS are obtained connecting these batteries in series. The operational characteristics of the battery used are shown in Table 4.2.

For a community of 30 dwellings and 50% of the penetration level of photovoltaic power, the simulation is carried for different ESS sizes. Each battery bank is modelled using the Copetti model (For details of Copetti model, see appendix A1). Due that the majority of individual users within a microgrid have a consistent and routine pattern of daily energy for each season (winter for this case study), then, this simulation can give a suggestion of the ESS size.

The real-time controller at microgrid level and deterministic EMS at main grid level is executed in Matlab environment and the cost function (J) defined in (4.24) is evaluated for selecting the smaller size that achieves in a better way the desired operational behaviour for this case study:

Table 4.2: Characteristics of Trojan T-105 Lead-Acid Battery

Nominal Voltage	6V
Minimum Operation Voltage	5.25V
Maximum Operation Voltage	6.75V
Maximum Current	165A
Maximum SoC	0.8
Minimum SoC	0.2
Nominal Capacity	165Ah
Maximum Instantaneous Power	1C

$$J = \beta_1 \frac{RMSE^{w}}{RMSE^{w/o}} + \beta_2 \frac{Energy^{w}_{Export}}{Energy^{w/o}_{Export}} + \beta_3 \frac{(EFC_{\text{desired}} - EFC)^2}{EFC_{\text{desired}}} + \beta_4 LPSP + \beta_5 (1 - LF)^2 \tag{4.24}$$

$RMSE^{w}$ and $RMSE^{w/o}$ are the root mean square errors for a microgrid with ESS and without ESS, respectively. This term in the cost function (J), represents the capability of the microgrid for following the reference power (P_{mgref}) sent by the higher level in the hierarchical EMS proposed as is shown in (4.25):

$$RMSE = \sqrt{\frac{\sum_{k=1}^{T} \left(P_{mgref}(k) - P_{grid}(k)\right)^2}{T}} \tag{4.25}$$

$Energy^{w}_{Export}$ and $Energy^{w/o}_{Export}$ are the exported energy to the main grid (sold energy by the microgrid) for a microgrid with ESS and without ESS, respectively. In this approach, an ESS that avoids injecting energy surpluses into the main grid and promoted the self-consumption is desired.

The Equivalent Full Cycles (EFC), given by (4.26), are the number of full discharges that a battery bank performs throughout its time use [124]:

$$EFC = \frac{E_{\text{dis}}(Ah)}{C_n} \tag{4.26}$$

where $E_{\text{dis}}(Ah)$ is the discharge energy during the simulation time, and C_n is the nominal battery capacity. The EFC is a metric associated with the life cycle of the ESS, therefore

in this approach, one cycle per day is the desired EFC (EFC_{desired}) in the third term of the cost function (J) in (4.24).

The loss of power supply probability ($LPSP$) is the ratio between the energy deficiency (ED) and the total energy demands for a period of time [125, 126]. In this approach, the energy deficiency occurs when $(P_{net}(k) - P_{mgref}(k))T_s > 0$, which means that the available maximum power of the ESS (P_{max}^{dischg}) cannot fulfil the load, and therefore the energy deficiency is supplied from the main grid. When this case happens, means that the microgrid cannot follow the power reference (P_{mgref}) in a perfect manner, and therefore $P_{grid} = P_{mgref} + ED$. A lower value of the $LPSP$ indicates a higher probability that the load will be satisfied. For domestic applications, the recommended $LPSP$ value is less or equal to 10% [127]. As in the work of [128], in this study, the $LPSP$ is defined as:

$$LPSP = \frac{\sum_{k=1}^{T} T_k}{T}, \tag{4.27}$$

where T_k is the simulation time in which an energy deficiency occurs and T is the total simulation time. Finally, as the work of [41], the Load Factor (LF), given by (4.28), is a measure used to quantify the ratio between the average grid power (P_{grid}^{AVG}) and peak grid power (P_{grid}^{max}) during a given period. An improvement to the LF value indicates the peak load reduction:

$$LF = \frac{Avg(P_{\text{grid}})}{\max(P_{grid})} \tag{4.28}$$

The terms $\beta_{\text{i}}(\text{i} = 1, \ldots, 5)$ in the cost function are the weighting factors. For this study, the weighting factor β_1, associated with the RMSE, is a slightly bigger than the other ones because one of the objectives is tried to follow the power reference (P_{mgref}) sent by the higher level. Table 4.3 shows the results of the terms used to compute the cost function in (4.24) for ten different ESS sizes. The exported energy without ESS, $Energy_{Export}^{w/o}$ is 40.54KWh, and exported energy with ESS, $Energy_{Export}^{w}$ is zero for all the ESS sizes used in the simulation, therefore, this term does not affect the cost function. $EFC_{\text{desired}} = 7$ due that the results shown in the Table 4.3 correspond to the simulation of typical one week of the winter season. The results suggest that an ESS with 135KWh nominal capacity is the smaller battery bank that achieves the desired operational behaviour, which corresponds to 4.5KWh per dwelling. However, an ESS with 120KWh of capacity has a similar behaviour than the previous one, as shown in Table 4.3. With this ESS size, 4kWh per dwelling is used.

Finally, it is important to remark that the results could change is another battery technology, different strategies control and/or different operational requirement for the microgrid and main grid are considered. The fuzzy prediction interval model for obtaining the expected value and quantifying the uncertainty of the net power P_{net} of microgrid is presented in the next section.

Table 4.3: Performance Indices of Cost Function in (4.24)

Battery Capacity (KWh)	**RMSE (KW)**	**RMSE$^{w/o}$ (KW)**	**EFC (Cycles)**	**LPSP (%)**	**LF**	**J**
75	1.77	9.61	7.97	6.35	0.371	0.871
90	1.78	10.67	7.52	5.95	0.389	0.721
105	1.90	11.68	7.14	5.65	0.389	0.676
120	1.51	12.32	6.79	4.76	0.388	0.612
135	1.22	12.91	6.40	3.78	0.387	0.606
150	1.11	13.40	6.09	3.54	0.385	0.656
165	1.12	13.91	5.81	3.14	0.383	0.736
180	1.04	14.47	5.58	2.62	0.381	0.805
195	1.01	15.09	5.37	2.56	0.380	0.889
210	0.95	15.59	5.21	2.54	0.378	0.959

4.4.2 Fuzzy Prediction Interval for Net Power of Microgrid

The load (P_L) and photovoltaic power (P_{PV}) from a town in the UK considered in this study are used to develop the fuzzy prediction interval model. A period of 90 days correspond to the winter season is used, which is divided into training, validation and test data. The training data are obtained as the average value of the measured data with a one-minute resolution. The maximum value of the net power (P_{net}) is 67.57kW and the minimum value is -45.09kW and a sample time of 30 minutes is used.

The relevant regressors obtained during the model identification process for the net power of the microgrid, given by $P_{net} = P_L - P_{PV}$ are shown in (4.29):

$$\begin{aligned}\hat{P}_{net}(k) = f^{fuzzy}(&P_{net}(k-1), P_{net}(k-2), P_{net}(k-8), P_{net}(k-25), P_{net}(k-26), P_{net}(k-32),\\ &P_{net}(k-38), P_{net}(k-42), P_{net}(k-43), P_{net}(k-44), P_{net}(k-46), P_{net}(k-48))\end{aligned} \tag{4.29}$$

Four rules correspond to the optimal structure for the fuzzy model. Note that exogenous variables are not included in the model. In this study, the prediction interval model is tuned at a desired prediction interval coverage probability *(PICP)* of 90% for all prediction horizons. The *PICP* is used to quantify the number of measured values that fall within the interval defined by the model, and *PINAW* is used to measure the width of the interval. Additionally, the *RMSE* and *MAE* are included as performance indices to evaluate the accuracy of the prediction model associated with the expected value.

Table 4.4 shows the performance indices for three different prediction horizons used with the test dataset. The results suggest that the fuzzy prediction interval was effectively tuned to approximately 90% of the desired *PICP*, and the interval width *(PINAW)* increases with the prediction horizon, however, this width corresponded to the minimum width for characterizing the uncertainty of the net power of the microgrid (P_{net}).

Table 4.4: Performance Indices of Fuzzy Prediction Interval Model

Performance	**Prediction Horizon**		
Indices	**One-hour ahead**	**Six-hours ahead**	**One-day ahead**
RMSE (kW)	4.5136	5.0471	5.1974
MAE (kW)	3.2995	3.7316	3.7530
PINAW (%)	22.73	27.62	28.02
PICP (%)	88.22	89.79	89.83

Fig. 4.5 shows one-day ahead prediction intervals, tuned with 90% coverage probability, using a rolling horizon strategy. In this figure, three days of the test dataset are presented. Furthermore, the expected value ($\hat{P}_{net}$) and lower ($\underline{\hat{P}}_{net}$) and upper ($\overline{\hat{P}}_{net}$) bounds provided by the prediction interval have been used to develop both the deterministic and robust EMS as was explained in previous section.

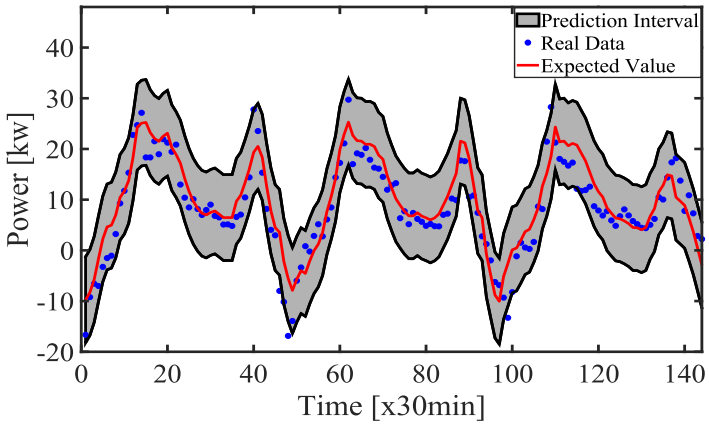

Figure 4.5: One-day ahead Prediction Interval for Power Net tuned at $PICP = 90\%$

4.4.3 Hierarchical EMS Results

In this case study, an ESS based on lead-acid batteries with 135KWh capacity is selected, based on the results obtained from the methodology presented in Section 4.4.1. Simulation results from the deterministic EMS (Section 4.3.1) and robust EMS (Section 4.3.2) for the higher level management of the microgrid are presented next, and they are compared with a basic EMS without ESS, where the energy required to satisfy the energy balance in the microgrid is either bought or sold from the main grid.

Fig. 4.6 shows the behaviour of the hierarchical EMS algorithms (Deterministic and Robust EMS) for operation over two days. The green line shows the original load demand of the community, the red line shows the power reference (P_{mgref}) obtained during the optimization process from the higher level (MPC controller), and the blue line shows the actual main grid

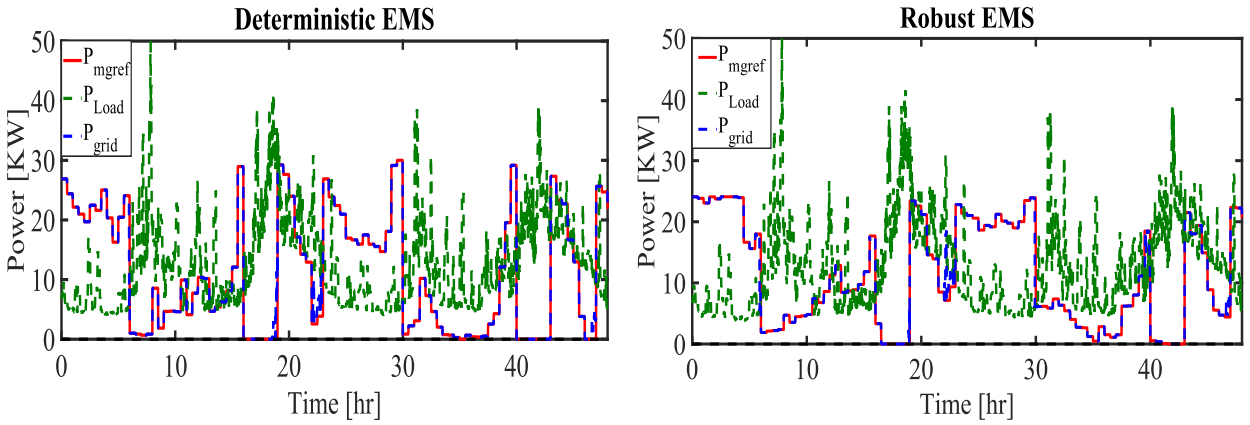

(a) (b)

Figure 4.6: Performance of Hierarchical EMS Proposed a) Deterministic Approach; b) Robust Approach

power when the EMS is used. The results show that both approaches have the capacity to follow the power reference reasonably well and reduce the peak load power drawn from the main grid. The tracking errors occur when the available maximum battery power for charging or discharging are less than the ESS power required by the microgrid (see rules in Section 4.2). This, in turn, could happen due to prediction errors and/or the errors by the linearization of the SoC and the available maximum power of ESS made in the higher level Energy Profiler.

From Fig. 4.6, it can see that the Robust EMS has a flatter power reference than the deterministic EMS, which is better for the distribution network operator. Results are consistent with the energy prices (see Table 4.1). For instance, the time block of 16:00 to 19:00 hours is the most expensive time to draw power from the main grid, but using the EMS the actual power drawn from the main grid is close to zero. During this time period, the peak load reduction occurs through the use of the ESS. The opposite behaviour occurs during morning hours (0:00-06:00 and 23:00-24:00) where the energy price is much cheaper.

Table 4.5 shows the energy costs, the tracking error of the power reference (P_{mgref}) measured by the *RMSE*, the equivalent full cycles *(EFC)*, and the loss of power supply probability *(LPSP)* of one-week simulation using the deterministic and robust EMS approaches.

Table 4.5: Performance Indices during a simulation of one week duration

EMS Strategy	**Cost (£)**	**RMSE (kW)**	**EFC Cycles**	**LPSP (%)**
Deterministic EMS	168.01	1.22	6.40	3.780
Robust EMS	165.28	1.14	6.07	2.927

The energy cost of the microgrid for one week without the ESS is £255.43. Note that the energy required to satisfy the energy balance in the microgrid is only bought or sold from the main grid. Therefore, a reduction of £87.42 corresponding to 34.22% is achieved using the deterministic EMS, and a reduction of £90.15 (35.29%) is achieved by the Robust EMS. Assuming this reduction is the average saving during each winter week a total of £1123.9 and £1159.1 are saved during this season with respect to the case without the ESS, with the deterministic EMS and Robust EMS, respectively.

Although the energy cost with the deterministic and robust approaches are similar, other metrics are also improved with the robust EMS, as shown in Table 4.5. The lower *RMSE* with the Robust EMS means that this approach follows in a better way the power reference (P_{mgref}) sent by the higher level to the microgrid (see Fig. 4.6). In addition, the lower *EFC* of the Robust EMS demonstrates fewer cycles of the ESS required for the same microgrid behavior which directly improves the state-of-the-health *(SoH)* and lifetime of the ESS. As battery ageing (measured by *SoH*) is a function of the elapsed time from the manufacture date, as well as the usage by consecutive charge and discharge actions, a lower *EFC* can improve the battery life time, and therefore, the replacement time of the battery bank could be longer with the Robust EMS compared to the deterministic EMS. Finally, the *LPSP* of 3.780% for the deterministic EMS corresponds to the percentage time which the microgrid cannot fulfil the load requirements using the reference power (P_{mgref}) defined by the higher level and the available resources of the microgrid (PV and ESS). The Robust EMS reduces this performance index to 2.927%. This is achieved because the robust approach compensates for the uncertainty into the ESS power and the power reference by means of the L gains (see Section 4.3.2). Therefore, this approach results in a better use of the ESS, as shown in the SoC behaviour (see Fig. 4.7).

The periods highlighted by the rectangles in Fig.4.7 show that the Robust EMS achieves a charge close to the maximum SoC before starting the discharging process which reduces the probability of loss of power supply. Additionally, Fig. 4.7 shows that the ESS works in the safe operation ranges. At all times the SoC is between 20% and 80% and the voltage is

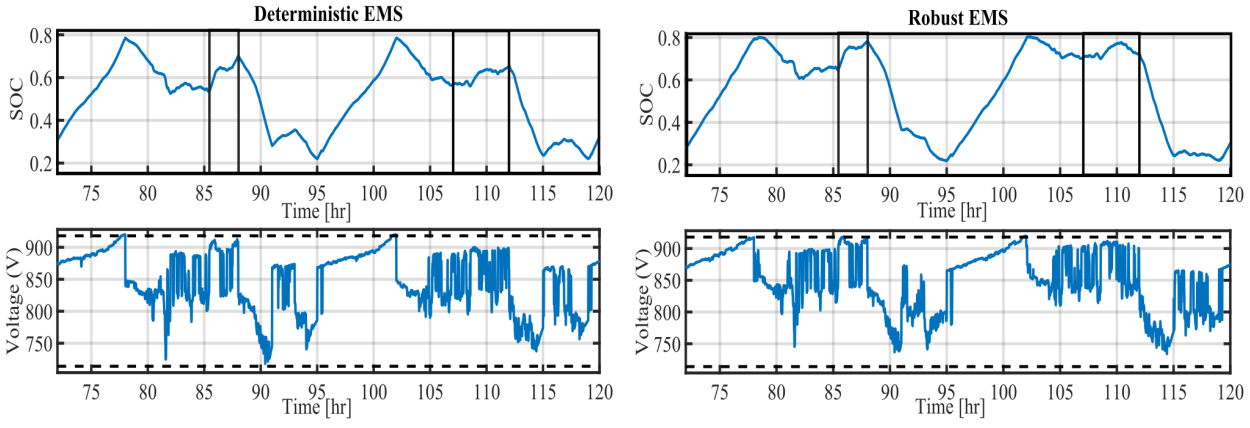

(a) (b)

Figure 4.7: Microgrid ESS SOC and Voltage Behaviour a) Deterministic EMS; b) Robust EMS

between the minimum and maximum values given by the manufacturer (dotted lines on the bottom figures).

Table 4.6 shows the amount of the energy bought by the community from the main grid during the different time periods associated with different tariff prices shown in Table 4.1. C1 correspond to the time with the cheaper price and C3 to the expensive price. As mentioned above, the operation of the hierarchical EMS's (deterministic and robust) is consistent with these price bands: more energy is bought at the cheaper price (C1) and less energy is bought at the expensive price (C3) compared to the scenario without the ESS strategy. The amount of the energy bought at the C2 price is similar for all EMS's strategies reported in Table 4.6. Additionally, deterministic and robust approaches avoid exporting energy to the main grid which is a required condition in this study and it is included in the constraints in the optimization.

Table 4.6: Energy Distribution at different Prices

EMS Strategy	**Export (kWh)**	**C1 (kWh)**	**C2 (kWh)**	**C3 (kWh)**
Without ESS	40.546	357.097	1087.877	436.215
Deterministic EMS	0.000	990.361	934.338	25.483
Robust EMS	0.000	994.081	931.231	15.321

Finally, with the purpose of quantifying the power profile of the main grid for the different controllers, several indexes of operation are presented in Table 4.7. These are the load factor (LF), the load loss factor (LLF), positive power peak (P^+), negative power peak (P^-), power variation range (PVR), maximum power derivative (MPD) and average power derivate (APD) are used and the results are shown in Table 4.7.

An improvement to the LF value indicates the reduction of peak load (see definition in Eq. 4.28). LLF, given by (4.30), is a measure of losses incurred as a result of peak power [41]:

$$LLF = \frac{Avg(P_{grid}^2)}{max(P_{grid}^2)} \tag{4.30}$$

Table 4.7: Quality Indices for Quantifying of the Power Profile of the Main Grid

EMS Strategy	**LF**	**LLF**	**P$^+$** (kW)	**P$^-$** (kW)	**PVR** (%)	**MPD** (kW/min)	**APD** (kW/min)
Without ESS	0.2119	0.0717	51.71	-14.86	100	19.67	1.1659
Deterministic EMS	0.3869	0.2452	30.00	0	45.06	29.63	0.1889
Robust EMS	0.4459	0.2880	25.90	0	38.91	22.48	0.1318

The power variation range (PVR) quantifies the ratio between the difference of the maximum ($P^{w}_{grid,max}$) and minimum ($P^{w}_{grid,min}$) grid power values when the deterministic or robust EMS are used and those maximum ($P^{w/o}_{grid,max}$) and minimum ($P^{w/o}_{grid,min}$) grid power values obtained without the ESS [129]:

$$PVR = \frac{P^{w}_{grid,max} - P^{w}_{grid,min}}{P^{w/o}_{grid,max} - P^{w/o}_{grid,min}} \tag{4.31}$$

The maximum power derivative (MPD) is the maximum value of the rate of change between two consecutive points of the main grid power in its absolute value [62, 130]:

$$MPD = \max(|\Delta P_{grid}(k)|) \tag{4.32}$$

where $\Delta P_{grid}(k) = P_{grid}(k) - P_{grid}(k-1)$. Finally, the average power derivate (APD) is the average of the absolute value of the rate of change of the main grid power:

$$APD = \frac{1}{T}\sum_{k=1}^{T} |\Delta P_{grid}(k)| \tag{4.33}$$

The LF increases from 0.2119 to 0.3869 when deterministic EMS is implemented compared to when there is no ESS. This LF value rises to 0.4459 with Robust EMS, therefore this EMS approach results in better peak power reduction. In a similar way, the LLF rises from 0.0717 to 0.2452 when the deterministic EMS is compared to the scenario with no ESS. The LLF value is 0.2880 for Robust EMS which means that this strategy has a significant reduction of losses incurred as a result of peak power.

The positive power peak (P^{+}) and negative power peak (P^{-}) for the hierarchical EMS proposed is limited by the constraints associated with the minimum and maximum power from the main grid as explained in the formulation of the optimization problem. Therefore, constraints in the EMS guarantee that no energy is exported to the main grid. On the other hand, the maximum main grid power (P^{max}_{grid}), in the optimization problem, is defined as 30kW. The Robust EMS works in a more conservative manner for the upper limit. It attempts to avoid sub-optimal operation due to worst case realizations: thus it allows smaller peaks ($P^{+} = 25.9kW$) than the deterministic EMS ($30kW$) (see also Fig. 4.8).

As can be seen in Table 4.7, the last three metrics are significantly improved using the hierarchical EMS proposed. The PVR is reduced to 45.06% and 38.91% compared to the case without the ESS when deterministic EMS and robust EMS respectively are used. Finally, the APD criterion has a significant reduction which corresponds to a flatter main grid power (see Fig. 4.8), although the maximum value of the ramp-rate of the power (measured by MPD) is low for the strategy without the ESS. It should be noted that the analyses presented in this section are representative of the specific microgrid described, with the given operational characteristics and limitations of the DG and ESS of this specific system. Therefore, changing the characteristics or penetration levels of these components could affect the results to some degree.

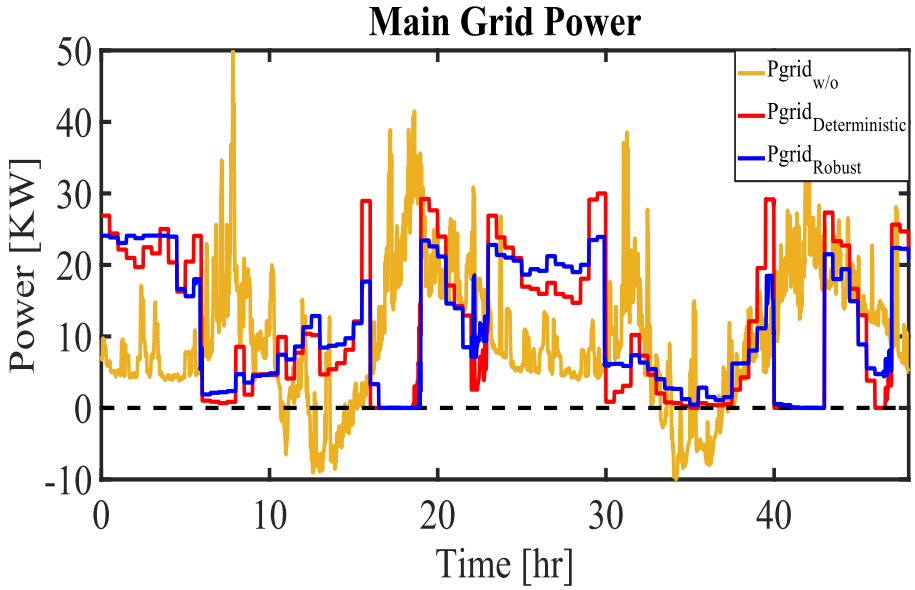

Figure 4.8: Main Grid Power Profiles

4.5 Discussion

In this chapter, a hierarchical two-level EMS was developed for energy community (microgrid) operation, considering the uncertainty of the renewable energy resources and electrical load consumption. At the lower (microgrid) level, a rule-based controller was implemented, whereas at the higher (main grid) level, a Robust MPC was used – the Energy Profiler. The aim was to incorporate the benefits of both non-optimal controllers and optimal controllers.

The hierarchical EMS proposed was tested using an energy community connected to the main grid made up of 30 dwellings with 50% photovoltaic power penetration level and as ESS of 135kWh. Results showed that the hierarchical EMS can benefit both the end user and the operator of the distribution network: the EMS is able to keep the community power flow close to the reference power defined by Robust MPC and provide minimum energy cost. Additionally, safe operation of the ESS and a peak load reduction were achieved.

Chapter 5

Hierarchical Energy Management System for Microgrid Coordination

This chapter proposes a hierarchical scheme based on two-level EMS for microgrid coordination which realises both short-term power balancing and long-term energy management, benefiting both the energy community members and the distribution network operator (DNO). The hierarchical two-level structure addresses both the uncertainty of the renewable energy resources and the variability in end-user consumption profiles. The performance of the proposed hierarchical EMS is tested with two case studies. The first case study corresponds to an energy community made up of two microgrids with different numbers of dwellings, renewable energy (Photovoltaic and Wind Energy) and ESS based on lead-acid batteries. The second case study corresponds to an energy community made up of three microgrids. For this latter case, a microgrid with a school demand profile is included with the aim to exploiting complementary power profiles.

5.1 Introduction

This chapter concerns the design of a hierarchical EMS for microgrid coordination, including the characterization of uncertainty associated with renewable DG and load. As it was explained in the previous chapter, in this thesis a two-level EMS is developed. The aim is to incorporate the benefits of schemes based on both receding horizon control and real-time decision-making. Therefore, the proposed EMS for microgrid coordination comprises a real-time control strategy which uses a rule-based approach at the lower level (for each microgrid) and a Robust MPC at the higher level as shown in Fig. 5.1.

In this framework, each microgrid has its own energy generation provided from a renewable energy sources (RES), non-controllable load and an ESS. The overarching aims of the EMS for the coordination of microgrids are to maximise self-consumption of the energy community (i.e. share energy between microgrids and minimise energy exported to the main grid) and to minimise the power drawn from the main grid during peak periods.

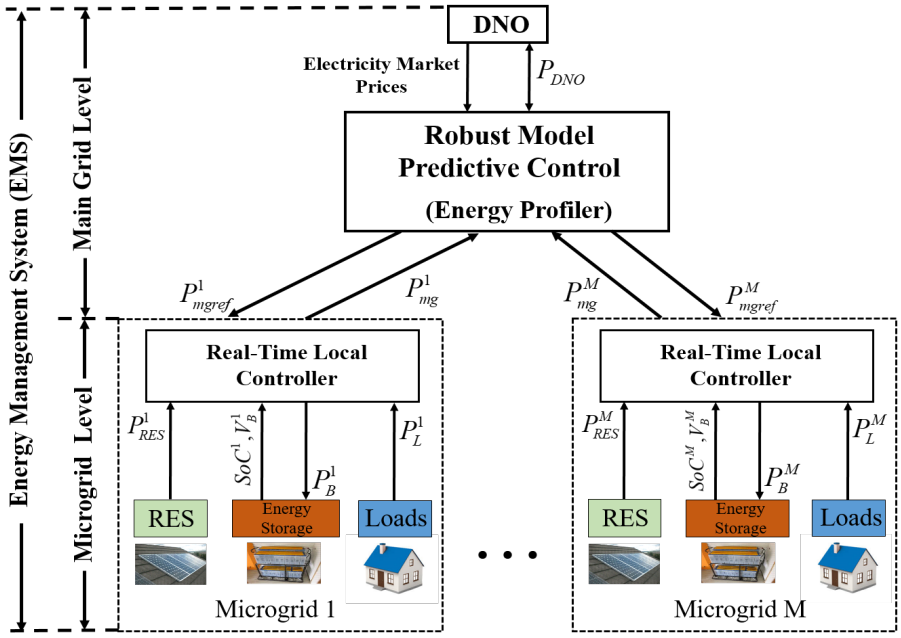

Figure 5.1: Hierarchical Control Structure for Microgrid Coordination

A centralized controller – the Energy Profiler – sets the power references P^{i}_{mgref} $\mathrm{i} = 0, \ldots, M$ for each $\mathrm{i}-th$ microgrid that make up the energy community. This Energy Profiler optimises the energy cost for the community over a prediction horizon, while considering safe limit constraints for each ESS at the microgrid level and power transfer to and from the main grid. A sample time of 30 min is considered, which defines the update frequency of P^{i}_{mgref}. A centralized controller – the Energy Profiler – sets the power references P^{i}_{mgref} $\mathrm{i} = 0, \ldots, M$ for each $\mathrm{i}-th$ microgrid that make up the energy community. This Energy Profiler optimises the energy cost for the community over a prediction horizon, while considering safe limit constraints for each ESS at the microgrid level and power transfer to and from the main grid. A sample time of 30 min is considered, which defines the update frequency of P^{i}_{mgref}.

The local real-time controller (at the microgrid level) used for every microgrid is the same that was explained in Section 4.2. In this framework, this controller controls the net power flowing from the point of common coupling (PCC) to the microgrid (P^{i}_{mg}) or vice versa so that it tracks the power reference (P^{i}_{mgref}) sent from the central Energy Profiler at the main grid level. The following sections present the details of the deterministic and Robust MPC strategies at the higher level: the Energy Profiler for microgrid coordination.

5.2 Model Predictive Control for Microgrid Coordination

At the main grid level, the power references (P^{i}_{mgref}) $\mathrm{i} = 0, \ldots, M$ are calculated taking into consideration the operation restriction of the microgrid level so that the local controller can follow the reference with a minimum tracking error, as well as the system works with minimum energy costs.

In this framework, the fuzzy prediction intervals models are used to anticipate the behaviour of the expected value over a prediction horizon, and the variability of both the demand and the energy available from the renewable resources. This information is used in the Energy Profiler design which uses the receding horizon control strategy. Finally, the same Time of Use (ToU) tariff showed in Table 4.1 (chapter 4) is used for buying energy from the main grid. In this scheme, three price levels are used called off-peak, mid-peak and peak (see Fig. 4.4). For the scenario without an ESS, 5p/kWh (pence of pound sterling per KWh) is used to quantify the financial benefit of the trade surplus energy exported to the main grid.

5.2.1 Deterministic Coordination of Microgrids

This section presents an extension of the deterministic EMS presented in Section 4.3.1 to energy communities that are made up of multiples microgrids (see Fig. 5.1). Therefore, at each discrete time instant k an optimization problem is solved to find the optimal sequence of $P^{\mathrm{i}}_{mgref}(k+j)$ with $\mathrm{i} = 1, \ldots, M$ and $j = 0, \ldots, N-1$ that minimizes the energy consumption of multiples microgrids during the prediction horizon N. $C(k+j)$ is the energy price and $P_{DNO}(k+j)$ is the total power bought from the main grid and therefore, it should meet the power balance with the sum of reference powers (P^{i}_{mgref}) of all the microgrids ($\mathrm{i} = 1, \ldots, M$) that make up the Energy Community:

$$P_{DNO}(k+j) = \sum_{\mathrm{i}=1}^{M} P^{\mathrm{i}}_{mgref}(k+j). \tag{5.1}$$

The above means that the microgrids can share energy between the members of the Energy Community, guaranteeing that the constraints imposed by the distribution network operator be achieved. Therefore, other constraints that must be considered in the optimization include the minimum and maximum main grid powers:

$$-P^{min}_{DNO} \leq P_{DNO}(k+j) \leq P^{max}_{DNO}. \tag{5.2}$$

Because the aims of the EMS are to maximise self-consumption (i.e. minimise energy exported to the main grid) and to minimise the power drawn from the main grid during peak periods, the minimum limit is $P^{min}_{DNO} = 0$ and the maximum power P^{max}_{DNO} can be defined in order to reduce the peak load, for example during peak periods. However, in the microgrid coordination approach, the reference power (P^{i}_{mgref}) of each microgrid can take negative values (sharing energy into the community) to achieve the defined aims of the energy community in a collaborative way. Additionally, that condition enlarges the feasible set of the optimization problem compared to the operation of energy community made up of an only microgrid, as was presented in chapter 4.

For this approach, the net power ($P^{\mathrm{i}}_{net} = P^{\mathrm{i}}_{L} - P^{\mathrm{i}}_{RES}$) of the i-th microgrid ($\mathrm{i} = 1, \ldots, M$) is given by its expected values $\hat{P}^{\mathrm{i}}_{net}(k+j)$ which are obtained by the fuzzy prediction interval models,where P^{i}_{L} is the demand of each microgrid and P^{i}_{RES} are the renewable energy

resources (PV and Wind) available in each microgrid. Therefore, the constraints associated to power balance for each microgrid are invoked in the optimization problem as:

$$P^{\mathrm{i}}_{mgref}(k+j) = \hat{P}^{\mathrm{i}}_{net}(k+j) - P^{\mathrm{i}}_{B}(k+j) \quad \text{for} \quad \mathrm{i} = 1, \ldots, M. \tag{5.3}$$

where P^{i}_{B} is the power profile of each ESS. The last constraints in the MPC optimization are associated to the ESS of each microgrid, and correspond to the evolution of the energy in the ESS (E^{i}_{B}) (see Eq. 5.4d), the minimum (E^{i}_{min}) and maximum (E^{i}_{max}) limits of battery capacity (see Eq. 5.4e) and the limits for charging ($P^{chg,\mathrm{i}}_{max}$) and discharging ($P^{\mathrm{dis}chg,\mathrm{i}}_{max}$) of the ESS (see Eq. 5.4f). These constraints are invoked in the optimization problem using the same simplified models used in chapter 4 for the ESS of the i-th microgrid. Therefore, with these considerations, and the fact the the EMS also aims to minimise costs, the optimal control problem to be solved at time k for all $j = 0, \ldots, N-1$ is given by:

$$J = \min_{\substack{P^1_{mgref}(k), \cdots, P^1_{mgref}(k+N-1) \\ \vdots \\ P^M_{mgref}(k), \cdots, P^M_{mgref}(k+N-1)}} \sum_{j=0}^{N-1} C(k+j) P_{DNO}(k+j)\, T_s \tag{5.4}$$

Subject to:

$$P_{DNO}(k+j) = \sum_{\mathrm{i}=1}^{M} P^{\mathrm{i}}_{mgref}(k+j) \tag{5.4a}$$

$$-P^{min}_{DNO} \leq P_{DNO}(k+j) \leq P^{max}_{DNO} \tag{5.4b}$$

$$P^{\mathrm{i}}_{mgref}(k+j) = \hat{P}^{\mathrm{i}}_{net}(k+j) - P^{\mathrm{i}}_{B}(k+j) \tag{5.4c}$$

$$E^{\mathrm{i}}_{B}(k+j+1) = E^{\mathrm{i}}_{B}(k+j) - T_s P^{\mathrm{i}}_{B}(k+j) \tag{5.4d}$$

$$E^{\mathrm{i}}_{min} \leq E^{\mathrm{i}}_{B}(k+j) \leq E^{\mathrm{i}}_{max} \tag{5.4e}$$

$$-P^{chg,\mathrm{i}}_{max}(k+j) \leq P^{\mathrm{i}}_{B}(k+j) \leq P^{\mathrm{dis}chg,\mathrm{i}}_{max}(k+j) \tag{5.4f}$$

Finally, only the first element of the sequence, $P^{\mathrm{i}}_{mgref}(k)$, is sent as a reference to each microgrid ($\mathrm{i} = 1, \ldots, M$) according to the RHC strategy, and the procedure is repeated at the next time instant $k+1$ (i.e. 30 min ahead).

5.2.2 Robust Coordination of Microgrids with Explicit Uncertainty Compensation

This section presents an extension of the Robust EMS presented in Section 4.3.2 to energy communities that are made up of multiples microgrids. In this approach, the uncertainty of the net power (P^{i}_{net}) of the microgrids is included explicitly in the formulation of the optimization problem using the uncertainty prediction given by the fuzzy prediction interval models.

The real values of the net power ($P^{\mathrm{i}}_{net}(k+j)$) for the i-th microgrid satisfy:

$$P^{\mathrm{i}}_{net}(k+j) = \hat{P}^{\mathrm{i}}_{net}(k+j) + \Delta\hat{P}^{\mathrm{i}}_{net}(k+j) \quad \text{for} \quad \mathrm{i} = 1, \ldots, M \tag{5.5}$$

where $\hat{P}^{\mathrm{i}}_{net}$ is the expected value of the prediction and $\Delta\hat{P}^{\mathrm{i}}_{net}(k+j)$ is the deviation of the actual value from the prediction. The deviations are uncertain, but satisfies:

$$\Delta\hat{P}^{\mathrm{i}}_{net}(k+j) \in [\Delta\hat{P}^{min,\mathrm{i}}_{net}(k+j), \Delta\hat{P}^{max,\mathrm{i}}_{net}(k+j)] \tag{5.6}$$

where

$$\Delta\hat{P}^{max,\mathrm{i}}_{net}(k+j) = \overline{\hat{P}}^{\mathrm{i}}_{net}(k+h) - \hat{P}^{\mathrm{i}}_{net}(k+h) \tag{5.7}$$

$$\Delta\hat{P}^{min,\mathrm{i}}_{net}(k+j) = \underline{\hat{P}}^{\mathrm{i}}_{net}(k+h) - \hat{P}^{\mathrm{i}}_{net}(k+h), \tag{5.8}$$

where $\overline{\hat{P}}^{\mathrm{i}}_{net}(k+j)$ and $\underline{\hat{P}}^{\mathrm{i}}_{net}(k+j)$ are the upper and lower bounds of the prediction interval, respectively, and $\hat{P}^{\mathrm{i}}_{net}(k+j)$ the expected value given by the prediction models. In this approach, these prediction interval models are designed to have a minimum interval width and guarantee that the future real values fall within the interval with a certain coverage probability.

As was presented in section 4.3.2, in this approach, the Robust MPC formulation includes the uncertainty explicitly in the optimization problem with linear gains $L(k+j)$ to compensate the uncertain terms. Then, following the same idea for microgrid coordination, the following control law (for each i-th microgrid) for the predicted inputs of the optimization at time k is proposed:

$$P^{\mathrm{i}}_{B}(k+j) = \hat{P}^{\mathrm{i}}_{B}(k+j) + L^{\mathrm{i}}(k+j)\Delta\hat{P}^{\mathrm{i}}_{net}(k+j) \tag{5.9}$$

$$P^{\mathrm{i}}_{mgref}(k+j) = \hat{P}^{\mathrm{i}}_{mgref}(k+j) + (1 - L^{\mathrm{i}}(k+j))\Delta\hat{P}^{\mathrm{i}}_{net}(k+j) \tag{5.10}$$

where $\hat{P}^{\mathrm{i}}_{mgref}(k+j)$, $\hat{P}^{\mathrm{i}}_{B}(k+j)$ and $L^{\mathrm{i}}(k+j)$ are the optimization variables, for $\mathrm{i} = 1, \ldots, M$ and $j = 0, \ldots, N-1$, and the gains $L^{\mathrm{i}}(k+j)$ satisfy:

$$0 \leq L^{\mathrm{i}}(k+j) \leq 1, \tag{5.11}$$

which indicates that the deviation of the real value from the prediction is compensated by $P^{\mathrm{i}}_{B}(k+j)$ and $P^{\mathrm{i}}_{mgref}(k+j)$ in a proportion defined by $L^{\mathrm{i}}(k+j)$ for $\mathrm{i} = 1, \ldots, M$. It is important to remark that with this control law (see Eqs 5.9 and 5.10), the power balance for each microgrid is satisfied with the expected values of P^{i}_{B}, P^{i}_{net} and P^{i}_{mgref}:

$$\hat{P}^{\mathrm{i}}_{mgref}(k+j) = \hat{P}^{\mathrm{i}}_{net}(k+j) - \hat{P}^{\mathrm{i}}_{B}(k+j). \tag{5.12}$$

Due that the optimization problem cannot be solved with uncertain values, the uncertain component $\Delta\hat{P}^{\mathrm{i}}_{net}(k+j)$ is considered in the constraints using the same criteria that was explained in section 4.3.2, and therefore the constraint which imposes the limits for P_{DNO} is invoked in the optimization problem as:

$$\sum_{\mathrm{i}=1}^{M}[\hat{P}^{\mathrm{i}}_{mgref}(k+j) - L^{\mathrm{i}}(k+j)\Delta\hat{P}^{max,\mathrm{i}}_{net}(k+j)] \leq P^{max}_{DNO} - \sum_{\mathrm{i}=1}^{M}\Delta\hat{P}^{max,\mathrm{i}}_{net}(k+j) \tag{5.13}$$

$$-\sum_{\mathrm{i}=1}^{M}[\hat{P}^{\mathrm{i}}_{mgref}(k+j) + L^{\mathrm{i}}(k+j)\Delta\hat{P}^{min,\mathrm{i}}_{net}(k+j)] \leq \sum_{\mathrm{i}=1}^{M}\Delta\hat{P}^{min,\mathrm{i}}_{net}(k+j) - P^{min}_{DNO} \tag{5.14}$$

The constraints associated with the ESS of each microgrid (Eqs. 5.4d, 5.4e, 5.4f) are reformulated as:

$$-T_s\sum_{n=0}^{j}\hat{P}^{\mathrm{i}}_{B}(k+n) - T_s\sum_{n=0}^{j}L^{\mathrm{i}}(k+n)\Delta\hat{P}^{max,\mathrm{i}}_{net}(k+n) \leq E^{\mathrm{i}}_{max} - E^{\mathrm{i}}_{B}(k) \tag{5.15}$$

$$T_s\sum_{n=0}^{j}\hat{P}^{\mathrm{i}}_{B}(k+n) + T_s\sum_{n=0}^{j}L^{\mathrm{i}}(k+n)\Delta\hat{P}^{max,\mathrm{i}}_{net}(k+n) \leq -E^{\mathrm{i}}_{min} + E^{\mathrm{i}}_{B}(k) \tag{5.16}$$

$$\hat{P}^{\mathrm{i}}_{B}(k+j) + L^{\mathrm{i}}(k+j)\Delta\hat{P}^{max,\mathrm{i}}_{net}(k+j) \leq P^{\mathrm{dis}chg,\mathrm{i}}_{max}(k+j) \tag{5.17}$$

$$-\hat{P}^{\mathrm{i}}_{B}(k+j) - L^{\mathrm{i}}(k+j)\Delta\hat{P}^{max,\mathrm{i}}_{net}(k+j) \leq P^{chg,\mathrm{i}}_{max}(k+j) \tag{5.18}$$

Finally, with all these considerations, the optimization problem to be solved at each time k is:

$$\begin{aligned} J = \min_{\substack{x^1(k),\ldots,x^1(k+N-1)\\ \vdots \\ x^M(k),\ldots,x^M(k+N-1)}} & \sum_{j=0}^{N-1} C(k+j)P_{DNO}(k+j)\ T_s \\ \text{subject to (5.11)-(5.18) all for } & j = 0,\ldots,N-1. \end{aligned} \tag{5.19}$$

where $x^{\mathrm{i}} = \{\hat{P}^{\mathrm{i}}_{mgref}, \hat{P}^{\mathrm{i}}_{B}, L^{\mathrm{i}}\}$ for $\mathrm{i} = 1,\ldots,M$. This optimization problem is linear and can be tackled with suitable solvers. In this case, by an interior-point algorithm. Among the benefits of this algorithm are its fast processing time and the low computational cost and the capability to traverse through the feasible region during its execution. Thus, the RHC strategy at the higher level MPC controller includes the following steps:

1. Get the initial condition at the initial discrete time k. The current states of the SoC^{i} for $\mathrm{i} = 1, \ldots, M$ are estimated by the UKF filter at the microgrid level which sends this information to the higher level.

2. The linear optimization problem finds the optimal sequences of the power reference (P^{i}_{mgref}) of each microgrid that minimizes the energy consumption during the prediction horizon, using the interior-point algorithm and considering all the constraints described in Eq. 5.19 and the initial conditions of the ESS of each microgrid. The expected value and the upper and lower bounds of the net power (P^{i}_{net}) of each microgrid are inputs variables of the MPC controller. These values are obtained by the fuzzy prediction interval models. In this case, the prediction horizon is one day, 48 steps with a sampling time of 30 minutes.

3. The first element of the sequence of the power reference (P^{i}_{mgref}) is sent to the real-time controller of each microgrid at the lower level of the EMS. The real-time controller set the charging/discharging power profile (P^{i}_{B}) of the ESS of each microgrid in order to track P^{i}_{mgref} sent by the Energy Profiler, based on the measurements (with a sample rate of one minute) of the power of both the microgrid consumption (P^{i}_{L}) and renewable energy resources (P^{i}_{RES}). Additionally, the real-time controller considers the safe operation limits of the each ESS obtained by the estimators of SoC and the maximum available power for charging and discharging.

4. The procedure for updating the power reference of each microgrid is repeated at time $k+1$ (i.e. 30 minutes ahead). Therefore, return to step 1.

Finally, when a high uncertainty level is considered in the robust optimization problem, the solution might be too conservative [63, 131]. In this approach, a possible alternative to ensure that the solution remains feasible with a high uncertainty level is to use bigger ESS compare with the deterministic approach, or to modify the limits associated with the power drawn from the main grid (see Eq. 5.4b) or the limits of the ESS capacity (see Eq. 5.4e). However, in this work, in order to avoid modify of the energy community characteristics described above, a trade-off between conservatism and uncertainty level is considered. Next, the uncertainty policy proposed for this purpose is described.

5.2.3 Uncertainty Policy

In this work, the uncertainty is handled by the fuzzy prediction interval models. As was explained in Chapter 3, the prediction interval aims to achieve the upper and lower bounds of the interval as narrow as possible and that the interval contains a certain percentage of measured data. Results in chapter 3 showed that given the desired coverage probability (e.g. 90%) the interval width increase as the prediction horizon increase and therefore, the uncertainty level is higher.

Based on the above results and to handle the level of conservatism of the robust solution a decreasing desired prediction interval coverage probability *(PICP)* is proposed in function of the prediction horizon, as follow:

$$PICP(j) = \left(\frac{PICP^f}{PICP^0}\right)^{\frac{j}{N-1}} PICP^0 \tag{5.20}$$

where $j = 0, \ldots, N-1$ is the prediction horizon, $PICP^0$ and $PICP^f$ are the initial and final desired $PICP$ over the prediction horizon, and $N = 48$ that corresponds one day ahead for this study. Fig. 5.2 shows an example of the proposed approach (Eq. 5.20), where $PICP^0 = 90\%$ and $PICP^f = 10\%$ are the initial and final desired $PICP$ over prediction horizon, respectively. Therefore, the upper and lower bounds of the fuzzy prediction interval models are tuned according to these desired $PICPs$ to avoid intervals too width for higher prediction horizon. Finally, the performance of the hierarchical EMS for microgrid coordination is tested based on two case studies which are detailed next.

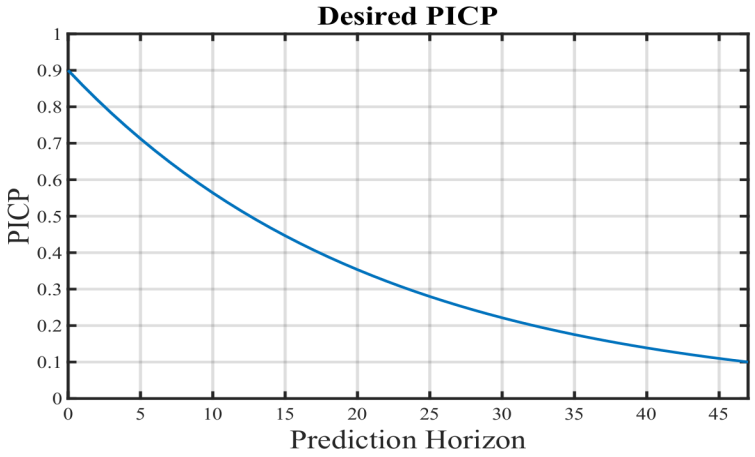

Figure 5.2: Desired PICP as function of Prediction Horizon

5.3 Case Studies

This section presents the results of the hierarchical EMS for the coordination of clusters of microgrids, which include the caracterization of uncertainty of renewable resources and load profiles. Two case studies are presented. The first case study corresponds to an Energy community made up of two microgrids with different numbers of dwellings, renewable energy (Photovoltaic and Wind Energy) and ESS based on lead-acid batteries. The second case study corresponds to an Energy community made up of three microgrids. For this latter case, a microgrid with a school demand profile is included with the aim to exploiting complementary power profiles such as daytime consumption profiles (like schools) and peak morning and evening consumption profiles (like households).

The data used for simulation correspond to winter season for all the case studies. The demand and photovoltaic power come from a town in the UK and wind power comes from Chile. Energy price used is the same as was explained in chapter 4 section 4.4 (see table 4.1). Fuzzy prediction interval models are used to predict the expected value and the uncertainty

of the net power of each microgrid of the energy community, and they are tuned according to the uncertainty policy described in the previous section. Simulation results for the microgrid coordination with the deterministic (Section 5.2.1) and the robust EMS (Section 5.2.2) are presented next, and they are compared with a basic EMS without ESS.

5.3.1 Case 1: Two Microgrids with Photovoltaic and Wind Energy

This case study corresponds to an energy community made up of two microgrids. The microgrid described in chapter 4 is used as the first microgrid for this energy community, and the second microgrid is composed of domestic demand, wind turbines and an ESS based on lead-acid batteries. Table 5.1 shows the characteristics of the energy community used to test the performance of the proposed EMSs.

Table 5.1: Energy Community Characteristics: Case Study 1

Energy Community	**Consumption Profiles**	**Rated Power of PV Generator**	**Rated Power of Wind Generator**	**ESS Capacity**
Microgrid 1	30 Dwellings	60KW	0KW	136KWh
Microgrid 2	60 Dwellings	0KW	35KW	180KWh

In this framework, the demand from the dwellings corresponds to non-controllable loads. The peak value of the load is 68KW and 120KW for the microgrid 1 and 2, respectively. With the ESS capacity chosen for the energy community, 3.5KWh capacity per dwelling is used. Therefore, the ESS capacity per dwelling is reduced compares with the case study reported in chapter 4, where 4.5KWh capacity per dwelling was used. Fig. 5.3 and Fig. 5.4 show both the load and renewable energy profiles (PV and Wind power) over 4 days for the microgrid 1 and 2, respectively.

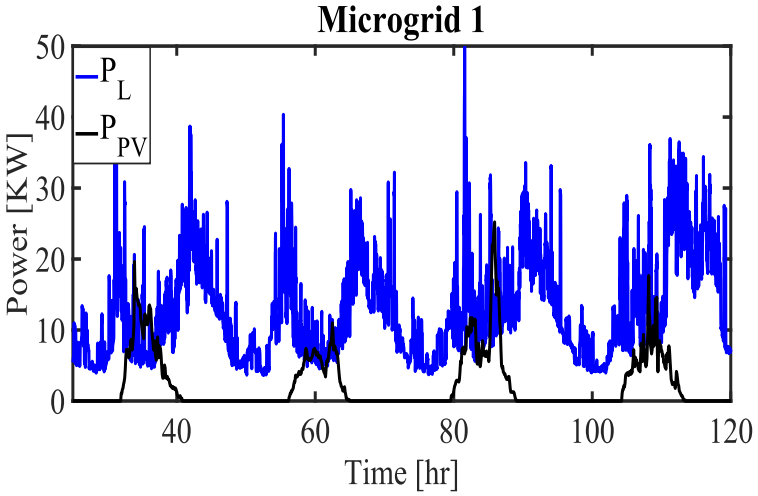

Figure 5.3: Profiles of Load and Photovoltaic Power over four days

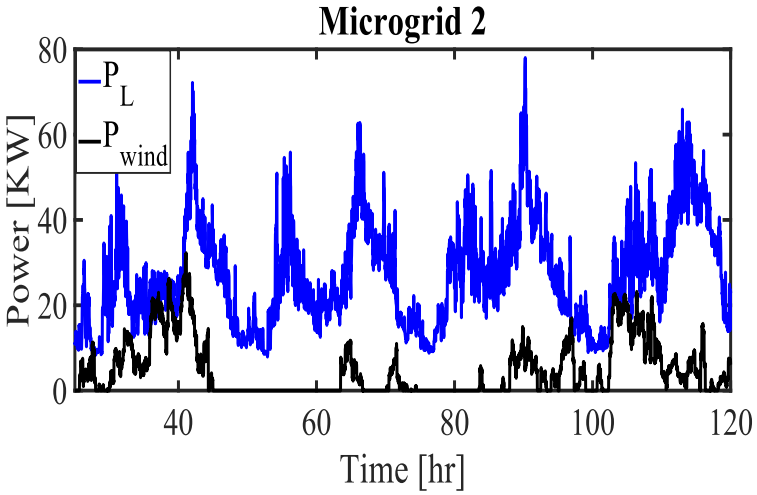

Figure 5.4: Profiles of Load and Wind Power over four days

For this case study, the desired *PICP* used for developing the fuzzy prediction interval models (for each microgrid) are 90% over the prediction horizon, which means that $PICP^0 = PICP^f$ in Eq. 5.20. Fig. 5.5 shows the responses obtained with the hierarchical EMSs (Deterministic and Robust) for an operation over two days of the energy community. It can also be seen that in both approaches the power reference (P^{i}_{mgref}), as sent by the higher level MPC controller to each microgrid (in red), can be tracked reasonably well by each lower level controller (P^{i}_{mg}, in blue). The tracking errors can happen due to errors associated to predictions of P^{i}_{net}, the linearization of the *SoC*, and/or the estimation of available maximum power of each ESS, all made in the higher level Energy Profiler.

Table 5.2 reports the *RMSE* of the tracking error of the power reference (P^{i}_{mgref}), the equivalent full cycles *(EFC)*, the loss of power supply probability *(LPSP)*, and the energy export for each microgrid of one-week simulation using the deterministic and robust EMSs (see chapter 4 for definition of *EFC* and *LPSP*). The lower *RMSE* with the Robust EMS means that there is a better tracking of the power reference (P^{i}_{mgref}) sent by the higher level to each microgrid of the energy community. The lower *EFC* of the Robust EMS means that fewer cycles which directly improves the state-of-the-health *(SoH)* and lifetime of the ESS.

The *LPSP*, which is the fraction of the time where each microgrid cannot fulfil the electrical demand requirements using the reference power (P^{i}_{mgref}) defined by the coordinator level and the available resources of each microgrid (Renewable Resources and ESS) of the energy community, is lower for the Robust EMS than the deterministic EMS. Additionally, as can be seen in Table 5.2, when the microgrids work in coordination manner, they can share energy between members of the community to maximise self-consumption and minimise the energy bought from the main grid. Finally, the behaviour obtained for the microgrid with 30 dwellings when it works in a coordinated way is similar than the behaviour reported in chapter 4 even with the reduction of ESS capacity per dwelling, as was mentioned above. This means that the microgrids that trading as energy communities can optimise the use of DG and the size of energy storage required.

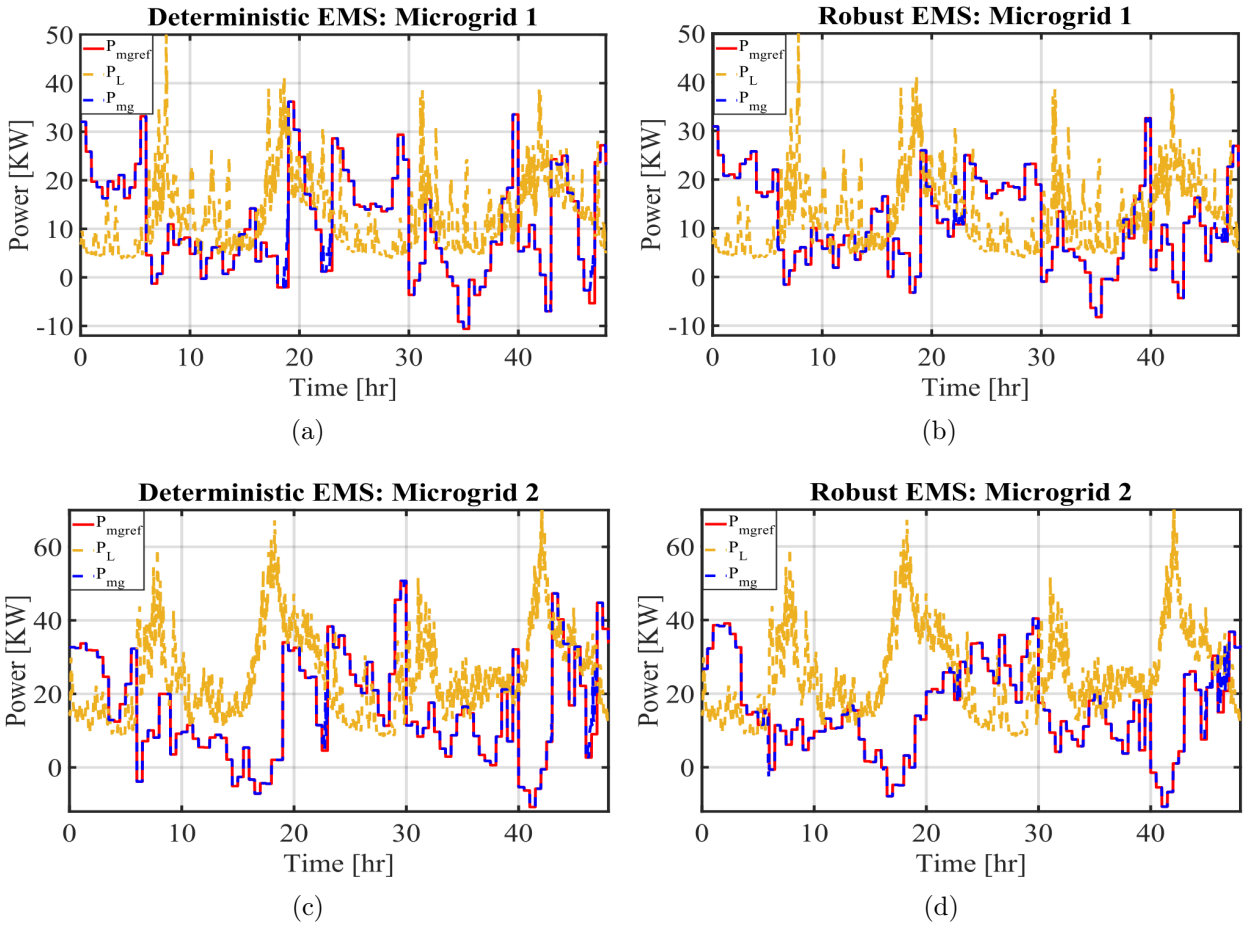

Figure 5.5: Performance of Hierarchical EMS for Microgrid Coordination a) Deterministic EMS: Microgrid 1; b) Robust EMS: Microgrid 1; c) Deterministic EMS: Microgrid 2; d)Robust EMS: Microgrid 2

Table 5.2: Performance Indices during a simulation of one Week duration: Case Study 1

EMS Strategy	RMSE (KW)	EFC Cycles	LPSP (%)	Shared Energy (KWh)
Deterministic:				
Microgrid 1	1.601	6.362	4.772	60.344
Microgrid 2	2.031	6.495	4.643	47.248
Robust:				
Microgrid 1	1.067	6.136	2.778	48.544
Microgrid 2	1.736	6.243	4.058	28.845

Table 5.3 shows the energy bought by the energy community from the main grid during the time periods associated with different tariff prices. As was explained in chapter 4, C1

identifies the time with the cheaper price and C3 that with the expensive price. The operation of both hierarchical EMSs is consistent with these price bands: more energy is bought at the cheaper price (C1) and less energy is bought at the expensive price (C3) compared to the case without ESS. The amount of the energy bought at the C2 price is similar for all EMSs strategies, as reported in Table 5.3. Additionally, deterministic and robust approaches do not export energy to the main grid since this requirement is added as a constraint in the optimization. Therefore, similar results were obtained regarding the energy distribution at different prices blocks compared with the operation of one microgrid reported in chapter 4.

Table 5.3: Energy Distribution at different Prices

EMS Strategy	**Export (KWh)**	**C1 (5p/kWh) (KWh)**	**C2 (12p/kWh) (KWh)**	**C3 (25p/kWh) (KWh)**
Without ESS	35.655	903.144	3133.138	1115.879
Deterministic	0.000	2306.259	2844.228	150.248
Robust	0.000	2342.289	2791.394	162.823

Finally, for further evaluation of the EMSs, several indexes of operation are presented in Table 5.4. These are the energy cost of the energy community, the load factor (LF), the load loss factor (LLF), positive power peak (P^+), negative power peak (P^-), power variation range (PVR), maximum power derivative (MPD) and average power derivate (APD) (See chapter 4 for detailed definitions).

The LF describes the flatness of the power response: values close to 1 are associated to flat responses while values close to 0 indicate the presence of large peaks. The LLF quantifies the losses incurred as a result of peak power: values close to 1 describe flat responses with small losses, while values close to 0 indicate large losses due to large peaks [41]. The PVR quantifies the ratio between the difference of the maximum and minimum power drawn from the main grid, for each EMS, and the same difference but for the case without ESS. The MPD is the maximum value of the rate of change between two consecutive points of the main grid power in its absolute value [62, 130]. And the APD is the average of the absolute value of the rate of change of the main grid power.

Table 5.4: Quality Indixes for the Power Profile of the Main Grid: Case Study 1

EMS Strategy	**Cost (£)**	**LF**	**LLF**	**P^+ (KW)**	**P^- (KW)**	**PVR (%)**	**MPD (KW/min)**	**APD (KW/min)**
Without Battery	698.32	0.2664	0.1028	114.31	-19.21	100	29.54	2.6841
Deterministic	494.18	0.4207	0.2673	75.00	0.00	56.17	71.48	0.5073
Robust	492.79	0.5043	0.3386	62.52	0.00	47.40	53.55	0.3897

The energy cost for the energy community without the ESS is £698.32. Therefore, a reduction of £204.14 is achieved using the deterministic EMS, and a reduction of £205.53 is

achieved by the Robust EMS. Even though the energy cost is similar for both EMSs (Deterministic and Robust), the quality indexes described above (see table 5.4) are significantly improved using the proposed hierarchical EMS compare with the case without ESS.

The positive power peak (P^+) and negative power peak (P^-) for the hierarchical EMS is limited by constraints as explained in Section 5.2. The limits are $P_{DNO}^{min} = 0kW$, which guarantees that no energy is exported to the main grid, and $P_{DNO}^{max} = 75kW$. The Robust EMS works in a more conservative manner for the upper limit. It attempts to avoid sub-optimal operation due to worst case realizations: thus it allows smaller peaks ($P^+ = 62.52kW$) than the deterministic EMS ($75kW$) (see also Fig. 5.6). Additionally, as discussed above, the operation of both hierarchical EMSs is consistent with energy prices bands, since energy from the main grid is the most expensive in the 16:00-19:00 hr time-block, therefore, the EMS makes this power draw be close to zero. Finally, Fig. 5.6 shows that the Robust EMS finds a flatter P_{DNO} than the deterministic EMS, which is good for the distribution network operator.

Overall, it can be seen that the deterministic and robust hierarchical EMSs provide improvements over the case without ESS, as they provide mechanisms for efficient energy management. Additionally, the Robust EMS provides small improvements over the deterministic EMS. These can be explained because the uncertainty management in the Robust EMS helps the system to be prepared for errors in the predictions that might yield sub-optimal decisions.

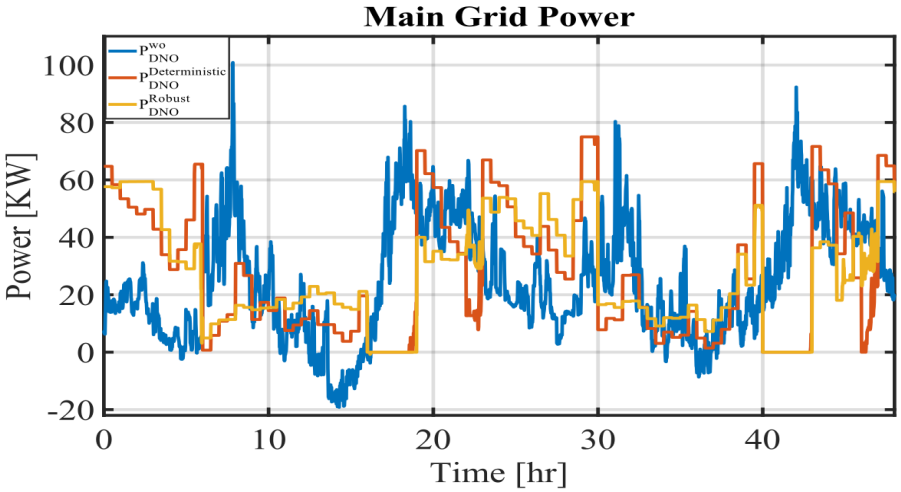

Figure 5.6: Main Grid Power Profiles: Case study 1

5.3.2 Case 2: Three Microgrids with Photovoltaic and Wind Generation including a School Load Profile

This case study corresponds to an energy community made up of three microgrids. The microgrids 1 and 2 of this energy community correspond to the microgrids described in the previous section (section 5.3.1). The third microgrid is a school with both photovoltaic and wind power, and an ESS based on lead-acid batteries. Table 5.5 shows the characteristics

of this energy community and Fig. 5.7 shows both the demand profile of the school and the aggregate demand of the microgrid 1 and 2 over four days. These days are Thursday to Sunday of a typical week, and as shown in Fig. 5.7 the load profile of the school decreases during the evening and changes significantly during the weekend. The peak value of the load from the school is 131.12KW. The electrical demand profile from Monday to Wednesday has a similar behaviour than shows in Fig. 5.7 for weekdays. Additionally, the holiday periods has a similar behaviour than weekend profiles.

Table 5.5: Energy Community Characteristics: Case Study 2

Energy Community	**Consumption Profiles**	**Rated Power of PV Generator**	**Rated Power of Wind Generator**	**ESS Capacity**
Microgrid 1	30 Dwellings	60KW	0KW	136KWh
Microgrid 2	60 Dwellings	0KW	35KW	180KWh
Microgrid 3	School	120KW	17.5KW	240KWh

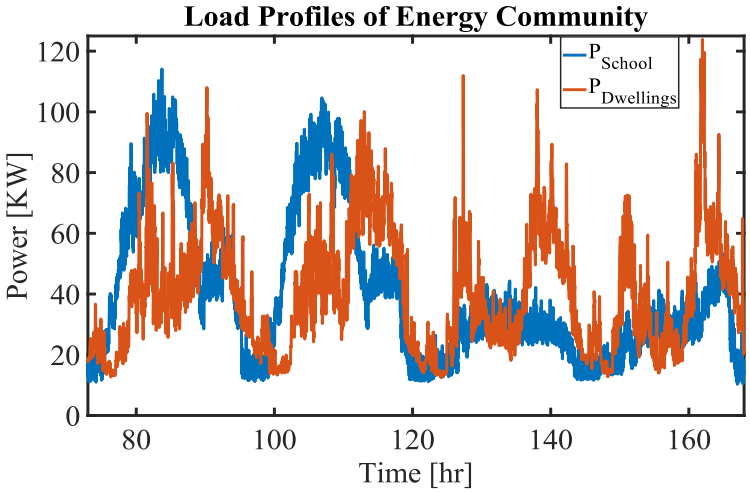

Figure 5.7: Demand Profiles of the School and Dwellings over four days

In this case study, fuzzy prediction interval models used to obtain the expected value and the uncertainty of the net power (P^{i}_{net}) of each microgrid are tuned using different initial ($PICP^0$) and final ($PICP^f$) desired $PICP$. Therefore, a $PICP^0 = 90\%$ and $PICP^f = 70\%$ are choisen in Eq. 5.20 in order to reduce the interval width for higher prediction horizon.

For this case study, similar results have been obtained compare with the case studies reported in previous sections (sections 4.4.3 and 5.3.1). In general, the proposed hierarchical EMS provides realistic power references (P^{i}_{mgref}) for each microgrid, minimizing the energy cost delivered to the community from the main grid. In consequence, each microgrid level controller tracks these references reasonably well, as shown in Fig. 5.8. Additionally, in this approach, the safe limit constraints for the ESS and power transfer to and from the main grid are considered.

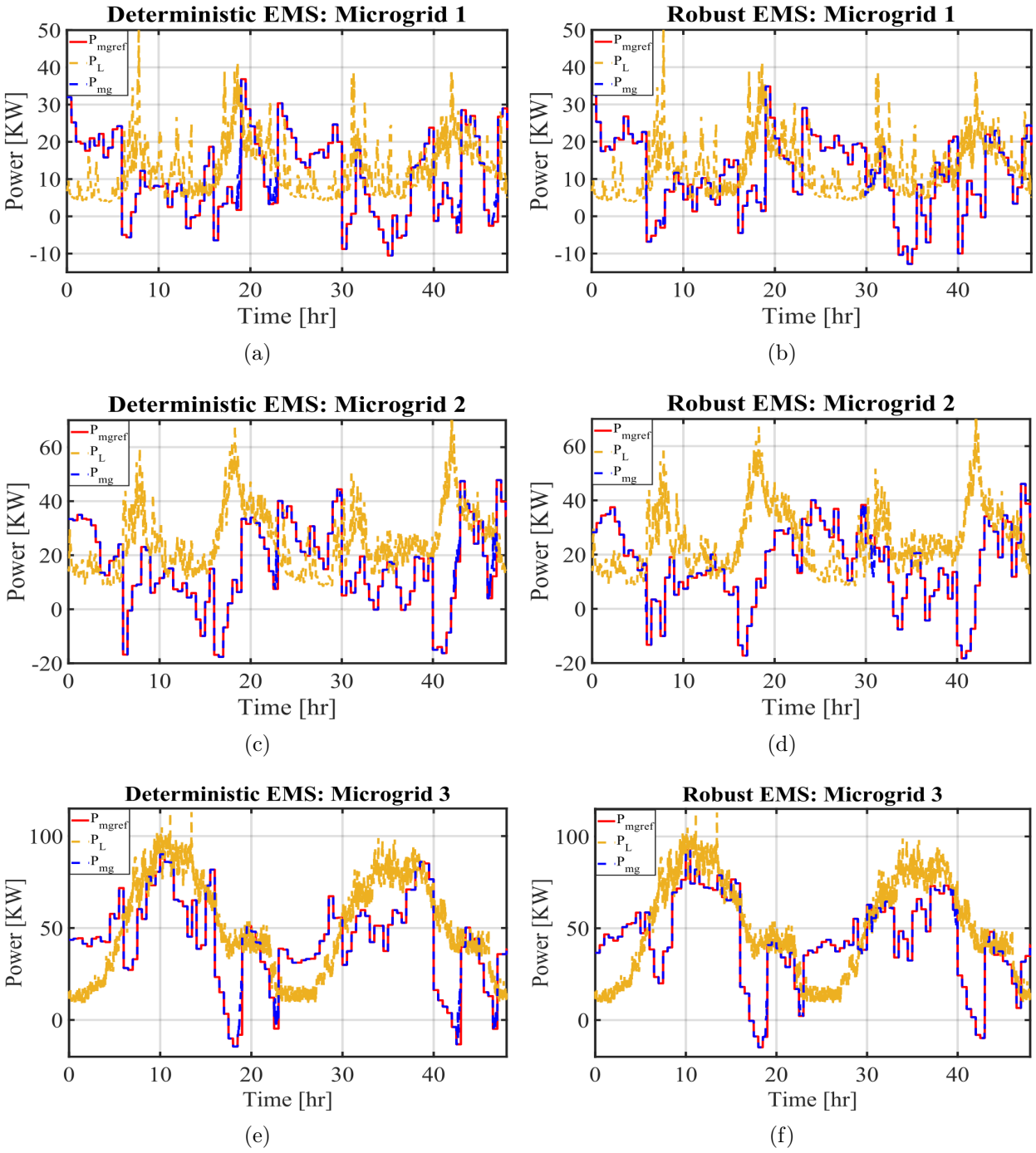

Figure 5.8: Performance of Hierarchical EMS for Microgrid Coordination a) Deterministic EMS: Microgrid 1; b) Robust EMS: Microgrid 1; c) Deterministic EMS: Microgrid 2; d) Robust EMS: Microgrid 2; e) Deterministic EMS: Microgrid 3; f) Robust EMS: Microgrid 3

The benefit of using complementary power profiles such as schools with daytime consumption and households with peak morning and evening consumption are presented in this case study. The above, it can see in results shown in Table 5.6. For instance, a better tracking of the power reference (P^{i}_{mgref}) sent by the higher level to each microgrid is achieved with the

Table 5.6: Performance Indices during a simulation of one Week duration: Case Study 2

EMS Strategy	RMSE (KW)	EFC Cycles	LPSP (%)	Shared Energy (KWh)
Deterministic:				
Microgrid 1	1.578	6.413	4.494	85.085
Microgrid 2	1.860	6.491	4.395	102.099
Microgrid 3	2.947	6.478	4.514	138.728
Robust:				
Microgrid 1	1.003	5.618	0.942	81.773
Microgrid 2	1.740	5.788	1.151	84.198
Microgrid 3	1.420	5.801	1.677	142.614

Robust EMS. This tracking error reduction is more significant for microgrid 1 and 3 when Robust EMS is compared to deterministic EMS. In a similar way, the state-of-the-health *(SoH)* and the lifetime of the ESS is improved when the Robust EMS is used. In general, regarding this metric (*EFC*) all the case studies reported in this work have obtained similar results, the Robust EMS achieves lower *EFC* when is compared to deterministic EMS. Therefore, this approach results in a better usage of the ESS which reduces the loss of power supply probability *(LPSP)*, as seen in table 5.6. The *LPSP* is reduced of 4.494% to 0.942% for microgrid 1, of 4.395% to 1.151% for microgrid 2, and of 4.514% to 1.677% for microgrid 3 when the Robust EMS is compare to deterministic EMS respectively. Overall, all the case studies reported in this thesis have obtained similar behaviour regarding this metric, and this happens because the robust approach compensates for the uncertainty of both renewable generation and electrical demand and can avoid the scenarios measured by the *LPSP*.

Additionally, Fig. 5.9 shows SoC behaviour of the microgrid 3 over two days. The results show that the ESS operates at all times in the safe operation ranges (SoC between 20% and 80% of the capacity of the ESS) for both deterministic and Robust EMSs. However, as it can seen in Fig 5.9, the Robust EMS results in a better usage of the ESS due that right before the discharging process, the Robust EMS achieves a charge closer to the maximum SoC, and try not to discharge ESS until the minimun SoC (20% of the capacity of the ESS). The above is a protection against of uncertainty and therefore, the Robust EMS are prepared for errors in the predictions, providing flexibility to ESS. Then, the energy community can improve the behaviour and reduce the energy bought from the grid. Finally, the microgrid 1 and 2 of this energy community have a similar SoC behaviour to that described previously.

The results show that the cooperation among microgrids has advantages for each microgrid of the energy community in terms of facing the deficiency or excess of energy production given by renewable energy behaviour. The above is another benefit of trading as energy communities, which optimise the use of DG and the size of ESS required. Table 5.6 reports the shared energy between members of the Energy Community (microgrids). This shared energy is used for the community in order to maximise self-consumption and minimise the

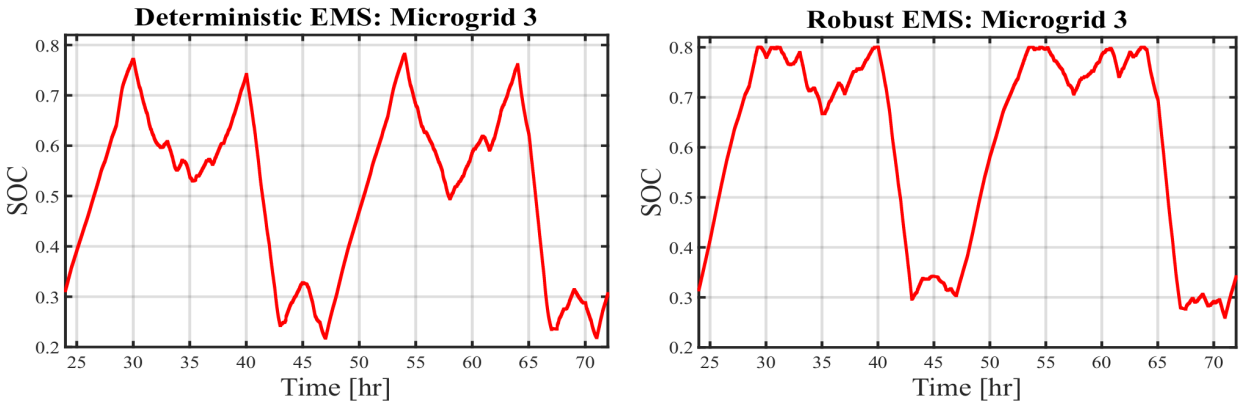

(a) (b)

Figure 5.9: Microgrid 3 ESS SoC Behaviour a) Deterministic EMS; b) Robust EMS

energy bought from the main grid. Microgrid 3 with daytime profiles, try to share more energy during the evening that corresponds to periods when the dwellings (microgrid 1 and 2) have one peak demand. In contrast, the microgrids 1 and 2 try to share more energy during peak demand of the school (during the day). Due to the chosen configuration for this energy community (i.e., penetration level of renewable energy, and size of ESS and load profiles of the microgrids), the electrical demand of the school during evening periods is similar to the demand of the microgrids made up of dwellings (with peak morning and evening load) at the same evening periods, despite that the school has peak day consumption (see Fig. 5.7). Therefore, for this case study, the benefits of using complementary power profiles is more significant (i.e., the microgrid 3 can share more energy) during the weekend and holidays, as shown in Fig. 5.10, compared to weekdays. In conclusion, for exploiting complementary power profiles, the planning of the energy community is an important aspect (planning is not on the scope of this work) because allows determining the optimal combination of DERs that made up of energy community to achieve the proposed goals. However, the proposed hierarchical EMS optimises the behaviour of the energy community based on available DERs and imposed constraints in the optimization problem.

Finally, Table 5.7 reports the energy cost of the energy community and several quality indices for quantifying of the power profile of the main grid. In general, in all the case studies reported, the energy cost is lower when the hierarchical EMSs (deterministic and Robust) are used compared to the case without ESS, therefore, this is one of the benefits achieved for using ESS at the distribution level. Additionally, energy cost is very similar for the both deterministic and Robust EMSs in all case studies. However, the load factor (LF), the load loss factor (LLF) and power variation range (PVR) metrics have improved significantly using the proposed hierarchical EMSs compare to the case without ESS and the Robust EMS has also improved these metrics compared to deterministic EMS, as shown in Table 5.7. The improvement of these metrics benefits directly to the network operator for electricity distribution systems, enabling increased penetration of DG.

As has been explained in previous sections, the positive power peak (P^{+}) and negative power peak (P^{-}) for the hierarchical EMS is limited by the constraints in the optimization

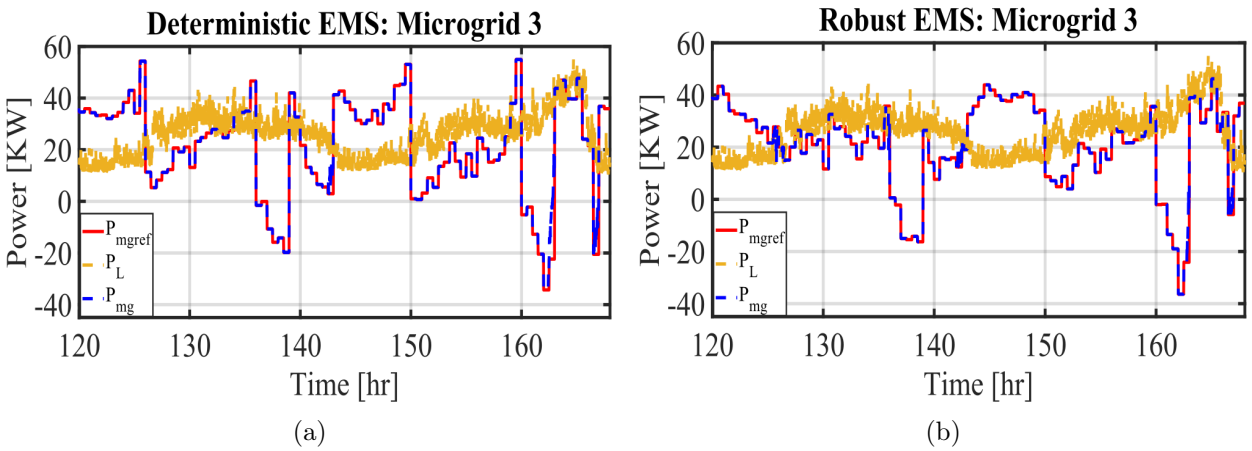

Figure 5.10: Performance of Hierarchical EMS for Microgrid 3 during Weekend a) Deterministic EMS; b) Robust EMS

Table 5.7: Quality Indixes for the Power Profile of the Main Grid: Case Study 2

EMS Strategy	Cost (£)	LF	LLF	P^+ (KW)	P^- (KW)	PVR (%)	MPD (KW/min)	APD (KW/min)
Without ESS	1472.23	0.3928	0.1840	172.34	0.00	100	33.87	4.6453
Deterministic EMS	1100.14	0.5737	0.4281	120.00	0,00	73.07	119.25	0.8071
Robust EMS	1105.65	0.6539	0.5225	104.43	0.00	63.59	97.50	0.6180

problem. For this work, the negative limit is $P_{DNO}^{min} = 0kW$, which guarantees that no energy is exported to the main grid, and the positive limit (P_{DNO}^{max}) is defined for limiting peak power levels. Therefore, the Robust EMS works in a more conservative manner due that it takes the values that are more constraining for the upper limit, and thus smaller peaks are obtained than the deterministic EMS, as shown in Table 5.7 and Fig. 5.11. Finally, the average power derivate (APD) has a significant reduction, corresponding to a flatter main grid power (see Fig. 5.11), although the maximum value of the ramp-rate of the power (measured by MPD) is lower for the case without the ESS (see Table 5.7).

5.4 Assumed Model Simplifications

The next paragraphs are intended to present all the considerations and simplifications assumed for the simulations of the study cases developed in this work, with the intention that these experiments can be replicated and/or adapted for future research works.

1. The microgrids that conform the Energy Community presented in this work only consider renewable distribution generation units (RESs), which are classified as DG non-dispatchable and energy storage systems (ESSs) based on batteries that are only dispatchable units in this scheme. The reason is that these types of microgrids could be

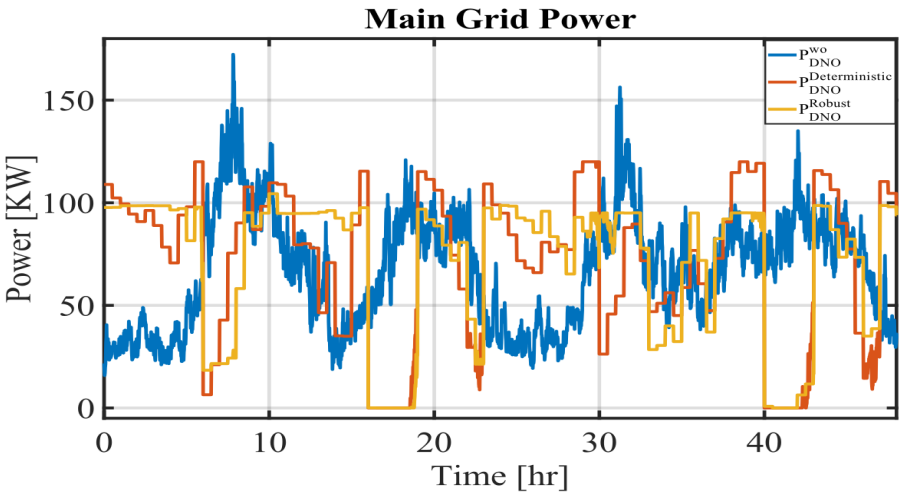

Figure 5.11: Main Grid Power Profiles: Case study 2

dwellings on a street or in a village, and they mainly incorporate renewable resources such as PV and wind generators. However, if thermal generation units are considered, then in the formulation of the Hierarchical EMS, binary on/off variables that solve unit commitment problems, where ramps between the generation units, on and off times, must be included. If this is the case, in the proposed Hierarchical EMS it becomes necessary to include the associated cost to the corresponding dispatchable DG so that the energy community can operate with the minimum cost and the technical constraints associated to these generation units.

2. For this study case, the operation of the energy community in island mode was not considered, and the main grid assumes the energy deficit that the microgrids might have in order to satisfy the power balance.

3. The used demand and renewable generation data (PV and wind) in all the study cases, both for operation and coordination, were measured data with one minute resolution. However, it the behavior of different microgrids want to be studied, for example including different profiles such as: factories, hospitals, etc, simulators that generate this type of data might be used. Examples of this are reported in [132] and [133]. In case of using of the data generated by the models, it is recommended to analyze the results with the support of Monte Carlo simulations in order to capture the stochasticity of the processes.

4. The data used for the simulations correspond to the winter season and the prediction interval models that capture the non-linearity and the uncertainty of the demand and renewable resources are trained for this winter data. However, in order to analyze the behavior of the operation and coordination of the energy community (microgrids) in other seasons, different prediction interval models can be used (for example, one per season) or if enough data is available to train the prediction interval model, a unique model can be developed using as a reference the Fuzzy or Neural Network models. Finally, the expected values and the upper and lower bounds of the prediction interval models are used in the formulation of the Robust EMS.

5. The renewable penetration levels and number of dwellings that conform each microgrid in the energy community were selected arbitrarily in order to evaluate the performance of the proposed Hierarchical EMS. However, a planning stage to determine the optimal size and topology of the microgrid can be done to guarantee and optimal future operation. The addition of more dwellings in each microgrid can reduce the variability of the demand allowing to predict in a better way by enabling the effective use of ESS at the distribution level.

6. In this work it is assumed a high flexibility on the grid. This means that energy can be transferred between the microgrids and the main grid without congestion issues, or voltage regulation problems, for example. Moreover, the power flows are not modelled since the grid is considered high flexible, it has the required capacity to deliver energy from and to the microgrids.

7. The main grid's power lower limit for this study case was set to zero with the purpose of not exporting energy to the main grid. Also, the main grid's maximum power limit was defined arbitrarily with the intention of reducing power peaks that are purchased to the main grid. Additionally, a Time of Use (ToU) tariff is used to buy energy from the main grid. In this scheme, three price levels are used: off-peak, mid-peak and peak. However, a real time price (RTP) for the energy price scheme can be used as these schemes tend to use hourly or half-hourly price differences to reflect the price on the wholesale market. Furthermore, a market scheme that allows to sell energy to the main grid with the intention to export the excess energy of the microgrid can be considered.

8. Regarding the ESS, lead-acid batteries were considered in this study. However, different technologies such as Li-ion, hydrogen of flywheels can be included. As mentioned before, this study considers state of charge (SoC) and maximum available power estimators for the charging and discharging process in order to operate the ESS within its safety limits. However, the degradation of the ESS was not considered since the simulation time (weeks) used to assess the performance of the Herarchical EMS is not enough to quantify the degradation suffered by the ESS. Although, if the degradation is considered in this scheme, its effect on the Hierarchical EMS can be neglected since the main grid would supply the necessary energy to balance the power equation but the energy cost will increase.

Although the scale demonstrated in this study is for small communities, it can potentially find value at the much larger scale which is currently being proposed for system "Aggregators" as part of a Smart Grid scenario operated by Distribution System Operatators (DSOs). Finally, this study also looks to determine how generalised design rules can be created for the design of the hierarchical control structure and incorporate, highest levels in the hierarchical approaches reported in the literature following the "Transferrable Design Rules" presented in this thesis.

5.5 Discussion

In this chapter, a hierarchical two-level EMS was developed for the coordination of multiple microgrids, considering both the uncertainty of the renewable energy resources and the variability in electrical load consumption. Two case studies were tested. The first community was made up of households profiles, renewable energy and ESS. The second community included an electrical demand of a school with daytime profiles. Results showed that this approach can benefit to both the end user, by reducing energy costs, and the distribution network operator, by limiting peak power levels and enabling increased penetration of DG.

A coordination between multiples microgrids improves the performance of the energy community because it allows to share the generated power and reduce the amount of energy bought from the main grid in the higher pricing hours and it also enlarges the feasible set of the optimization problem which allows lowering the ESS size guaranteeing optimal operation.

Chapter 6

Conclusions

From the literature review has been demonstrated that the active management of DERs provides an acceptable approach to integrate of large numbers of DERs within a distribution network, in order to exploit their potential benefits and avoid the costs of network reinforcement. Active management of a distribution network requires the integration of control strategies at different levels in a smart grid framework and communication technologies. In this thesis, the active management of DERs has been proposed using an EMS applied to "Energy Communities". The concept of energy communities enables energy exchange between the DERs of community members to maximise their self-consumption, minimise their energy costs, reduce peak power levels or a combination of these and other beneficial goals. An energy community could be considered to be a microgrid or cluster of microgrids if it is seen from the main distribution grid as a single element responding to appropriate control signals within defined electrical boundaries. The energy management system (EMS) is responsible for reliable, secure and economical operation of the energy communities, managing the power and the energy between generation sources and loads.

Therefore, the focus of this thesis has been on the design of hierarchical energy management system (EMS) for the operation and coordination of microgrids, including the uncertainty associated with both renewable distributed generation and electrical demand. The hierarchical EMS was designed in two levels: main grid level and microgrid level. At the microgrid level, a real-time local controller based on rules was proposed and at the higher level, Robust MPC controller was proposed to manage the uncertainty by means of fuzzy prediction interval models. The idea behind of use a hierarchal EMS was to exploit the benefit of both non-optimal controllers and optimal controllers which were adopted on different levels.

The role of the Robust MPC controller at the main grid level is to minimize the energy cost delivered to the energy community from the main grid. To achieve this goal, Robust MPC controller provides realistic power references for each community member (microgrids), such that the lower level controller can be tracked the power reference reasonably well based on the available resources and load of each microgrid. Therefore, the Robust MPC implements an optimization of the predicted performance cost of the energy community over a prediction horizon, while considering the uncertainty associated with predictions of the renewable gen-

eration and consumer load, safe limit constraints for the ESS and power transfer to and from the main grid. The uncertainty was included explicitly in the optimization problem using an alternative that compensates the uncertain terms with linear gains. Additionally, the lower level controller incorporates real-time estimators associated with the operation of the ESS: the maximum available power estimator and the SoC estimator in order to work in a safe operating area. This area is determined by current, voltage, and SoC limits.

Several case studies were used to test the performance of the hierarchical EMS for operation and coordination of microgrids. Robust EMS based on fuzzy prediction interval models was compared to the deterministic EMS and with a basic EMS without ESS, where the energy required to satisfy the energy balance in the energy community is either bought or sold from the main grid. The main conclusions obtained from these case studies can be summarized as follows:

- Prediction interval models provide a systematic framework for the representation of uncertainty and, therefore, they are suitable for loads and renewable energy forecasting in applications of energy communities. The proposed prediction interval models provide the upper and lower bounds of the predicted values given a coverage probability with the minimum interval width at future prediction horizons, providing more accurate information about the uncertainty modelled.

- The deterministic and Robust hierarchical EMSs provide improvements over the case without ESS, as they provide mechanisms for efficient energy management. The results show that incorporating ESS into the energy community benefit both end user, by reducing energy cost, and distribution network operator, by limiting peak power levels and enabling increased penetration of distributed generation.

- The hierarchical EMS is able to keep the community power flow close to the reference power defined by the higher level controller and provide minimum energy cost, among other benefits. Additionally, the benefits of Robust MPC are greater than those of deterministic MPC due to the uncertainty compensation, which helps the system to be prepared for errors in the predictions that might yield sub-optimal decisions.

- A coordination between multiples microgrids improves the performance of the energy community because it allows to share the generated energy and reduce the amount of energy bought from the main grid in the higher pricing hours and can optimise the size of ESS required for the community.

6.1 Future Work

From the development of this thesis, further research may be pursued on the following subjects:

- Regarding prediction interval models, other evaluation metrics for the prediction interval could be included in the optimization problem, and a Pareto analysis could be included in the multi-objective cost function to obtain the best compromise solution.

- Incorporate into the proposed hierarchical EMS, the degradation process of the ESS by means of an estimator of the state of health (SoH), as well as considering to incorporate demand side management strategies.

- Use a real time price (RTP) for the energy price scheme as these schemes tend to use hourly or half-hourly price differences to reflect the price on the wholesale market.

- Consider other energy communities such as factories, hospitals, commercial parks or other community loads as well as other types of distributed generation, for example, biomass-based generation or renewable generation could be included in the energy community to be controlled by the hierarchical EMS proposed.

- Employ other energy storage technologies e.g. hydrogen or flywheels, as well as considering other network asset limitations.

Appendices

A1 Battery Model

Copetti model is adopted for modelling the ESS based on lead-acid battery. The model considers an equivalent circuit that contains a constant voltage source and a variable polarisation resistance $R_{int}(I, SoC, T)$. The voltage source represents the relationship between V_{oc} and SoC, while R_{int} represents the battery electrochemical effects that oppose the current flow, as is shown in Fig. 1. As explained in [134], the Copetti model describes four operation modes for the battery system: charging zone, discharging zone, overcharging zone, and an intermediate zone that represents a soft transition between the charging/discharging modes.

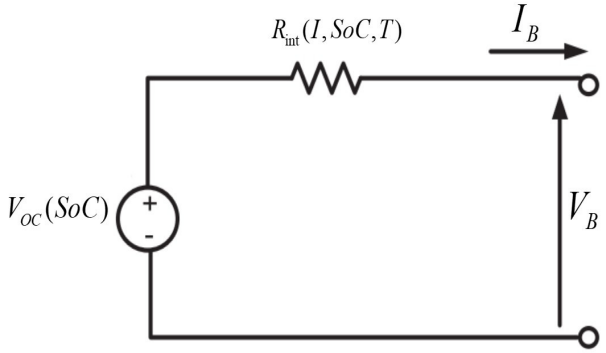

Figure 1: Circuital Representation of Battery for the Copetti Model

In this work, three operation zones are included: the discharging, charging and intermediate zones. The analytical expressions for the output voltage (V_B) in these zones are represented by equations (1), (2) and (3), respectively:

Discharge zone (V_B^{dc}): In this zone of work, the battery will give energy to the electrical system. The discharging and charging zones are the best zones for the work of the batteries:

$$V_B^{\mathrm{dc}}(k) = (V_{b0\mathrm{dc}} - K_{b0\mathrm{dc}}(1 - SoC_k)) - \frac{|I_k|}{C_{10}}\left(\frac{P_{1\mathrm{dc}}}{1 + |I_k|^{P_{2\mathrm{dc}}}} + \frac{P_{3\mathrm{dc}}}{SoC_k^{P_{4\mathrm{dc}}}} + P_{5\mathrm{dc}}\right)(1 - \alpha_{r\mathrm{dc}}\Delta T_k), \tag{1}$$

where P_{idc} (i $= 1, \ldots, 5$) are unknown coefficients associated with the polarisation resistance. C_{10} corresponds to the battery capacity (in AH) for 10h, and $\alpha_{r\mathrm{dc}}$ relates the model with the temperature variation (ΔT). The term $(V_{b0\mathrm{dc}} - K_{b0\mathrm{dc}}(1 - SoC_k))$ models the relationship of $V_{oc} - SoC$. In this work, the temperature effects are neglected.

Charge zone (V_B^c): In this operation zone, the battery takes energy to the electrical system. The efficiency of this zone decreases:

$$V_B^c(k) = (V_{b0c} + K_{b0\mathrm{dc}}SoC_k) + \frac{I_k}{C_{10}}\left(\frac{P_{1c}}{1 + {I_k}^{P_{2c}}} + \frac{P_{3c}}{(1 - SoC_k)^{P_{4c}}} + P_{5c}\right)(1 - \alpha_{rc}\Delta T_k), \tag{2}$$

where P_{ic} ($\mathrm{i} = 1, \ldots, 5$) are unknown coefficients associated with the polarisation resistance. α_{rc} relates the model with the temperature variation (ΔT). The term ($V_{b0c} + K_{b0\mathrm{dc}} SoC_k$) models the relationship of $V_{oc} - SoC$.

Transition zone (V_B^{cdc}): when the transition occurs between the discharging zone and the charging zone, the model used is shown as in (3), where I_δ is the current threshold for the transition:

$$V_B^{\mathrm{cdc}}(k) = \frac{V_B^c(I_\delta) - V_B^{\mathrm{dc}}(I_\delta)}{2I_\delta} I_k + \frac{V_B^c(I_\delta) + V_B^{\mathrm{dc}}(I_\delta)}{2}. \tag{3}$$

Finally, the unknown coefficients associated with the polarisation resistance were identified based on an optimisation method with a data training set.

On the other hand, the relationship between the open-circuit voltage (V_{oc}) and the state-of-charge (SoC) is obtained using an experimental test known as "voltage relaxation": a procedure that basically applies a known discharge profile to the battery for a given period, then forces a null discharge current (open circuit) for an appropriate "rest" time (usually an hour), and then measures the (V_{oc}) output voltage. In particular, the $V_{oc} - SoC$ curve in lead-acid batteries can be modelled using a linear-in-the-parameters structure (4):

$$V_{OC}(k) = a_n SoC^n(k) + a_{n-1} SoC^{n-1}(k) + \cdots + a_1 SoC(k) + a_0, \tag{4}$$

where a_{i} ($\mathrm{i} = 1, \ldots, n$) are model parameters. In this model, the SoC is calculated empirically as the integral of the instantaneous current. The discrete model of SoC is given by (5):

$$SoC(k) = SoC(k-1) - \frac{\eta T_s}{C_n} I(k-1), \tag{5}$$

where C_n is the nominal capacity, T_s is the sampling time, and $I(k-1)$ is the instantaneous discharge current. In the work presented in [119] an experimental system was designed and implemented in order to obtain experimental data by discharging a lead-acid battery bank, which is constructed with three batteries in series connection. The same system is used to charge the batteries according to the charging profile recommended by the manufacturers. With this experimental system, the SoC vs V_{oc} curve was estimated experimentally. This relationship can be written mathematically as (6):

$$V_{OC}(k) = 3.755 \cdot SoC^3(k) - 5.059 \cdot SoC^2(k) + 3.959 \cdot SoC(k) + 17.064 \tag{6}$$

A2 SoC Estimator

The state of charge (SoC) is defined as the amount of energy contained in an energy storage system (ESS). It is critical to the implementation of optimal control strategies for charging/discharging of the ESS to have information about the SoC of the battery. For this reason, it is important to have a method that is able to estimate the SOC, and according to a future-use profile, the online prediction of the SoC of the ESS that delivers results with appropriate accuracy and precision.

Several methods for SoC estimation are reported in the literature, such as electrochemical impedance spectroscopy, open-circuit voltage, and integral of the instantaneous current. However, these methods are only suitable for off-line studies. Long battery resting periods, and acquisition of costly equipment and/or high-precision sensors are some of the other disadvantages. In recent years, there has been growing interest in the use of stochastic filtering techniques (for instance, the Unscented Kalman Filter) to estimate the SoC of an ESS. In fact, experience has demonstrated that Bayesian estimators are well suited for real-time estimation problems that incorporate dynamic state transition models [117].

Due to the nonlinearity of the models for SoC, one of the most widely estimated use of it corresponds to the sub-optimal Bayesian methods of the Extended Kalman Filter (EKF) technique. The disadvantage of this method arises from errors in the linearization approximation. Another alternative presented is the Unscented Kalman Filter (UKF). It is outstanding for its good performance against problems with nonlinear equations, and its efficient computational ability. In this work, the implementation of UKF for estimating the SoC is presented [117].

In this approach, three state variables are considered: SoC, and the resistances of charging (R^{chg}) and discharging ($R^{\mathrm{dis}chg}$). The equation that describes the SoC is defined for the integral of the instantaneous current (see Eq. 7), and the states corresponding to resistances are variables that evolve artificially, with only noise added to the process, as is shown in (8) and (9):

$$SoC_{k\backslash k-1} = SoC_{k-1} - \frac{\eta \cdot T_s}{C_n} \cdot I_{k-1} + w^1_{k-1} \tag{7}$$

$$R^{\mathrm{dis}chg}{}_{k\backslash k-1} = R^{\mathrm{dis}chg}{}_{k-1} + w^2_{k-1} \tag{8}$$

$$R^{chg}{}_{k\backslash k-1} = R^{chg}{}_{k-1} + w^3_{k-1}, \tag{9}$$

where T_s is the sampling time; C_n is the nominal capacity of the battery; η is the efficient; I_{k-1} is the current; and w^1_{k-1}, w^2_{k-1} and w^3_{k-1} are the process noise. The observation equation is defined as the battery voltage, and it is based on a simple model as is shown in Fig. 2 and equation (10):

$$V_B(k) = Voc_k(SoC) + \delta R^{\text{dischg}} I(k) + (1-\delta) R^{chg} I(k) + v_k, \tag{10}$$

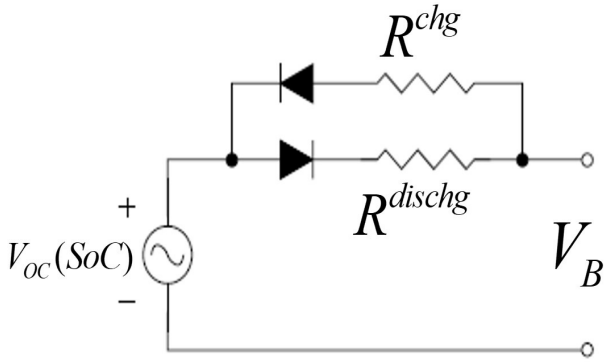

Figure 2: Simple Model for the Battery Voltage

where $I(k)$ is the current in the time instant k, and v_k is the observation noise. The relationship between the open-circuit voltage (V_{oc}) and the state-of-charge (SoC) is obtained using an experimental test known as "voltage relaxation" (for more details see Appendix A1). In this work, negative current is defined for discharging, and positive current for charging. Thus, the δ term indicates the operation mode of the battery, as shows in (11):

$$\delta = \begin{cases} 1 & if \;\; I(k) \leq 0 \\ 0 & if \;\; I(k) > 0 \end{cases} \tag{11}$$

Additionally, the Outer Feedback Correction Loops (OFCL) is included as a method to ensure accuracy and precision of the estimates. The OFCLs, typically measure the model quality, and improve the performance of the algorithm, either modifying the structure of the model, or updating the hyper-parameters that define the noises of the process or observation. In this case, the noise of the process is modified as shown below:

$$\begin{aligned}
&\text{if} : t > t_{\min}, \\
&then : \\
&\quad \mathrm{e}_{acum} = \mathrm{e}_{acum} + |\mathrm{e}_{obs}| \\
&\text{if} : \mathrm{e}_{acum} \leq \mathrm{e}_{Th} \\
&\quad std(w_1(t)) = \max(p_1 std(w_1(t)), \underline{std_1)} \\
&\quad std(w_2(t)) = \max(p_2 std(w_2(t)), \underline{std_2)} \\
&\quad std(w_3(t)) = \max(p_3 std(w_3(t)), \underline{std_3)} \\
&else : \\
&\quad \mathrm{e}_{acum} = 0 \\
&\quad std(w_1(t)) = q_1 std(w_1(t)) \\
&\quad std(w_2(t)) = q_2 std(w_2(t)) \\
&\quad std(w_3(t)) = q_3 std(w_3(t)),
\end{aligned}$$

where t_{min} is the time during which the OFCL starts to work; e_{obs} is the observation error, given by the difference between the output measurement and the output estimate; e_{acum} is the accumulative observation error; e_{th} is the decision threshold where the noise process begin to change. If the accumulative error is less than the threshold, the standard deviations of the noise decrease; in the opposite case the noise standard deviation increases. p_i ($i = 1, 2, 3$) are constant values between 0 and 1. q_i ($i = 1, 2, 3$) are constant values greater than 1. Finally, $\underline{std}_1, \underline{std}_2$ and $\underline{std}_3$ are lower bounds, under which standard deviations they cannot be reduced.

A3 Maximum Available Power Estimator

The method adopted for estimating the maximum available power that may be sourced by the battery bank, and the maximum power for the charging process, is presented in this appendix. These values must be calculated carefully in such a way that the battery bank will not be damaged by over/under charge (SoC), or voltage, or by exceeding a design current or power limit [115, 116, 135].

The first method for calculating the maximum discharging and charging current limits ($I_k^{\mathrm{dis},SoC}/I_k^{chg,SoC}$) includes the maximum and minimum values of the SoC permitted in the operation of the battery bank, and the second method calculates the current limits ($I_k^{\mathrm{dis},volt}/I_k^{chg,volt}$) considers operation voltage limits.

In the first adopted method (maximum and minimum values of the SoC permitted), given a constant current I_k, the SoC recurrent relationship is given by (12):

$$SoC(k+L) = SoC(k) - \frac{\eta L T_s}{C_n} I_k, \tag{12}$$

where L is the time horizon where the power for charging or discharging may be maintained constant without violating present operational design limits, for this case the SoC [135]. $SoC(k+L)$ is the predicted SoC L seconds into the future, $SoC(k)$ is the present SoC, C_n is the capacity in ampere-seconds and η is the Coulombic efficiency factor. If the SoC is limited by the minimum and maximum values ($SoC_{\min} \leq SoC(k) \leq SoC_{\max}$), then the I_k can be calculated such that these limits are not exceeded by (13) and (14):

$$I_k^{\mathrm{dis},SoC} = \frac{SoC(k) - SoC_{\min}}{\frac{\eta L T_s}{C_n}} \tag{13}$$

$$I_k^{chg,SoC} = \frac{SoC(k) - SoC_{max}}{\frac{\eta L T_s}{C_n}} \tag{14}$$

where $I_k^{\mathrm{dis},SoC}$ is the maximum discharge current and $I_k^{chg,SoC}$ is maximum charge current based on SoC limits method of the battery bank. This method is safe and reasonable when the actual SoC is close to its limits avoiding over-discharged or over-charged.

The second adopted method for calculating the maximum discharge and charge current includes voltage limits [115]. The Eq. 15 presents correct prediction when the simple model (see Fig. 2 in appendix A2) of the battery bank and the time horizon L are considered. In this method, L is the time horizon where the power for charging or discharging may be maintained constant without violating voltage limits ($V_{\min} \leq V_B(k) \leq V_{\max}$). In Eq. (15), the current (I_k) is assumed constants between the $k-th$ sampling time t_k and $(k+L)-th$ sampling time t_{k+L}:

$$V_B(k+L) = Voc(SoC(k+L)) - RI(k), \tag{15}$$

For solving Eq. (15) a Taylor-series expansion to linearize the equation is used, which gives the results shown in Eq. 16 (for more details see [135]):

$$V_B(k+L) \approx Voc(SoC(k)) - I(k)\frac{\eta L T_s}{C_n}\frac{\partial Voc(SoC(k))}{\partial SoC(k)} - RI(k), \tag{16}$$

Finally, the maximum discharge current ($I_k^{\mathrm{dis},volt}$) and charge current ($I_k^{chg,volt}$) obtained by voltage limits method are given by (17) and (18):

$$I_k^{\mathrm{dis},volt} = \frac{Voc(SoC(k)) - V_{\min}}{\frac{\eta L T_s}{C_n}\frac{\partial Voc(SoC(k))}{\partial SoC(k)} + R^{\mathrm{dis}chg}}, \tag{17}$$

$$I_k^{chg,volt} = \frac{Voc(SoC(k)) - V_{\max}}{\frac{\eta L T_s}{C_n}\frac{\partial Voc(SoC(k))}{\partial SoC(k)} + R^{chg}}, \tag{18}$$

The voltage limits method cannot be accurate over the entire SoC range, particularly near extreme values of the SoC [115]. Once the current limits based on the SoC and voltage methods have been calculated, the maximum discharge ($I_k^{\mathrm{dis}chg}(k)$) and charge ($I_k^{chg}(k)$) currents with all limits enforced are computed by (19) and (20):

$$I_k^{\mathrm{dis}chg}(k) = \min(I_{\max}, I_k^{\mathrm{dis},SoC}, I_k^{\mathrm{dis},volt}), \tag{19}$$

$$I_k^{chg}(k) = \max(I_{\min}, I_k^{chg,SoC}, I_k^{chg,volt}), \tag{20}$$

where I_{max} and I_{min} are design limits for the maximum discharge and minimum charge currents respectively, given by the manufacturer. The maximum discharging ($P_{max,k}^{\mathrm{dis}chg}$) and charging ($P_{max,k}^{chg}$) powers are calculated as the product of the maximum current (discharge or charge) and the predicted future voltage (see the Eq. 16) over the horizon time (L) by (21) and (22):

$$P_{\max,k}^{\mathrm{dis}chg} = I_k^{\mathrm{dis}chg} V_B(k+L) \tag{21}$$

$$P_{\max,k}^{chg} = I_k^{chg} V_B(k+L) \tag{22}$$

The accuracy of both methods (SoC and voltage) in calculating the maximum discharging and charging currents depends on the precision of the estimation of the SoC. In this work, the estimations of the SoC is obtained based on UKF, as was explained in appendix A2.

Bibliography

[1] M. Falahi, S. Lotfifard, M. Ehsani, and K. Butler-Purry. Dynamic model predictive-based energy management of DG integrated distribution systems. *IEEE Transactions on Power Delivery*, 28(4):2217–2227, Oct 2013.

[2] F. Katiraei, R. Iravani, N. Hatziargyriou, and A. Dimeas. Microgrids management: Controls and operation aspects of microgrids. *IEEE Power and Energy Magazine*, 6(3):54–65, May 2008.

[3] D. E. Olivares, A. Mehrizi-Sani, A. H. Etemadi, C. A. Cañizares, R. Iravani, M. Kazerani, A. H. Hajimiragha, O. Gomis-Bellmunt, M. Saeedifard, R. Palma-Behnke, G. A. Jiménez-Estévez, and N. D. Hatziargyriou. Trends in Microgrid Control. *IEEE Transactions on Smart Grid*, 5(4):1905–1919, July 2014.

[4] A. P. Meliopoulos, G. J. Cokkinides, R. Huang, and E. Farantatos. Integrated smart grid hierarchical control. In *2012 45th Hawaii International Conference on System Sciences*, pages 1967–1976, Jan 2012.

[5] A. Fazeli. *The application of a novel deterministic algorithm for controlling the power flow through real time dispatch of the available distributed energy resources within a microgrid*. PhD thesis, University of Nottingham, 2014.

[6] J. Vasiljevska, J. A. P. Lopes, and M. A. Matos. Multi-microgrid impact assessment using multi criteria decision aid methods. In *2009 IEEE Bucharest PowerTech*, pages 1–8, June 2009.

[7] S. Parhizi, H. Lotfi, A. Khodaei, and S. Bahramirad. State of the Art in Research on Microgrids: A Review. *IEEE Access*, 3:890–925, 2015.

[8] B. M. Eid, N. A. Rahim, J. Selvaraj, and A. H. El Khateb. Control methods and objectives for electronically coupled distributed energy resources in microgrids: A review. *IEEE Systems Journal*, 10(2):446–458, June 2016.

[9] P. P. Padhi, R. K. Pati, and A. A. Nimje. Distributed generation: Impacts and cost analysis. *International Journal of Power System Operation and Energy Management*, 1(3):91–96, 2012.

[10] DNV GL Energy. A review of distributed energy resources. Technical report, New

York Independent System Operator, September 2014.

[11] Department of Energy office of Electricity Delivery and Energy Reliability. Summary Report : 2012 DOE Microgrid Workshop. Technical report, Office of Electricity Delivery and Energy Reliability Smart Grid R&D Program, 2012.

[12] R. H. Lasseter. Microgrids and distributed generation. *Journal of Energy Engineering*, 133(3):144–149, 2007.

[13] R. H. Lasseter. Microgrids. In *2002 IEEE Power Engineering Society Winter Meeting. Conference Proceedings (Cat. No.02CH37309)*, volume 1, pages 305–308, Jan 2002.

[14] J. C. Vasquez, J. M. Guerrero, J. Miret, M. Castilla, and L. Garcia de Vicuna. Hierarchical control of intelligent microgrids. *IEEE Industrial Electronics Magazine*, 4(4):23–29, Dec 2010.

[15] J. A. Peças, A. Madureira, and F. Nuno Gil. Operation of Multi-Microgrids. In N. Hatziargyriou, editor, *Microgrid: Architectures and Control*, pages 165–205. Wiley-IEEE Press, 2014.

[16] N. Hatziargyriou, H. Asano, R. Iravani, and C. Marnay. Microgrids: An Overview of Ongoing Research, Development, and Demonstration Projects. *IEEE Power & Energy Magazine*, July/August:78–94, July 2007.

[17] A. Ipakchi and F. Albuyeh. Grid of the future. *IEEE Power and Energy Magazine*, 7(2):52–62, March 2009.

[18] S. Massoud Amin and B. F. Wollenberg. Toward a smart grid: power delivery for the 21st century. *IEEE Power and Energy Magazine*, 3(5):34–41, Sept 2005.

[19] R. H. Lasseter. Smart distribution: Coupled microgrids. *Proceedings of the IEEE*, 99(6):1074–1082, June 2011.

[20] H. A. Khan, Z. Xu, H. Iu, and V. Sreeram. Review of technologies and implementation strategies in the area of smart grid. In *2009 Australasian Universities Power Engineering Conference*, pages 1–6, Sept 2009.

[21] F. Bouhafs, M. Mackay, and M. Merabti. Links to the future: Communication requirements and challenges in the smart grid. *IEEE Power and Energy Magazine*, 10(1):24–32, Jan 2012.

[22] H. Karimi, H. Nikkhajoei, and R. Iravani. Control of an electronically-coupled distributed resource unit subsequent to an islanding event. *IEEE Transactions on Power Delivery*, 23(1):493–501, Jan 2008.

[23] D. E. Olivares, C. A. Cañizares, and M. Kazerani. A Centralized Energy Management System for Isolated Microgrids. *IEEE Transactions on Smart Grid*, 5(4):1864–1875, July 2014.

[24] G. Pepermans, J. Driesen, D. Haeseldonckx, R. Belmans, and W. D'haeseleer. Distributed generation: definition, benefits and issues. *Energy Policy*, 33(6):787 – 798, 2005.

[25] L. I. Dulău, M. Abrudean, and D. Bică. Effects of distributed generation on electric power systems. *Procedia Technology*, 12:681 – 686, 2014.

[26] P. Chiradeja. Benefit of distributed generation: A line loss reduction analysis. In *2005 IEEE/PES Transmission Distribution Conference Exposition: Asia and Pacific*, pages 1–5, Aug 2005.

[27] J. M. Guerrero, P. C. Loh, T. Lee, and M. Chandorkar. Advanced control architectures for intelligent microgrids—part ii: Power quality, energy storage, and ac/dc microgrids. *IEEE Transactions on Industrial Electronics*, 60(4):1263–1270, April 2013.

[28] R. Hidalgo, C. Abbey, and G. Joós. A review of active distribution networks enabling technologies. In *IEEE PES General Meeting*, pages 1–9, July 2010.

[29] S. Abapour, K. Zare, and B. Mohammadi-Ivatloo. Dynamic planning of distributed generation units in active distribution network. *IET Generation, Transmission Distribution*, 9(12):1455–1463, 2015.

[30] O. Palizban, K. Kauhaniemi, and J. M. Guerrero. Microgrids in active network management – part II: System operation, power quality and protection. *Renewable and Sustainable Energy Reviews*, 36:440–451, 2014.

[31] A. Fazeli, E. Christopher, C. M. Johnson, M. Gillott, and M. Sumner. Investigating the effects of dynamic demand side management within intelligent Smart Energy communities of future decentralized power system. In *2011 2nd IEEE PES International Conference and Exhibition on Innovative Smart Grid Technologies*, pages 1–8, Dec 2011.

[32] A. An, B. Zheng, H. Zheng, C. Zheng, and P. Du. Benefit analysis and evaluation of distributed generation in distribution network under active management. In *2016 Chinese Control and Decision Conference (CCDC)*, pages 6031–6035, May 2016.

[33] J. M. Guerrero, M. Chandorkar, T. Lee, and P. C. Loh. Advanced control architectures for intelligent microgrids—part i: Decentralized and hierarchical control. *IEEE Transactions on Industrial Electronics*, 60(4):1254–1262, April 2013.

[34] A. Bidram and A. Davoudi. Hierarchical Structure of Microgrids Control System. *IEEE Transactions on Smart Grid*, 3(4):1963–1976, Dec 2012.

[35] K. De Brabandere, K. Vanthournout, J. Driesen, G. Deconinck, and R. Belmans. Control of microgrids. In *2007 IEEE Power Engineering Society General Meeting*, pages 1–7, June 2007.

[36] A. Kiani and A. Annaswamy. Distributed hierarchical control for renewable energy integration in a smart grid. In *2012 IEEE PES Innovative Smart Grid Technologies*

(ISGT), pages 1–8, Jan 2012.

[37] A. Kiani Bejestani, A. Annaswamy, and T. Samad. A hierarchical transactive control architecture for renewables integration in smart grids: Analytical modeling and stability. *IEEE Transactions on Smart Grid*, 5(4):2054–2065, July 2014.

[38] L. I. Minchala-Avila, L.E. Garza-Castañón, A. Vargas-Martínez, and Y. Zhang. A review of optimal control techniques applied to the energy management and control of microgrids. *Procedia Computer Science*, 52:780–787, 2015.

[39] A. Fazeli, M. Sumner, E. Christopher, and M. Johnson. Power flow control for power and voltage management in future smart energy communities. In *3rd Renewable Power Generation Conference (RPG 2014)*, pages 1–6, Sept 2014.

[40] A. Fazeli, M. Sumner, C. M. Johnson, and E. Christopher. Coordinated optimal dispatch of distributed energy resources within a smart energy community cell. In *2012 3rd IEEE PES Innovative Smart Grid Technologies Europe (ISGT Europe)*, pages 1–10, Oct 2012.

[41] A. Fazeli, M. Sumner, M. C. Johnson, and E. Christopher. Real-time deterministic power flow control through dispatch of distributed energy resources. *IET Generation, Transmission Distribution*, 9(16):2724–2735, 2015.

[42] W. Su and J.Wang. Energy management systems in microgrid operations. *The Electricity Journal*, 25(8):45–60, 2012.

[43] M. Mao, P. Jin, N. D. Hatziargyriou, and L. Chang. Multiagent-Based Hybrid Energy Management System for Microgrids. *IEEE Transactions on Sustainable Energy*, 5(3):938–946, July 2014.

[44] O. Palizban, K. Kauhaniemi, and J.M. Guerrero. Microgrids in active network management — Part I: Hierarchical control, energy storage, virtual power plants, and market participation. *Renewable and Sustainable Energy Reviews*, 36:428–439, 2014.

[45] M. F. Zia, E. E., and M. Benbouzid. Microgrids energy management systems: A critical review on methods, solutions, and prospects. *Applied Energy*, 222:1033–1055, 2018.

[46] J. Mattingley, Y. Wang, and S. Boyd. Receding Horizon Control. *IEEE Control Systems Magazine*, 31(3):52–65, June 2011.

[47] J. Silvente, G. M. Kopanos, E. N. Pistikopoulos, and A. Espuña. A rolling horizon optimization framework for the simultaneous energy supply and demand planning in microgrids. *Applied Energy*, 155:485–501, 2015.

[48] R. Palma-Behnke, C. Benavides, F. Lanas, B. Severino, L. Reyes, J. Llanos, and D. Sáez. A Microgrid Energy Management System Based on the Rolling Horizon Strategy. *IEEE Transactions on Smart Grid*, 4(2):996–1006, June 2013.

[49] Q. Jiang, M. Xue, and G. Geng. Energy management of microgrid in grid-connected

and stand-alone modes. *IEEE Transactions on Power Systems*, 28(3):3380–3389, Aug 2013.

[50] M. Brandstetter, A. Schirrer, M. Miletić, S. Henein, M. Kozek, and F. Kupzog. Hierarchical Predictive Load Control in Smart Grids. *IEEE Transactions on Smart Grid*, 8(1):190–199, Jan 2017.

[51] L. Valverde, C. Bordons, and F. Rosa. Integration of Fuel Cell Technologies in Renewable-Energy-Based Microgrids Optimizing Operational Costs and Durability. *IEEE Transactions on Industrial Electronics*, 63(1):167–177, Jan 2016.

[52] M. M. A. Abdelaziz, M. F. Shaaban, H. E. Farag, and E. F. El-Saadany. A multistage centralized control scheme for islanded microgrids with pevs. *IEEE Transactions on Sustainable Energy*, 5(3):927–937, July 2014.

[53] M. Pereira, D. Limon, D. Muñoz de la Peña, L. Valverde, and T. Alamo. Periodic economic control of a nonisolated microgrid. *IEEE Transactions on Industrial Electronics*, 62(8):5247–5255, Aug 2015.

[54] I. A. Sajjad, G. Chicco, and R. Napoli. Effect of aggregation level and sampling time on load variation profile - A statistical analysis. In *17th IEEE Mediterranean Electrotechnical Conference*, pages 208–212, April 2014.

[55] Z. Wu, X. Zhang, J. Brandt, S. Zhou, and J. LI. Three Control Approaches for Optimized Energy Flow With Home Energy Management System. *IEEE Power and Energy Technology Systems Journal*, 2(1):21–31, March 2015.

[56] A. K. Daud and M. S. Ismail. Design of isolated hybrid systems minimizing costs and pollutant emissions. *Renewable Energy*, 44:215–224, 2012.

[57] M. Hosseinzadeh and F. R. Salmasi. Power management of an isolated hybrid AC/DC microgrid with fuzzy control of battery banks. *IET Renewable Power Generation*, 9(5):484–493, 2015.

[58] R. Davies, M. Sumner, and E. Christopher. Energy storage control for a small community microgrid. In *7th IET International Conference on Power Electronics, Machines and Drives (PEMD 2014)*, pages 1–6, April 2014.

[59] S. Faquir, A. Yahyaouy, H. Tairi, and J. Sabor. A type-1 fuzzy logic algorithm to manage the flow of energy in a stand-alone PV/wind/battery hybrid system. In *2015 Intelligent Systems and Computer Vision (ISCV)*, pages 1–6, March 2015.

[60] L. Roiné, K. Therani, Y. Sahraei Manjili, and M. Jamshidi. Microgrid energy management system using fuzzy logic control. In *2014 World Automation Congress (WAC)*, pages 462–467, Aug 2014.

[61] I. Yahyaoui, I. Ouachani, M. Ammous, M. Chaabene, and F. Tadeo. Energy management for a photovoltaic-wind system with non-controlable load. In *IREC2015 The Sixth International Renewable Energy Congress*, pages 1–5, March 2015.

[62] D. Arcos-Aviles, J. Pascual, L. Marroyo, P. Sanchis, and F. Guinjoan. Fuzzy Logic-Based Energy Management System Design for Residential Grid-Connected Microgrids. *IEEE Transactions on Smart Grid*, 9(2):530–543, March 2018.

[63] J. D. Lara, D. E. Olivares, and C. A. Cañizares. Robust Energy Management of Isolated Microgrids. *IEEE Systems Journal*, pages 1–12, 2018.

[64] S. Talari, M. Yazdaninejad, and M. Haghifam. Stochastic-based scheduling of the microgrid operation including wind turbines, photovoltaic cells, energy storages and responsive loads. *IET Generation, Transmission Distribution*, 9(12):1498–1509, 2015.

[65] D. E. Olivares, J. D. Lara, C. A. Cañizares, and M. Kazerani. Stochastic-Predictive Energy Management System for Isolated Microgrids. *IEEE Transactions on Smart Grid*, 6(6):2681–2693, Nov 2015.

[66] A. Papavasiliou, S. S. Oren, and R. P. O'Neill. Reserve Requirements for Wind Power Integration: A Scenario-Based Stochastic Programming Framework. *IEEE Transactions on Power Systems*, 26(4):2197–2206, Nov 2011.

[67] A. Sobu and G. Wu. Optimal operation planning method for isolated micro grid considering uncertainties of renewable power generations and load demand. In *IEEE PES Innovative Smart Grid Technologies*, pages 1–6, May 2012.

[68] A. Parisio and L. Glielmo. Stochastic model predictive control for economic/environmental operation management of microgrids. In *2013 European Control Conference (ECC)*, pages 2014–2019, July 2013.

[69] W. Wu, J. Chen, B. Zhang, and H. Sun. A Robust Wind Power Optimization Method for Look-Ahead Power Dispatch. *IEEE Transactions on Sustainable Energy*, 5(2):507–515, April 2014.

[70] A. Khodaei. Provisional Microgrids. *IEEE Transactions on Smart Grid*, 6(3):1107–1115, May 2015.

[71] Y. Zhang, N. Gatsis, and G. B. Giannakis. Robust Energy Management for Microgrids With High-Penetration Renewables. *IEEE Transactions on Sustainable Energy*, 4(4):944–953, Oct 2013.

[72] J. Yi, P. F. Lyons, P. J. Davison, P. Wang, and P. C. Taylor. Robust Scheduling Scheme for Energy Storage to Facilitate High Penetration of Renewables. *IEEE Transactions on Sustainable Energy*, 7(2):797–807, April 2016.

[73] I. Škrjanc. Fuzzy confidence interval for pH titration curve. *Applied Mathematical Modelling*, 35(8):4083–4090, 2011.

[74] M. Khodayar, J. Wang, and M. Manthouri. Interval deep generative neural network for wind speed forecasting. *IEEE Transactions on Smart Grid*, 2018.

[75] A. Kroll and H. Schulte. Benchmark problems for nonlinear system identification and

control using soft computing methods: Need and overview. *Applied Soft Computing*, 25:496–513, 2014.

[76] H. M. D. Kabir, A. Khosravi, M. A. Hosen, and S. Nahavandi. Neural network-based uncertainty quantification: A survey of methodologies and applications. *IEEE Access*, 6:36218–36234, 2018.

[77] N.A. Shrivastava, K. Lohia, and B. K. Panigrahi. A multiobjective framework for wind speed prediction interval forecasts. *Renewable Energy*, 87(Part 2):903–910, 2016.

[78] R. Dybowski and S. J. Roberts. *Confidence intervals and prediction intervals for feed-forward neural networks*, page 298–326. Cambridge University Press, 2001.

[79] T. Heskes. Practical confidence and prediction intervals. *Advances in Neural Information Processing Systems*, 9:176–182, Oct. 1997.

[80] M. Ramezani, M. Bashiri, and A. C. Atkinson. A goal programming-topsis approach to multiple response optimization using the concepts of non-dominated solutions and prediction intervals. *Expert Systems with Applications*, 38(8):9557–9563, 2011.

[81] A. C. Rencher and G. B. Schaalje. *Linear models in statistics*. John Wiley & Sons, Inc, USA, 2 edition, 2008.

[82] L. G. Marín, N. Cruz, D. Sáez, M. Sumner, and A. Núñez. Prediction interval methodology based on fuzzy numbers and its extension to fuzzy systems and neural networks. *Expert Systems with Applications*, 119:128–141, 2019.

[83] D. Sáez, F. Ávila, D. Olivares, C. Cañizares, and L. G. Marín. Fuzzy Prediction Interval Models for Forecasting Renewable Resources and Loads in Microgrids. *IEEE Transactions on Smart Grid*, 6(2):548–556, March 2015.

[84] F. Valencia, J. Collado, D. Sáez, and L. G. Marín. Robust Energy Management System for a Microgrid Based on a Fuzzy Prediction Interval Model. *IEEE Transactions on Smart Grid*, 7(3):1486–1494, May 2016.

[85] I. Škrjanc, S. Blazic, and O. Agamennoni. Interval fuzzy model identification using l_∞-Norm. *IEEE Transactions on Fuzzy Systems*, 13(5):561–568, Oct 2005.

[86] F. Valencia, D. Sáez, J. Collado, F. Ávila, A. Marquez, and J. J. Espinosa. Robust energy management system based on interval fuzzy models. *IEEE Transactions on Control Systems Technology*, 24(1):140–157, Jan 2016.

[87] Y. Xiang, J. Liu, and Y. Liu. Robust energy management of microgrid with uncertain renewable generation and load. *IEEE Transactions on Smart Grid*, 7(2):1034–1043, March 2016.

[88] L. G. Marín, F. Valencia, and D. Sáez. Prediction interval based on type-2 fuzzy systems for wind power generation and loads in microgrid control design. In *2016 IEEE International Conference on Fuzzy Systems (FUZZ-IEEE)*, pages 328–335, July

2016.

[89] Y. Zhang and L. Xie. Online dynamic security assessment of microgrid interconnections in smart distribution systems. *IEEE Transactions on Power Systems*, 30(6):3246–3254, Nov 2015.

[90] A. Ouammi, H. Dagdougui, L. Dessaint, and R. Sacile. Coordinated model predictive-based power flows control in a cooperative network of smart microgrids. *IEEE Transactions on Smart Grid*, 6(5):2233–2244, Sept 2015.

[91] J. Wu and X. Guan. Coordinated multi-microgrids optimal control algorithm for smart distribution management system. *IEEE Transactions on Smart Grid*, 4(4):2174–2181, Dec 2013.

[92] M. Fathi and H. Bevrani. Statistical cooperative power dispatching in interconnected microgrids. *IEEE Transactions on Sustainable Energy*, 4(3):586–593, July 2013.

[93] L. Che, M. Shahidehpour, A. Alabdulwahab, and Y. Al-Turki. Hierarchical coordination of a community microgrid with ac and dc microgrids. *IEEE Transactions on Smart Grid*, 6(6):3042–3051, Nov 2015.

[94] W. Xi, Q. Xiaoyan, J. Runzhou, L. Dan, W. Gang, and L. Qian. Economic operation of multi-microgrids containing energy storage system. In *2014 International Conference on Power System Technology*, pages 1712–1716, Oct 2014.

[95] C. Zhang, X. Liu, X. He, and C. Li. The output optimization of multi-microgrids connected to distribution network during peak, flat and valley periods. In *2014 IEEE PES Asia-Pacific Power and Energy Engineering Conference (APPEEC)*, pages 1–5, Dec 2014.

[96] N. Nikmehr and S. Najafi Ravadanegh. Optimal power dispatch of multi-microgrids at future smart distribution grids. *IEEE Transactions on Smart Grid*, 6(4):1648–1657, July 2015.

[97] Z. Wang, B. Chen, J. Wang, M. M. Begovic, and C. Chen. Coordinated energy management of networked microgrids in distribution systems. *IEEE Transactions on Smart Grid*, 6(1):45–53, Jan 2015.

[98] R. Ak, Y. Li, V. Vitelli, E. Zio, E. López Droguett, and C. M. Couto Jacinto. NSGA-II-trained neural network approach to the estimation of prediction intervals of scale deposition rate in oil & gas equipment. *Expert Systems with Applications*, 40(4):1205–1212, 2013.

[99] F. Veltman, L. G. Marín, D. Sáez, L. Guitierrez, and A. Núñez. Prediction Interval Modeling Tuned by an Improved Teaching Learning Algorithm Applied to Load Forecasting in Microgrids. In *2015 IEEE Symposium Series on Computational Intelligence*, pages 651–658, Dec 2015.

[100] A. Khosravi, S. Nahavandi, D. Creighton, and A. F. Atiya. Comprehensive review of

neural network-based prediction intervals and new advances. *IEEE Transactions on Neural Networks*, 22(9):1341–1356, Sept 2011.

[101] A. Khosravi, S. Nahavandi, D. Creighton, and A. F. Atiya. Lower upper bound estimation method for construction of neural network-based prediction intervals. *IEEE Transactions on Neural Networks*, 22(3):337–346, March 2011.

[102] A. Khosravi, S. Nahavandi, and D. Creighton. A prediction interval-based approach to determine optimal structures of neural network metamodels. *Expert Systems with Applications*, 37(3):2377 – 2387, 2010.

[103] J.M. Mendel. *Uncertain rule-based fuzzy logic systems: Introduction and new directions*. Springer International Publishing, 2nd edition, 2017.

[104] K. H. Lee. *First course on fuzzy theory and applications*. Springer-Verlag, (Chapter 5), Berlin, 1 edition, 2005.

[105] N. N. Karnik and J. M. Mendel. Operations on type-2 fuzzy sets. *Fuzzy Sets and Systems*, 122(2):327–348, 2001.

[106] Robert Babuška. *Fuzzy modeling for control*. Kluwer Academic Publishers, Boston, USA, 1st edition, 1998.

[107] R. Gencay and Min Qi. Pricing and hedging derivative securities with neural networks: Bayesian regularization, early stopping, and bagging. *IEEE Transactions on Neural Networks*, 12(4):726–734, July 2001.

[108] D. Sáez and R. Zuniga. Cluster optimization for Takagi & Sugeno fuzzy models and its application to a combined cycle power plant boiler. In *Proceedings of the 2004 American Control Conference*, volume 2, pages 1776–1781, June 2004.

[109] H. Quan, D. Srinivasan, and A. Khosravi. Short-term load and wind power forecasting using neural network-based prediction intervals. *IEEE Transactions on Neural Networks and Learning Systems*, 25(2):303–315, Feb 2014.

[110] E. Elbeltagi, T. Hegazy, and D. Grierson. Comparison among five evolutionary-based optimization algorithms. *Advanced Engineering Informatics*, 19(1):43–53, 2005.

[111] D. C. Tran, Z. Wu, and V. X. Nguyen. A new approach based on enhanced pso with neighborhood search for data clustering. In *2013 International Conference on Soft Computing and Pattern Recognition (SoCPaR)*, pages 98–104, Dec 2013.

[112] S. Chen, S. A. Billings, and P. M. Grant. Non-linear system identification using neural networks. *International Journal of Control*, 51(6):1191–1214, 1990.

[113] Y. Xu, M. Zhang, Q. Zhu, and Y. He. An improved multi-kernel rvm integrated with ceemd for high-quality intervals prediction construction and its intelligent modeling application. *Chemometrics and Intelligent Laboratory Systems*, 171:151–160, 2017.

[114] I. Richardson and M. Thomson. One-Minute Resolution Domestic Electricity Use Data, 2008-2009 [computer file]. *Colchester, Essex: UK Data Archive [distributor]*, 2010.

[115] G. L. Plett. High-performance battery-pack power estimation using a dynamic cell model. *IEEE Transactions on Vehicular Technology*, 53(5):1586–1593, Sept 2004.

[116] F. Sun, R. Xiong, H. He, W. Li, and J. E. E. Aussems. Model-based dynamic multi-parameter method for peak power estimation of lithium–ion batteries. *Applied Energy*, 96:378–386, 2012.

[117] R. Van der Merwe and E. A. Wan. The square-root unscented Kalman filter for state and parameter-estimation. In *2001 IEEE International Conference on Acoustics, Speech, and Signal Processing. Proceedings*, volume 6, pages 3461–3464, May 2001.

[118] C. Tampier, A. Pérez, F. Jaramillo, V. Quintero, M. E. Orchard, and J. F. Silva. Lithium-ion battery end-of-discharge time estimation and prognosis based on Bayesian algorithms and outer feedback correction loops: A comparative analysis. In *Proceedings of the Annual Conference of the Prognostics and Health Management Society, PHM*, volume 6, pages 182–195, 2015.

[119] C. Burgos, D. Sáez, M. E. Orchard, and R. Cárdenas. Fuzzy modelling for the state-of-charge estimation of lead-acid batteries. *Journal of Power Sources*, 274:355–366, 2015.

[120] D. A. Pola, H. F. Navarrete, M. E. Orchard, R. S. Rabié, M. A. Cerda, B. E. Olivares, J. F. Silva, P. A. Espinoza, and A. Pérez. Particle-Filtering-Based Discharge Time Prognosis for Lithium-Ion Batteries With a Statistical Characterization of Use Profiles. *IEEE Transactions on Reliability*, 64(2):710–720, June 2015.

[121] A. Pérez, R. Moreno, R. Moreira, M. Orchard, and G. Strbac. Effect of Battery Degradation on Multi-Service Portfolios of Energy Storage. *IEEE Transactions on Sustainable Energy*, 7(4):1718–1729, Oct 2016.

[122] P. J. Goulart, E. C. Kerrigan, and J. M. Maciejowski. Optimization over state feedback policies for robust control with constraints. *Automatica*, 42(4):523–533, 2006.

[123] Green Energy UK and Tide — a new way to take control. https://www.greenenergyuk.com/Tide. Accessed: 2018-10-16.

[124] D. Parra, S. A. Norman, G. S. Walker, and M. Gillott. Optimum community energy storage for renewable energy and demand load management. *Applied Energy*, 200:358–369, 2017.

[125] M. Kharrich, Y. Sayouti, and M. Akherraz. Optimal microgrid sizing and daily capacity stored analysis in summer and winter season. In *2018 4th International Conference on Optimization and Applications (ICOA)*, pages 1–6, April 2018.

[126] H. Zahboune, S. Zouggar, G. Krajacic, P. S. Varbanov, M. Elhafyani, and E. Ziani. Optimal hybrid renewable energy design in autonomous system using Modified Electric

System Cascade Analysis and Homer software. *Energy Conversion and Management*, 126:909–922, 2016.

[127] R. Ayop, N. M. Isa, and C. W. Tan. Components sizing of photovoltaic stand-alone system based on loss of power supply probability. *Renewable and Sustainable Energy Reviews*, 81:2731–2743, 2018.

[128] B. Ould Bilal, V. Sambou, P. A. Ndiaye, C. M. F. Kébé, and M. Ndongo. Multi-objective design of PV-wind-batteries hybrid systems by minimizing the annualized cost system and the loss of power supply probability (LPSP). In *2013 IEEE International Conference on Industrial Technology (ICIT)*, pages 861–868, Feb 2013.

[129] D. Arcos-Aviles, J. Pascual, L. Marroyo, P. Sanchis, F. Guinjoan, and M. P. Marietta. Optimal Fuzzy Logic EMS design for residential grid-connected microgrid with hybrid renewable generation and storage. In *2015 IEEE 24th International Symposium on Industrial Electronics (ISIE)*, pages 742–747, June 2015.

[130] J. Pascual, J. Barricarte, P. Sanchis, and L. Marroyo. Energy management strategy for a renewable-based residential microgrid with generation and demand forecasting. *Applied Energy*, 158:12–25, 2015.

[131] D. Bertsimas and M. Sim. The price of robustness. *Operations Research*, 52(1):35–53, Jan4 2004.

[132] A.D. Hansen, P. Sørensen, L.H. Hansen, and H. Bindner. Models for a Stand-Alone PV System. Technical report, Risø National Laboratory, 2000.

[133] I. Richardson, M. Thomson, D. Infield, and C. Clifford. Domestic electricity use: A high-resolution energy demand model. *Energy Build*, 42(10):1878–1887, 2010.

[134] J.B. Copetti and F. Chenlo. Lead/acid batteries for photovoltaic applications. test results and modeling. *Journal of Power Sources*, 47(1):109–118, 1994.

[135] R. Xiong, H. He, F. Sun, X. Liu, and Z. Liu. Model-based state of charge and peak power capability joint estimation of lithium-ion battery in plug-in hybrid electric vehicles. *Journal of Power Sources*, 229:159 – 169, 2013.